A PHOSPHORESCENCE METHOD TO PROBE PROTEIN DYNAMICS

GUSZTÁV SCHAY

SUPERVISOR: PROF. JUDIT FIDY D.SC.

Doctoral School of Biology
Doctoral school leader: Prof. Anna Erdei D.Sc.
Structural Biochemistry doctoral programme , Eötvös Lóránd University
Programme leader: Prof. László Gráf D.Sc.

Department of Biophysics and Radiation Biology
Semmelweis University
June 2012

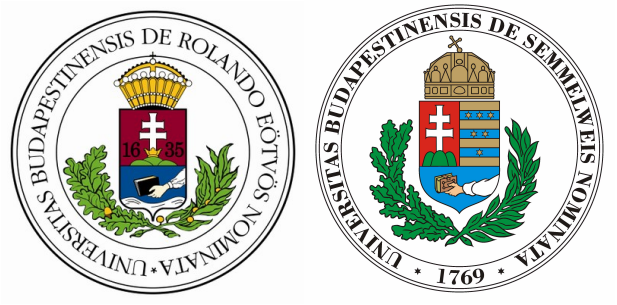

ABSTRACT

A new phosphorescence-based method is presented, by which the activation of slow (ms - s time-scale) global dynamics of proteins can be monitored. It is shown, that the activation of this slow, global dynamics is specific for the protein. A simple model is also presented by which the activation energy and entropy can be calculated (estimated) from the experimental data. The new method is presented in the case of human hemoglobin. The experiments were performed also in the presence of allosteric effector molecules, which modify the oxygen-binding of hemoglobin. As a consequence of the presence of these effectors we have observed changes in the activation of the collective dynamics of hemoglobin, changes in the dissociation constant of the tetramer obtained by pressure perturbation, and also changes in the isothermal compressibility obtained by fluorescence line narrowing spectroscopy. All these changes are in accordance with the efficiency of the effectors in modifying the oxygen binding of hemoglobin. This shows that changes in the global, slow dynamics of hemoglobin, caused by allosteric effectors may play a significant role in the regulation of hemoglobin function. The phosphorescence-based method is also applied to two other proteins, namely phosphoglycerate kinase, and dUTP-pyrophosphatase. In the case of phosphoglycerate kinase it was shown that the activation of the dynamics is asymmetric, and depends on the presence of both domains. Apparently, the hinge-bending motion is not essential for the inter-domain communication: there is a collective dynamics of the two domains even when hinge bending is blocked. In the case of dUTP-pyrophosphatase it was shown that the C-terminal arm-like structures of the trimeric molecule have a distinct dynamics in the apo-enzyme and in the substrate-bound form. It may thus be hypothesized that the special type of dynamics being monitored in these experiments may be important in the regulation of multi-domain proteins.

CONTENTS

LIST OF TABLES

BZF Bezafibrate

DMSO dimethyl sulfoxide

DPG 2,3-diphospho-glycerate

dUPNPP 2´-deoxyuridine-5´-(α,β-imido)triphosphate

DUT dUTP-ase

HEPES 4-(2-hydroxyethyl)-1-piperazineethanesulfonic acid

IDF inhomogeneous distribution function

IHP Inositol hexaphosphate

Mb Human Myoglobin

MEM Maximum Entropy Method

MWC Monod-Wyman-Changeux model of allostery in hemoglobin

oxy-HbA oxygen - saturated, R-state HbA

Pd-CP Palladium coproporphyrin

PGK Phosphoglycerate kinase

TRP Tryptophan residue

Zn-HbA [α-FeO2]2-[β-Zn]2-HbA

Zn-PP zinc protoporphyrin-IX

FLN Fluorescence Line Narrowing Spectroscopy

HbA Human Hemoglobin A

From where then does wisdom come,
and where is the resting-place of knowledge?
For it is kept secret from the eyes of all living,
unseen by the birds of the air...

...for we see now through a mirror obscurely,
and then face to face.

— Bible [1]

GENERAL INTRODUCTION

There is so much to say about the selected citation from the Bible. Beyond its deep theological message - which shall not be discussed in this thesis - it can be understood in a broader context covering all wisdom and knowledge, including the purpose of our lives. At the same time, it also holds in a much more limited context: the knowledge of science.
Since science and philosophy have seemingly departed from each other, it might appear a little confusing to start a PhD dissertation in the field of science with a discussion about general wisdom. However, ultimately science is all about "wisdom" in a special way: we would like to acquire knowledge about nature, about the world around us, and - as a result of a motivation working deeply inside us - about the purpose of our lives. Although science does not go into the details about the latter, it is still one of the hidden, but important, driving forces behind scientific research.
During the years of my PhD work, I have built instruments, collected and analyzed data and tried to build a model around to be at least self-consistent. In spite of all these endeavors, even if a model is self-consistent, even if it also fits the experimental data and the numbers it delivers appear to make sense, we shall never forget this thousands of years old but still ever true message: *"we are looking at nature through a mirror"*.

This is a general introduction only, for more detailed, scientific introductions please see the individual parts, each has its own.

Before going on, there is an important note:
I think science is not only about new discoveries and knowledge, but it is also enlightening. It is an important part of being a scientist to enjoy the sparks of possibly wild ideas, to see them emerge and of course

1 Bible, Joung's literal translation, *Job* 28,20-21. and *I.Corinthians* 13,12.

then sometimes see them being destroyed. This dynamics of ideas makes science unique among most of the professions, and relates it closely to art. In this thesis, I will make an attempt to reflect this duality of science: both being some sort of loose, easy art, and being at the same time rigorously precise and logical. Therefore I will deliberately use different language styles in this thesis. My own thoughts, speculations and view will be presented in a relaxed language style, while results and discussions which are already published, or being submitted to journals - thus having passed the rigorous logic and found to have a solid basis - will be written in a formal style to emphasis their separation from speculations, and freely floating ideas. This introduction is more an introduction to the thesis itself, than an introduction to the science in it. The latter will be given for each chapter separately, since they are so different, it did not seem logical to have a single introduction split into several parts. Many different questions are raised and discussed, and also three different molecules are addressed, although mostly from a given viewpoint. This common viewpoint is the perspective of the new optical method developed during my PhD work. Therefore, this short introduction has three goals:

- present the questions raised before and mostly *during* the work.
- present the structure of the thesis.
- and finally acknowledge all the the support I got during the years.

This thesis tries to summarize the results of the last couple of years in a *retrospective* way. Looking backwards often yields a completely different perspective, which may be somehow useful to better understand connections between pieces of a big puzzle. This case is not an exception, and therefore, to show *how* the specific questions, goals were raised before and also *during* the work, I will shortly "tell the story": How the research began, what did we expect, and how those ideas emerged, which now form the basis of this thesis.

This part of the introduction is mostly about the story *from my personal perspective.*

When I started my PhD-work under the supervision of Prof. Judit Fidy, she just started a new project - in collaboration with Prof. Yonetani - with human hemoglobin (HbA[2]). It was assigned as my PhD project. We did not think then to develop a new method, rather it was our intention to build upon the expertise already available in Prof. Fidy's group in the field of high resolution fluorescence spectroscopy, and pressure perturbation methods, and use these techniques in a collaborative effort, to gain

2 Each abbreviation will appear in parenthesis when used for the first time.

further insights into the mechanism of allosteric control in HbA.
During the long decades of experimental and theoretic work being done on HbA many models have emerged to describe the phenomenon of oxygen binding, and allostery. Most of these models are already parts of basic biochemistry textbooks, and as such are considered as basic science. However, many details are still not perfectly understood and described by these methods, and the topic is still a field of active research. Just including the last three years, over 23000 entries are found with a simple search using the keyword "hemoglobin", and while many of them analyze the genetic code behind diseases, there are also new papers about structural insights of the molecule itself. This shows, that even today open questions (and possible answers) regarding for example ligand migration pathways [77] still exist. Prof Yonetani's group is well known in the field of hemoglobin, one of his most cited works publishes the new "global allostery" model [155]. In this model the allosteric effectors (which are small molecules, that can bind to HbA to modify its oxygen binding) are proposed to bind to *both* oxygen-containing, and deoxygenated forms of hemoglobin to modify the interaction between all of the monomers. Since our special spectroscopic techniques are capable to somehow monitor changes in this interaction, a collaboration was formed, and we started to work with fluorescent hybrid HbA, in which two of the heme-groups was exchanged to fluorescent porphyrin. Heme itself is non-fluorescent, so this substitution was essential to open the way for the application of our spectroscopic techniques. We have started with a pressure perturbation study, since pressure is known to influence interfaces between molecules, and as such, it is perfect tool to study a tetramer such as hemoglobin. We found that allosteric effectors modify the interaction between the two dimers in HbA in both oxygenation states, and also determined the respective dissociation constants [117]. These findings supported the "global allostery" model.
The fluorescent porphyrins are perfect candidates also for high resolution fluorescence spectroscopy. A particular method used in our group is fluorescence line narrowing spectroscopy (FLN) which can be extended with pressure perturbation to estimate the isothermal compressibility of the protein [126]. In the case of HbA we have seen only a minuscule change in the compressibility of the protein in most cases. This was surprising to me, and *seemed to be controversial* to the fact that in the case of the interfaces we did find a definite trend in the effect of these modifier molecules. These FLN experiments were the first ones which pointed towards the need of an optical method capable of monitoring slow, possibly

ms timescale dynamical events. Since FLN is based on fluorescence emission, and requires very low temperatures (below 10K), it is not sensitive to any type of dynamics which may not be activated at this temperature. The only resolution to this controversy was then to assume that most of the changes manifesting in the change of the interactions between subunits come from a type of dynamics to which the FLN-based method is not sensitive. Taking into account that HbA is a fairly large molecule, I had the idea that maybe its size is large enough to have its own "internal universe" with slow, collective motions. And what if these motions are the ones which are primarily influenced by the presence of various allosteric effectors? Could it be, that these are the motions that may play a role in the control of the whole tetramer? Of course these were wild *speculations*, but triggered the question, that maybe using a different method, which is sensitive to this time-range, it may show a more pronounced difference between complexes of HbA and different allosteric effectors. The fact, that the special mixed-metal Zinc-hybrids are not only fluorescent, but also phosphorescent, gave an instant push to try experiments based of phosphorescence. Moreover, in the previous years I was using phosphorescence spectroscopy during my diploma-thesis work in the design of a novel test method for antibiotic susceptibility [116, 115], so I had quite a bit of experience in avoiding the usual pitfalls (controlling different sources of quenching) associated with the method. The first experiments quickly showed, that there is an interesting effect, however to have reliable data, many instrumental developments had to be made. The main difficulty arose from the fact that in these phosphorescence experiments the signal level was extremely low: A typical experiment had to run for about 3 weeks non-stop if no problems, such as power or cooling water outages occurred. I had to build an automatic system (see Appendix: Chapter A) to circumvent all these problems, and enable reliable non-stop data acquisition. These developments are not strictly part of the scientific results, but indirectly still are: without the system built, the data collection would not have been possible. The appendix to this thesis describes these developments. This part is more about engineering than science itself, therefore it is separated from the actual text of the thesis.

Of course there are methods, such as NMR, to investigate these effects, and this is a very active area of research, with the ever-increasing capabilities of NMR, localized events can also be monitored.

This was the birth of the "departmental legend", that I want a system which acquires data while I am on vacation, maybe sailing. It is partly true: It did acquire data also during those times.

I have used a special technique: I have deliberately *not* deoxygenated the samples before freezing them, to have O_2 molecules being trapped inside the protein matrix, and I have avoided the use of glass-forming substances, such as glycerol. Both turned out to be essential, and *we have observed something, which was not seen before*: The results from these temper-

ature studies showed a phase transition in the average phosphorescence lifetime, and we have shown that this can be interpreted in terms of an activation of slow (ms - s timescale), global dynamics specific to HbA, and distinct from the already well-known "glass-transition" observed in glassy solutions of proteins. We have also shown that this dynamics is sensitive to the presence of allosteric effectors, and with a simple theoretical model we could also calculate the energy and entropy change of the system associated to the activation of this special dynamics. This was also an answer to some of the questions raised before. Now, knowing that with this new method - technique - we can calculate these interesting parameters, it became an important question, if this is limited to the special case of hybrid, fluorescent HbA, or is it maybe more general, and applicable to other proteins as well? This was the time, when *the whole project started to deviate from HbA, and we turned into the direction of slow, global dynamics of proteins in general.*

In a summer break I have asked my colleague Szabolcs Osváth, who then worked with phosphoglycerate kinase (PGK) if he had some samples in the fridge for me to run a test. He had several different constructs. It turned out, that despite the signal levels being even lower than in the case of HbA, a similar transition could be observed, and more experiments then followed this initial one. We have shown, that indeed, inter-domain communication in PGK does manifest in the transition. We have shown that millisecond timescale *inter-domain communication in PGK also exist without the well-known "hinge-bending" motion*. This is surprising, since it shows that even if the boundary of the molecule is "fixed" (e.g., being embedded in, and bound to a solid, such as ice in this case) important motions, that may play a significant role in the function, still exist. Of course this technique is not capable of providing structural details, but the observed changes in the transitions may indicate that this specific timescale of a few hundreds of microseconds to seconds may well be very important in the function of enzymes.

At about this time Prof Fidy has started a new joint project with Prof. Beáta Vértessy on the structural dynamics of dUTP-pyrophosphatase[11] (DUT), and this new experimental method became part of the project. DUT is known to be a homo-trimer, in which each of the three active sites are built from parts of each three monomer. The whole structure looking at it from the top resembles a triangle, in which each monomer has a long "arm", which reaches both other monomers, and the end of this arm is one of the building parts of an active site. Prof Vértessy's group constructed a single-tryptohan (Trp) mutant of the protein, which

was another perfect molecule for the new method. We have shown, that the apo-enzyme behaves distinctly to the enzyme in complex with 2´-deoxyuridine- 5´ - (α,β-imido) triphosphate (dUPNPP). The dynamics of the "arm" region somewhat resembles the dynamics of the solvent in the apo-enzyme, while it is close to the dynamics of a globular fold in the complex with dUPNPP.

In this thesis the emphasis is laid on the new phosphorescence-based method, and thus its structure is built around it:

PART I : Demonstration of the method in the case of HbA.

- Description of the method and the theoretical model.
- Correlation with other results on HbA: measurement of the tetramer $\rightleftharpoons$ dimer dissociation constant by pressure-perturbation method, and estimation of changes in the isothermal compressibility measured by fluorescence line narrowing.
- Short summary.

PART II : Application to other proteins:

- PGK - communication without hinge-bending.
- dUTPase - preliminary results on the dynamics of the arm region.
- General conclusions

After the bibliography, I have inserted an appendix, which is a description of the engineering work, and new instrumentation developed during the research project. This is not strictly part of the thesis itself, but for the engineering-oriented reader it contains some interesting additional details about the instrumentation and software I have developed during the work.

Now, before the first part is started, I want to express my gratitude to all of those, who participated in this exciting work. I am very grateful to Prof Judit Fidy, my supervisor, for all of her support and patience she had with me during the long years of work. She was not only an exciting partner in discussions, and a very precise critic if it was the need for that

[3], but she also did everything to coach me to become a scientist. Without all these years together, I would surely not enjoy science as much, as I do now. I am also indebted to my colleagues, particularly to the whole "LSL" group[4], especially András Kaposi, Ferenc Tölgyesi (my diploma-thesis supervisor), Levente Herényi, László Smeller and Szabolcs Osváth. The "coffee-house meetings[5]" at lunchtime were fruitful times: I floated most of the ideas during these informal conversations, many technical and experimental questions were answered, or we just simply had a great time together. I have learnt the FLN technique together with Krisztián Szigeti, we had a lot of fun, e.g., in the beginning when we desperately tried to align the ring-laser for two days without success, and then András "gold-handed" Kaposi just came by, and tweeked here and there a bit, and whoila!... I am also grateful to Károly Módos who introduced me to the Propeller microcontroller platform, which was then heavily used in the instrumental developements. I am also very grateful to all of my other colleagues, if I would list all the names, then I would need to list the staff of the Department of Biophysics and Radiation Biology of Semmelweis University in the last approximately ten years. I am fortunate to be part of a great team - now lead by Prof. Miklós Kellermayer - built not only of excellent scientists, but also great people and friends. Without their constant support nothing presented in this thesis would have ever been possible.

I am also grateful to my family, without their support and love I would have never become a scientist, may God bless them with both of His hands. I am also grateful to the Kapernaum Foundation, which is a Christian mission for children with multiple (mental and physical) disability. The best ideas for my research always came during the days (and vacations) spent as a volunteer with them. After a week spent together I always re-started work full of ideas and energy.

3 And it was in many cases. As the reader will see, I like to formulate ideas, specualtions, also in the cases when they are only based on limited data. While this is interesting, a check needs to be kept on them.

4 Luminescence Spectroscopy Laboratroy

5 © Csaba Böde, our former collegue. We always laughed the loudest, when he wanted to work on something urgent. In other times, at the end of the day he told great stories about railways. We were all stunned that he knows the European railway time-table by heart...

Part I

DYNAMICAL TRANSITION IN HEMOGLOBIN

1

THE DYNAMICAL TRANSITION

1.1 INTRODUCTION

The conformational dynamics of proteins is known to be extremely complex phenomenon [56, 57]. It is a hierarchical network of specific motions across several orders of magnitude of spatial and temporal scales. Some dynamic components are observable even at cryogenic temperatures [158], whereas others become activated around the "glass transition temperature" of proteins and the timescale may extend from picoseconds to the time range of seconds [39, 97, 29, 27, 51, 108]. It is therefore experimentally demanding to monitor a wider scale of these motions in a single research approach [130, 16], since the various experimental and computational methods refer to specific time windows of motions. Most of the results have been obtained on myoglobin, which has thus become "the H-atom of biophysics" [40] due to its advantageous properties as a model system [19]. The time-window of the applied methods in most cases was far in the sub-millisecond range [55]. Motions involved in biologically relevant reactions (e.g. domain motions, closure of loops), however, mostly take place in the millisecond-second range. It is therefore of functional significance to develop and utilize techniques that address this longer timescale of protein dynamics [56, 33, 129, 15]. Although the functional significance of conformational dynamics is becoming more and more accepted[57], our understanding of its regulation and the exact mechanisms of action in macromolecular interactions is far from complete[17]. Especially intriguing questions are related to the role of the protein environment in its internal fluctuations. These important questions may involve coupling to the dynamics of the hydration layer, the bulk buffer, the crowded environment of the cell, or to motions in any specific interface bordering the molecule [41, 88, 156, 1, 79, 80, 47]. The answer must be found for each time and amplitude scale of the involved motions. It has been suggested, for example, that a strong coupling occurs between the internal protein dynamics and fast fluctuations in the hydration shell, whereas slower motions on a larger scale are slaved to fluctuations in the bulk solvent [42]. The experimental techniques applied in the studies often involve optical measurements at cryogenic temperatures on samples

containing high percentages of glycerol. It is also relevant to investigate how this circumstance may influence the conclusions concerning the dynamic coupling of protein and its environment. The following questions were raised:

1. Is there a specific thermal activation of large-scale protein dynamics in the time-window of a few tens of milliseconds up to a few hundreds of milliseconds?
2. If yes, can this transition be described by the well-known theory of "glass-transition"?
3. What is the significance of the protein environment, can the contribution of the protein be separated from that of it's environment?

To answer these questions we have developed a new optical method based on phosphorescence lifetime detection, and an ideal model system is one having in the molecule multiple suitable chromophores for spectroscopy. Therefore we have chosen a Zn-hybrid modified HbA, which has 6 Trp residues in the tetramer, and two phosphorescent porphyrins in its two β-subunits.

1.2 METHODS

1.2.1 *Sample preparation*

Sodium chloride, dimethyl sulfoxide (DMSO) and 4 - (2-hydroxyethyl) - 1 - piperazineethanesulfonic acid (HEPES) were purchased from Aldrich-Sigma (St. Louis). All samples were prepared in 100 mM HEPES, pH 7.4 with double-distilled water. Hybrid human HbA with zinc-protoporphyrin (Zn-PP) substituting the heme in the β subunits, $[\alpha\text{-FeO2}]_2$-$[\beta\text{-Zn}]_2$-HbA (Zn-HbA) was prepared in Takashi Yonetani's Laboratory at the University of Pennsylvania [141] :

In short, HbA was prepared from human blood as described in [142] according to the method of Drabkin [30]. HbA was promptly converted to the carbonmonoxy-form (CO-HbA) and stripped of organic phosphates by the method of Berman [14], and further purified by ion exchange chromatography. The final HbA solution was eluted in pH 7.4, 5 mM HEPES buffer. The α and β subunits were isolated from CO-HbA, and the subunit was converted to apoprotein by the acid-acetone method and then incubated with Zn-PP to create β-zinc subunits. Finally, the α-Fe and β-zinc

Figure 1: Reference absorption spectrum of Zn-HbA.

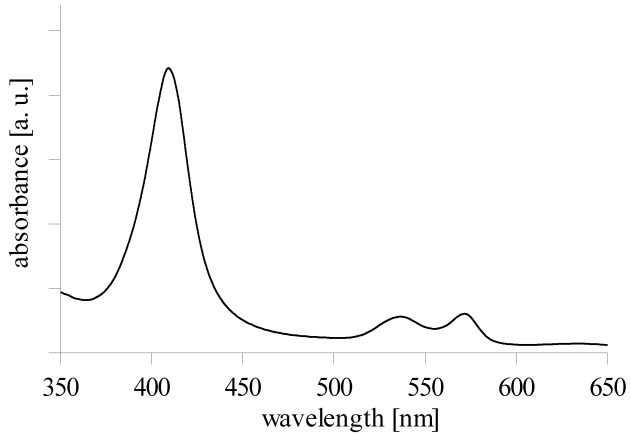

subunits were mixed and incubated in the cold for 2 days. The (α-Fe-CO)$_2$-(β-Zn)$_2$ form was then converted to the O_2 bound (oxy-) form of (α-Fe-O_2)$_2$-(β-Zn)$_2$-HbA by strong illumination and a flow of pure oxygen above the sample, which was kept on ice. Samples were transferred to Budapest on dry ice and stored at -80°C until use after fast-freezing in liquid nitrogen. Sample quality after thawing was controlled before further experiments by recording an absorption spectrum, and overlaying with the spectrum recorded on the fresh samples at the University of Pennsylvania. Only samples with no detectable difference were used. The control spectrum is shown in Figure 1. It can be seen, that the Zn-hybrid has a well-defined absorption-peak in the Soret-region around 410 nm, and also a structured Q-band around 550 nm. The position and shape of the spectrum in these regions is very sensitive to structural changes in the porphyrins themselves, and the protein matrix around them. This sensitivity is a well-known, common feature of porphyrin-containing proteins and is routinely used to control sample quality.

Human myoglobin (Mb) from Aldrich-Sigma was used as purchased. The protein concentration was adjusted to 60 μM in all experiments.

We have also used Zn-PP, as a special case, deprived of the protein, dissolved in DMSO. We have chosen this solvent, since Zn-PP has an acceptable solubility in this medium, its polarity is not very far from water, and it has no phase transition in the temperature range used in these experiments.

1.2.2 *Phosphorescence decay measurements at various temperatures.*

The conclusions in this chapter are based on phosphorescence lifetime data obtained on samples in thermal equilibrium, at various temperatures, starting upwards from 8 K. The samples were equilibrated for 4 hours at 8 K before starting the heating cycle to ensure thermodynamic equilibrium. Then temperature was changed in 5 or 10 K increments, and the samples were equilibrated at the target temperature for 45 minutes before the start of the phosphorescence decay measurement. At each temperature the triplet state lifetimes of the chromophores, namely Zn-PP, palladium coproporphyrin (Pd-CP) or Trp-s of the proteins were measured using the time-domain mode of an EAI CD900 spectrometer (Edinburgh Analytical Instruments, Edinburgh, U.K.) equipped with a μF900 Xe flash lamp of an energy of approximately 1 mJ/pulse and a pulse width of 2 μs FWHM (full width at half maximum). Excitation and emission wavelengths were 409, 384 or 290 nm and 723, 668 or 421 nm (for Zn-PP, Pd-CP and Trp, respectively), with 5 nm bandpass. The phosphorescence emission was very weak due to strong light scattering and quenching effects. To reach an acceptable signal/noise ratio for evaluation, up to14 000 consecutive flashes were summed with a time resolution of 80 μs. The long data collection time involved the possibility of photobleaching, which was controlled by repeated data collection periods and lifetime evaluation. Consecutive decays showed no detectable difference in signal intensity, and the shape of the emission spectrum also did not change. This confirms that no significant photobleaching was caused by the long data-collection. Phosphorescence photons were detected by a photomultiplier tube (R928, Hamamatsu Photonics, Shimokanzo, Japan) operated in single photon counting mode, and cooled to 255 K (C65972 water-cooled, Peltier operated PMT-cooler). After amplification, data were collected by a Norland 5000 multichannel analyzer card (Viking Instruments, Madison, U.S.A), and a custom-made multiscaler, controlled by an integrated data-acquisition software, which I have developed. The software also controlled the cryostat, used for adjusting the temperature of the sample, and the safety subsystem responsible for protection against power and cooling-water outages. The system is described in detail in appendix A of the thesis.

1.2.3 *Evaluation of phosphorescence decay curves*

The experimental goal was to characterize the dynamic state of the selected protein at various temperatures by the phosphorescence lifetime of a specific embedded chromophore. This parameter of chromophores in an ensemble of protein molecules representing also an ensemble of dynamic conditions is considered heterogeneous since both the heterogeneous conformational environment and the heterogeneity of the quenching conditions affect the individual lifetimes. We used the average lifetime of the heterogeneous lifetime-population as a dynamic parameter. Two approaches have been applied to determine reliable average lifetimes. We analyzed the decay curves by the method of Maximum Entropy (MEM) yielding lifetime distributions and fitted the decay data (I(t) functions) with the sum of exponential decay functions of discrete lifetime values:

$$I(t) = \sum_{i=1}^{n} A_i \cdot e^{-t/\tau_i} \tag{1}$$

where A_i and τ_i are the amplitudes and lifetimes of the individual components, respectively, and n is the number of exponentials used for the fitting. According to our experience, an acceptable least squares fit required 3 ... 5 discrete exponentials. The ensemble average $<\tau>$ was taken into consideration, since this is the parameter, which can be also approximated with the help of a simple thermodynamic model. The correct average can be calculated as a weighted average of the individual lifetime values, since the photon-statistics from every homogeneous sub-population with a given τ_i lifetime follows an exponential function. Let the probability of a photon being emitted at time t be :

$$P(emission\,at\,time\ t) \sim A_i \cdot e^{\frac{-t}{\tau_i}} \tag{2}$$

The total number of photons emitted from this population is thus:

$$N_i = \int_0^\infty A_i \cdot e^{\frac{-t}{\tau_i}} dt = A_i \tau_i \tag{3}$$

Thus, the weighting factor in the summation for each τ_i is $N_i = A_i\tau_i$. The average lifetime can then be expressed as:

$$< \tau >= \frac{\sum_{i=1}^{n} N_i \tau_i}{\sum_{i=1}^{n} N_i} = \frac{\sum_{i=1}^{n} A_i \tau_i^2}{\sum_{i=1}^{n} A_i \tau_i} \tag{4}$$

Table 1: Parameters of the selected discrete exponential fittings. The remarks show the classification of the lifetimes as well. The lifetimes below 0.2 ms are arising from the 80μs sampling time-quantization, and were discarded from further analysis, therefore these are not shown in the table, but are shown in Figure 2.

77 K		215 K		235 K		
τ [ms]	amplitude [a.u.]	τ [ms]	amplitude [a.u.]	τ [ms]	amplitude [a.u.]	*remark*
0.9	8746	0.2	14941	0.6	17502	*instrument response*
		2.0	18741	2.2	61590	*strongly quenched*
5.7	5604	6.3	39639	4.0	37911	*medium quenched*
23.6	41042	15.9	35777	10.1	7068	*long lifetime*
35.0	22805	31.3	6206	25.6	1379	

The <τ> values also represent the ensemble average: if every single state had been resolved, then A_i values would represent the number of molecules in the *i*-th state, having a lifetime of τ_i, and the summation would be over the whole ensemble, thus *n* would be the number of dynamic states. This value is then approximated by Equation (4) , where the individual lifetime values are either determined by the discrete exponential fitting method, or by the Maximum Entropy Method[20] (MEM). MEM inversions were obtained by importing the data into a custom-made program (by Károly Módos) for the analysis of dynamic light scattering data. In the case of the calculation of <τ> from MEM-data, the summation is over the whole discretized lifetime distribution.

Based on repeated lifetime acquisitions and different methods of calculation of <τ> values[1], the relative error in all experiments was less than 5%, except for the Trp, where the signal level was very low due to strong quenching and energy-transfer to the heme-groups. In the case of Trp data the relative error of the average lifetime values was 5 ... 15%. Sample decay curves are shown in Figure 2 together with the corresponding MEM-derived lifetime distributions. It can be seen, that the discrete-exponential method provides a very good fit to the data, the error functions do not show any residual structure, and the lifetimes match the corresponding MEM curve. In the case of the Trp data the signal/noise ratio

1 Comparison yielded a difference between MEM-based average values and discrete exponential-based ones of less than 5%. Also the difference between average lifetime values between two <τ>-s of individual lifetime data is less than 5%

Figure 2: Sample decay curves of Zn-HbA at various temperatures. The fitted curve is shown in red, the result of the MEM is shown on the right together with the lifetime and relative weight of the discrete exponentials.

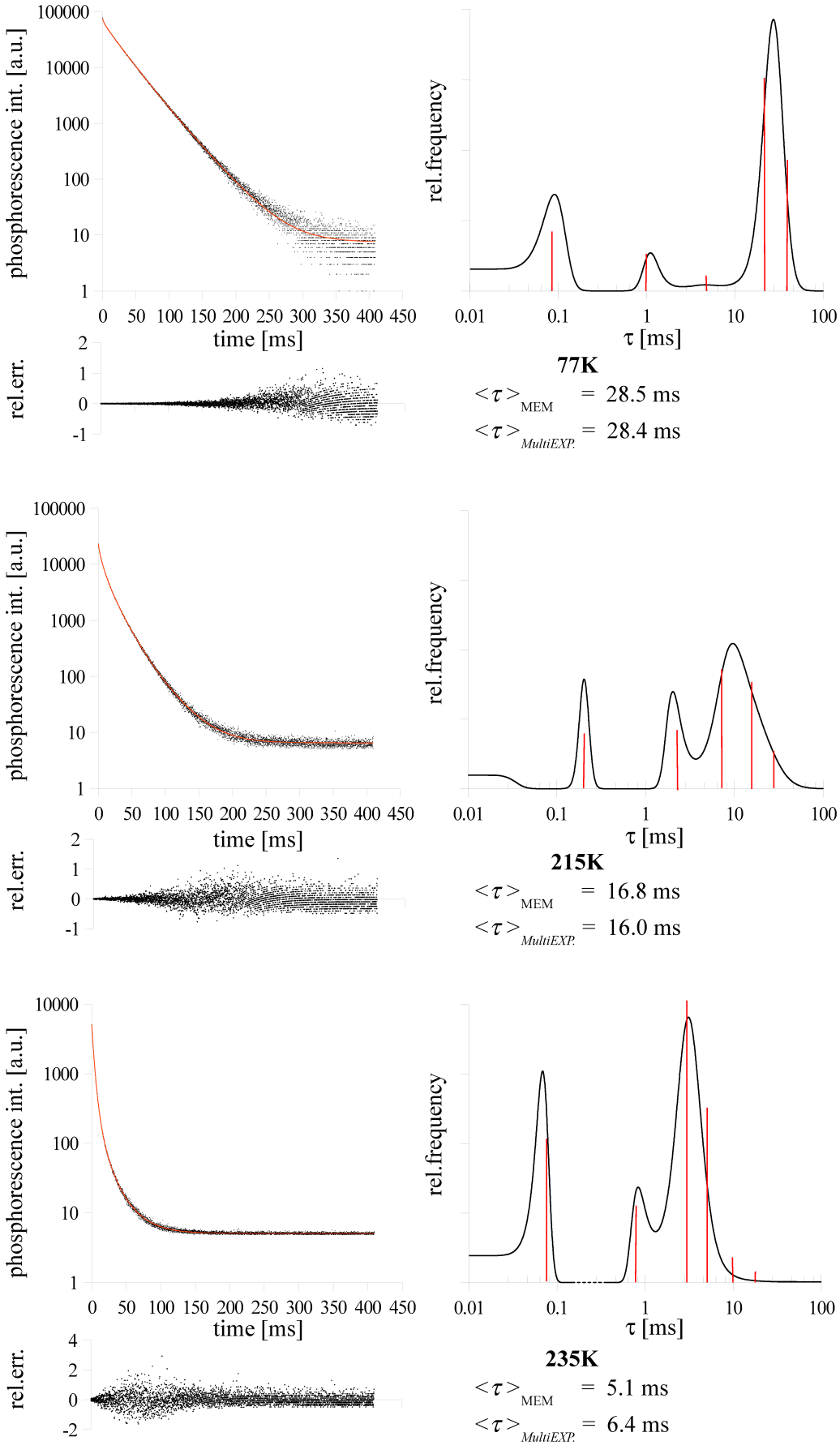

was too low, to obtain a reliable MEM inversion, however the discrete exponential fitting was still stable. Therefore, to maintain consistency we have used the <τ> based on the latter calculation for further analysis. The results of the multiple discrete-exponentials fitting is presented in Table 1. The shortest lifetime is marked "instrument response" since it is still influenced by the sampling method, but we decided to include it in the analysis. It can also be seen, that all lifetime components show a decrease with increasing temperature, and the maxima of the amplitudes shift to shorter lifetimes.

1.2.4 *Adjusting the temperature of the sample*

The adjustment of the initial low temperature of the sample and of the higher temperatures was done by using a Cryophysics M22 type closed cycle Helium refrigerator (Cryophysics SA, Geneva, Switzerland) and Lake Shore M330 temperature controller (Lake Shore Inc. Westerville, USA). The cryostat was also controlled by the integrated data-acquisition software. Using the cryostat, its cold finger of copper must be brought into and kept in good thermal contact also under vacuum conditions. The sample of 80 µl volume was contained in a quartz (UV fused silica) tube of 2.7 mm inner diameter, sealed gas-tight with a conical Teflon stopper. The techniques required for this study had to achieve the following conditions:

1. to bring the sample to 8 K fast enough to avoid phase separation and bulk crystallization of the aqueous sample
2. to maintain the thermal contact of sample and cold finger in a broad temperature range from 8 K up to 273 K.
3. reproducibility of the structural conditions in the sample.

These conditions had to be tested as thoroughly and rigorously as possible.

COOLING TO 8 K. Fast cooling was achieved by using a copper adapter attached to the cold finger prepared with an indium coated hole that contained the sample tube with a tight fit. Prior to the insertion of the sample, the copper housing was pre-cooled to 77 K by liquid nitrogen. The positioning of the sample in the cryostat was fast and the low temperature of the housing promoted fast cooling, moreover the sample could also

be pre-cooled to 77 K by liquid nitrogen prior to insertion into the housing as well. The data obtained by this method, however, showed that the good thermal contact between the sample tube and cold finger could not be *reliably* maintained at higher temperatures (> 200 K) due to the different thermal expansion of copper and quartz. This method was useful, however, as a control, since it provides an extremely rapid cooling, and it is also the same cooling method used routinely in biochemistry to safely store proteins avoiding structural damage or alteration.

MAINTAINING THE THERMAL CONTACT OF SAMPLE-TUBE AND COLD FINGER IN A BROAD TEMPERATURE RANGE. I have designed another copper adapter fixing the contact of the sample-tube and the cold finger. This sample holder consisted of two parts, an indium-coated part was fixed to the cold-finger of the cryostat, and a second part was mounted to it with screws. The quartz tube was inserted between these two parts, and springs were used to firmly press the tube to the indium coating. This design finally achieved the good thermal contact in the full temperature range of the experiments. In this method, however, the positioning of the sample in the cryostat required more time than to just put it in a hole, thus pre-cooling to 77 K made no sense[2]. The cold finger in this method was first pre-cooled to 240 K by the cryostat. At this temperature the tube was fixed, the cryostat closed, evacuated and continued cooling to 8 K by the highest cooling rate. Phosphorescence lifetime data were determined at various increasing temperatures starting from 8 K on samples cooled either by the "fast cooling" method (with pre-cooling to 77 K) or by the second method (with pre-cooling to 240 K) for comparison. The data showed identical temperature dependence in the two cases if the temperature stayed below approximately 230 K, as shown in Figure 3. It can be seen, that up to 200 K the two curves overlap perfectly, but above that moderate deviations start to appear. These deviations were sometimes larger than shown in Figure 3, due to the instability of the contact between the quartz tube and the copper sample holder. The perfect overlap up to 200 K, however, could always be reproduced. The absolute errors of the $<\tau>$ values are also shown in Figure 3, and it can be seen that the size of the error-bars are comparable to the symbol sizes. To avoid cluttering

2 Since the cryostat has to be open during the positioning of the sample, humidity in the air, and also other substances may freeze onto the surfaces at 77K. This "snow" later causes a failure in reaching temperatures below 30K, and also a severe degradation of the transparency of the cuvette. Therefore if the cryostat has to be open for more than a few seconds, it can not be cooled to 77K, but only to around 240K.

Figure 3: a: Comparison of the average lifetime (<τ>) values for Zn-HbA measured using the two different protocols: "fast cooling" (red) and extreme rapid cooling (grey). A cooling path (returning from 230 K) is shown in black. The error bars indicate the estimated absolute error of the <τ> values.
b: Comparison of the <τ> values of fast cooling protocol (red curve, and red axis) and deliberately slow cooling protocol (brown curve and axis). The error bars indicate the estimated absolute error of the <τ> values.

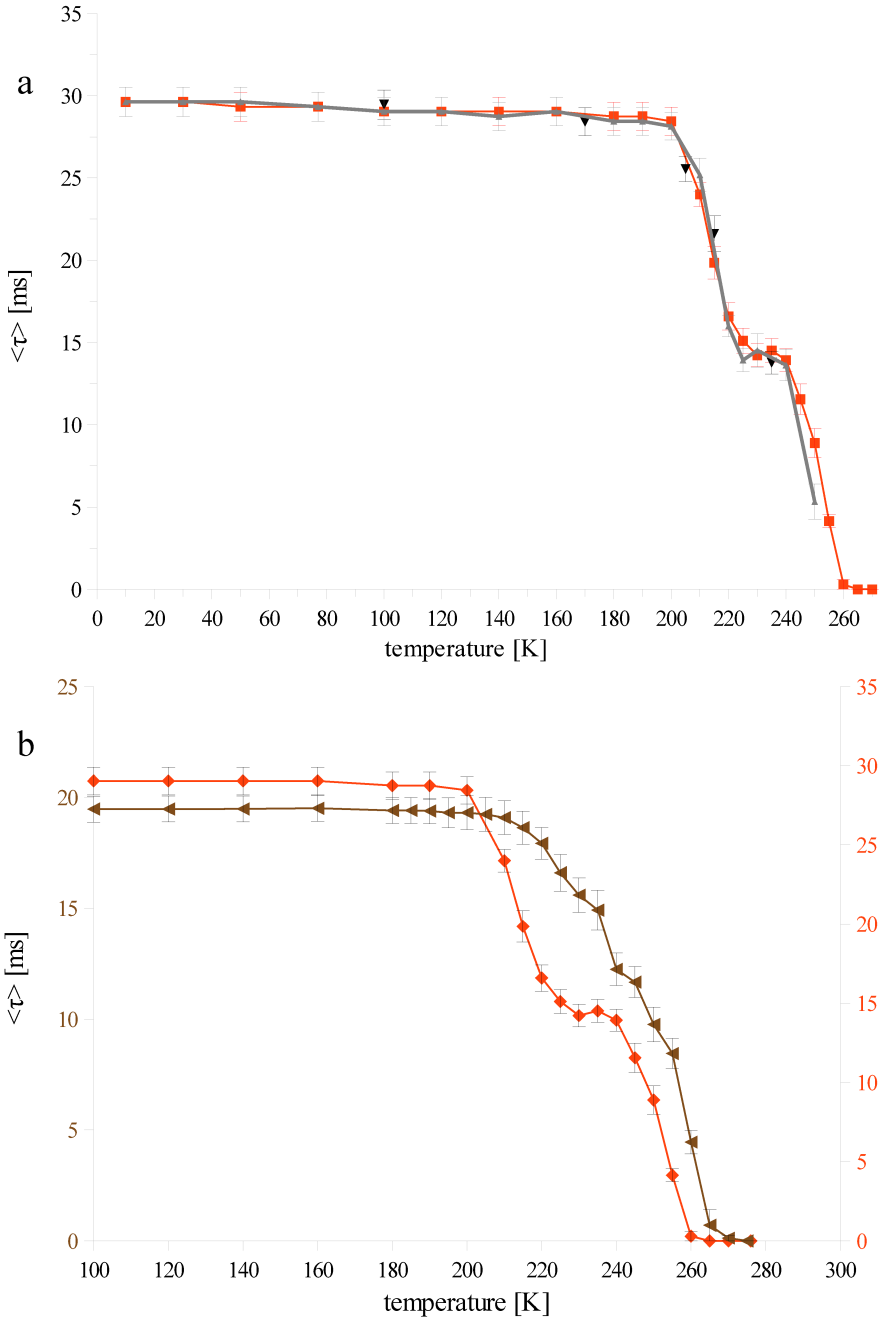

of the graphics, I will only show error-bars if the relative error is more than 5% (typically in the case of Trp data). Based on the results of this control study, we selected the second method for cooling protocol in the reported experiments and considered it a "fast cooling" technique. We found that the results obtained by this protocol were reliable within the whole temperature range of the studies.

1.2.5 *Further control experiments*

Since I was developing a new method, it was essential to make careful control experiments, to verify sample quality, repeatability of the experimental conditions, etc. The most important control experiments we designed are outlined below.

REPRODUCIBILITY-REVERSIBILITY. In the experiments we detected phosphorescence lifetime data under thermally activated quenching conditions. The quenched emission signal at higher temperatures (above 200 K) was very week and thus long data collection times were needed. A total measurement time covering the whole temperature range spanned over several days up to a week, sometimes even longer. Still, parallel experiments involving larger steps on the temperature scale[3] were performed and proved the reproducibility of the data. Besides reproducibility, we found also complete reversibility of the temperature effect (as can be seen in Figure 3, black points) on the phosphorescence lifetime if the temperature did not exceed 230 K. This experience showed that the selected time period of thermal equilibration at each temperature (45 min) was sufficient in our temperature dependence protocol. Since the structure of the cold sample is crucial in such an experiment we controlled the effect of the cooling rate also by using a *deliberately slow* cooling method. In this method the sample was gradually cooled from 270 K to 8 K during five hours. From 8 K, the sample was then heated stepwise to 270 K the same way as with the method used regularly, and phosphorescence decay curves were measured. Figure 3also shows the average phosphorescence lifetimes calculated from these decays (brown line). It is apparent, that besides the lifetime being altered, the two-step behavior is also missing in this curve: it starts to decline from the long lifetime plateau of the cryo-

Of course reversibility is only expected if there is no phase-transition (the second transition corresponds to the solid to liquid phase transition of the bulk solvent) in the bulk solvent. If yes, then an inverse-directional temperature scan by 5K steps would be very different than the fast-cooling, and therefore would not *yield the same results.*

3 At some randomly selected temperature points two or more decay curves were taken, and fitted individually. This provided a measure both for the relative error of the lifetime determination, and for the repeatability of the decay curves. It also served as a control to rule out possible photobleaching or sample degradation.

genic range at a higher temperature than in the case of the fast-cooled sample. We found that in the samples prepared in this slow cooling protocol, precipitates were also formed. This shows that if the cooling rate is not sufficiently fast, the structure of the solidified sample is most probably inhomogeneous, and this condition leads to partial denaturation.[4] This could partly arise from freeze-concentration, which can be significant if the cooling rate is slow. The striking difference of the this curve and the curves corresponding to the two other cooling methods shows that by a sufficiently rapid cooling method these effects can be avoided.

Above a certain cooling rate it seems that sample quality is not affected.

ABSORPTION SPECTROSCOPY It is accepted that the optical absorption spectrum of the heme in heme proteins is a sensitive monitor of deterioration or alteration of the protein structure around the heme. In Figure 4 we show the control of the cooling effect based on absorption spectroscopy. Spectra of Zn-HbA are shown at room temperature under three conditions: the spectrum before the experiment (black curve), the spectrum after the usual cooling-warming cycle protocol of our lifetime experiments (green curve), and the spectrum after the slow cooling protocol (red curve). It is seen and evident from the difference absorption curve (50x magn., grey dashed line) that the usual cooling protocol did not change the environment of the Zn-porphyrins in the protein. The slow cooling protocol caused protein precipitation, and also a distorted absorption spectrum after the cycle as shown in the figure. This further confirms that the fast cooling protocol, which was used can be considered "safe" for the protein.

CONTROL FOR THE PROTEIN CONCENTRATION POSSIBLY AFFECTED BY FREEZING It is well known, that by cooling a solution the effect of freeze-concentration may have an important role. In these experiments it is essential to estimate this effect as well. For this test we have chosen

4 If we consider our interpretation of the lifetime data (see in the discussion: quenching due to the activation of collective dynamics of the protein), then this lack of the first step is consistent with the denaturation of the protein: The deterioration of the protein structure probably eliminates the structural cavities of the intact structure, the places where oxygen can be trapped [136, 25]. If these cavities are lost, the oxygen content of the protein matrix would be largely reduced, and collisional quenching with oxygen molecules will only occur if they are allowed to enter the matrix from the bulk solvent. This becomes significant only when the mobility in the bulk phase is sufficiently increased, which corresponds to the second step in the temperature profile. Indeed, the quenching in the deteriorated sample starts to occur in this temperature range. This consideration further supports our interpretation of the lifetime data, that is, these oxygen molecules may play important role in the quenching effect under intact conditions.

Figure 4: Absorption spectra of Zn-HbA. Freshly thawn Zn-HbA is shown in black (identical to Figure 1) and after an experiment involving the fast cooling technique (green curve) together with the difference spectrum at 50x magnification (grey dotted line). Spectrum taken after the deliberately slow cooling technique is shown in red. Curves are shifted along the absorbance axis for clarity.

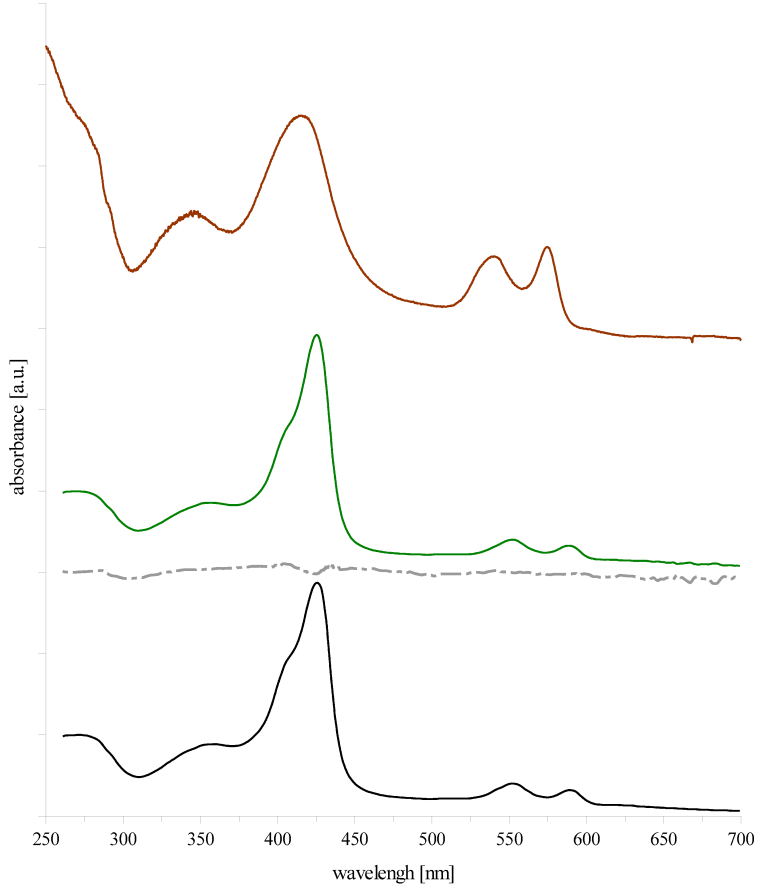

the recombinant Trp mutant forms of yeast Phosphoglycerate Kinase [95]. We performed the same thermally activated phosphorescence quenching studies on protein solutions of 20 µmolar concentration by the fast cooling protocol. It is known that this protein precipitates above 40 µmolar concentration, thus any significant freeze-concentration would case precipitation. We did not observe any precipitation after the thermal cycle. This shows, that while freeze-concentration can not be totally excluded, the protein is surely not concentrated by more than a factor of 2 during the cooling process.

THE OXYGEN CONTENT OF THE SAMPLES In most experiments, the protein solutions were saturated with the oxygen of air by carefully and slowly bubbling air into the samples for 5 minutes prior to the experiment. However, according to our hypothesis (as discussed later) the O_2 molecules embedded in the system play an important role in the observed effect. Therefore it was important to design a "negative control", i.e. significantly decrease the O_2 content of the samples. The goal was to achieve partial oxygen saturation without inducing structural changes in the protein. These partially oxygen-saturated Zn-HbA samples were prepared using a special procedure: As a first step, the temperature of the *unsealed* sample (in air-saturated form) was rapidly decreased to 250 K. At this temperature, the pressure was reduced to 10^{-2} mbar, and this low pressure was maintained for ½ hour. Subsequently, the sample was sealed and further cooled to 8 K. The measurements were then carried out starting from this state like those performed with oxygen-saturated samples. Possible denaturation or change in the redox state of the heme during experiments were controlled by recording the absorption spectrum. No significant changes were detected in the 270-700 nm wavelength range after the thermal cycles, or after partial deoxygenation.

1.3 RESULTS OF THE DYNAMICAL TRANSITION

In this section I will summarize the first group of results obtained by the new phosphorescence quenching method.

1.3.1 *Phosphorescence lifetime of Zn-PP in HbA as a function of temperature*

The intrinsic phosphorescence lifetime of Trp has been suggested for and successfully applied to monitoring the internal dynamics of proteins at

room temperature [45]. Since molecular oxygen is a very effective collisional quencher of phosphorescence [145], these studies have been always performed *in the absence of oxygen*. In this new method I have decided to - instead of deoxygenation - *saturate* the samples with air (oxygen) and register the phosphorescence lifetime in thermal equilibrium at various temperatures starting from 10 K up to 273 K, to detect the activation of quenching effects. The chromophores were Zn-PP, substituting the heme in the ß subunits of Zn-HbA and the tryptophans of the protein. In low temperature optical studies transparency is usually maintained by the addition of cryosolvent. I wanted to refrain from changing the physical parameters of the sample (protein and solvent), and therefore avoided this method. Figure 2 shows examples of phosphorescence decay data of Zn-PP in Zn-HbA on a semi-logarithmic plot at various temperatures, the decay curves arising from discrete fittings (see Equation (1)) and the error of the fittings. Although the signal was low due to significant light scattering, with sufficient data collection time, acceptable signal/noise levels could be reached even at higher temperatures, where quenching effects became activated. The discrete lifetime components, the corresponding amplitudes and the $<\tau>$ values are shown in Table 1. The phosphorescence decay data were also evaluated by MEM. The two approaches yielded results with remarkably good agreement, the ensemble average lifetime values calculated by Equation (4) in both cases agreed very well, and followed the same trend in function of temperature, as can be seen in Figure 2. Lifetime components of 100 μs range appeared in both methods of evaluation. Based on the analysis of the instrument response function and on the fact that the phosphorescence decay was recorded with 80 μs resolution, these were considered as experimental artifacts and were omitted from data evaluation. The next shortest component in both approaches was in the lifetime range of 0.9 ... 5 ms. This component - of low population at lower temperatures - seemed unaffected by the temperature, and remained almost the sole component close to 273 K. We attributed this signal to such chromophores which have trapped oxygen molecules in their immediate vicinity of specific configurations. These chromophores are expected to be significantly and strongly quenched, as the trapping of oxygen molecules in the vicinity acts as a seemingly high quencher concentration[31]:

$$\frac{\tau_0}{\tau} = 1 + K_{SV}[Q] = \frac{F_0}{F} \qquad K_{SV} = k_q \tau_0 \qquad k_q \sim D \tag{5}$$

In Equation (5), the Stern-Volmer equation, the lifetime (τ) and the emission intensity (F) of a given chromophore under different quenching con-

ditions is given (τ_0 and F_o are the values without quenching). *[Q]* is the quencher (mostly O_2) concentration, and K_{SV} is the dynamic quenching constant, which is proportional to - among several other factors - the diffusion coefficient (D) of the quencher in the matrix around the chromophore. It can be seen, that if either *[Q]*, or D change, both cause a change in τ. Trapping of O_2around the chromophore may act primarily as an increase in *[Q]*. The trapping may further cause modified diffusion (D) of the oxygen, which can then also contribute to further increase of the quenching efficiency by increasing the quenching rate (k_q). The Stern-Volmer equation is originally expressed for a single chromophore, but can be extended to population averages as well, then instead of a single τ we take the population average <τ> , and of course then all the other parameters are population averages as well (<K_{SV}> , <D> , etc.)

The normalized average lifetime of Zn-PP in Zn-HbA as a function of temperature is shown in Figure 3. The lifetime does not change significantly from 10 K up to about 180 K, thus in this temperature range there is no significant change in the quenching process as well. Above this temperature, additional quenching effects become activated and the lifetime drops in two markedly separated steps on the temperature scale. The first step begins at around 190 K and becomes complete at around 230 ... 235 K. The second step follows the first one and completely eliminates the signal[5]. Importantly, the phenomenon is fully reversible along a cooling path if reverted below 250 K – an example is also shown in the figure (a: black triangles).

Evidently, this stepwise behavior of the average lifetime vs. temperature graphs shows two transitions in the quenching process. Both transitions arise from the fact that dynamic quenching is changed, becoming more and more activated. The nature, origin of these dynamic activations are different in the two cases, however.

5 At least, the signal is not detectable with the instrument used in these experiments. Since the drop of the lifetime is accompanied by a drop in the intensity (F) as well, according to the Stern-Volmer equation, if the quenching constant is increased, after a certain point the signal level will drop below the detectable level. Of course theoretically this is not a complete elimination of the signal, but technically it is. Therefore on the graphs I will show a lifetime of 0 in these cases, to indicate this fact.

Table 2: <τ> data of the chromophores at 10K temperature.

sample	<τ> ± s.d. at 10K [ms]
Zn-PP in HbA	28.7 ± 0.6
Trp in HbA	212 ± 22
Trp in Mb	605 ± 44
Pd-CP in HEPES	2.14 ± 0.11
Zn-PP in DMSO, at 100 K	0.11 ± 0.05

1.3.2 *Mechanisms underlying the two steps of phosphorescence quenching of Zn-HbA*

To examine the contribution of the protein matrix to dynamic activation, the phosphorescence lifetime measurement was also performed on a chromophore sample *deprived of the protein*. Because the solubility of Zn-PP is extremely poor in aqueous buffer, we measured the emission of Pd-coproporphyrin (Pd-CP) instead under buffer conditions identical with those of the protein samples. Pd-CP is a porphyrin very similar to Zn-PP, only a few atoms differ in the two structures. But Pd-CP's phosphorescence emission is much stronger, partly due to the well-known heavy-atom effect [54, 7][6]. Based on literature data from NMR studies on the thermal activation of the mobility of protons coordinated to buffer components in aqueous solutions[138], referring to the same temperature range as in our experiments (discussed below), it can be supposed that the structural coupling of the Zn- or Pd-porphyrin derivatives to the solvent matrix cannot be significantly different. Data starting from 120 K are shown in Figure 5 (blue curve). For comparison, the data for Zn-HbA are also included (red curve), all data are normalized, and error bars are omitted for clarity. The data were fitted with two sigmoidal functions based on a simple thermodynamic model (see later) in the case of the first transition, and a simple sigmoidal curve for the second transition. To better characterize the two steps in the quenching effect, the negative derivative functions of the fitted curves are also presented. The data are normalized for better comparison, the absolute <τ> values are listed in Table 2.

From all figures, where the error bar sizes are comparable to the symbol size, the error bars are omitted for clarity.

In the case of Pd-CP, in the low temperature range, a gradual and slight quenching effect appears to be activated. Then, well above the tempera-

6 It is known that when heavy atoms (high atom number) are included in aromatic systems, the phosphorescence efficiency generally greatly increases.

Figure 5: Normalized average phosphorescence lifetime values of Zn-HbA (red curve) and Pd-CP (blue curve). The negative derivative functions are also shown. The lines are fitted functions to the original data shown with symbols. (Our own model function to the first transition and a sigmoid curve to the second)

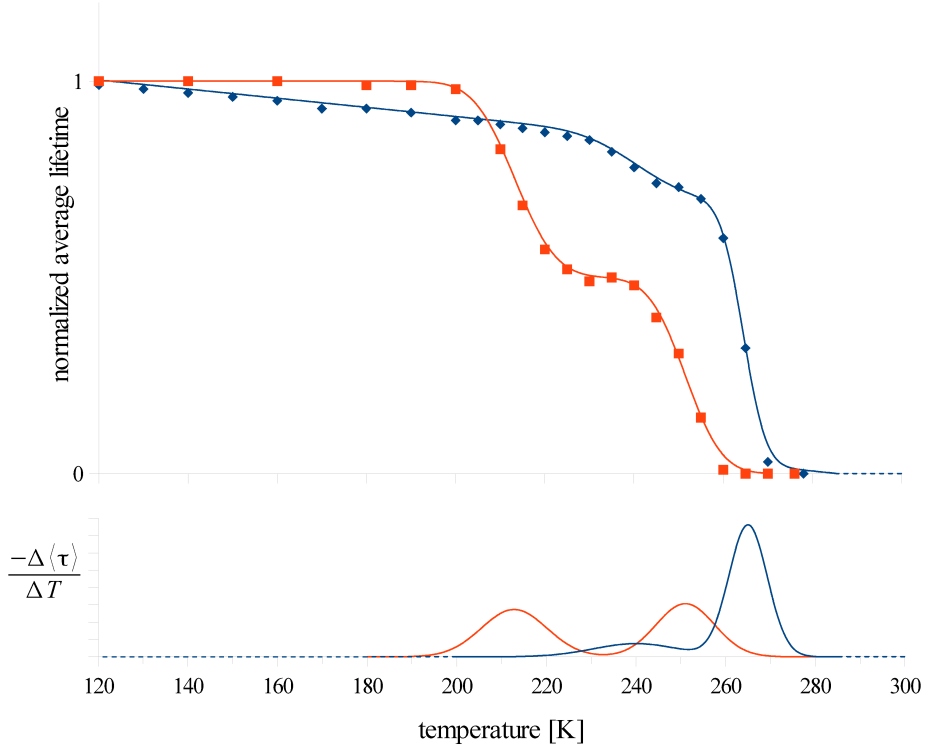

Figure 6: Normalized average lifetime data of Zn-PP in DMSO (green line and symbols). For comparison Zn-HbA data is also shown (red curve).

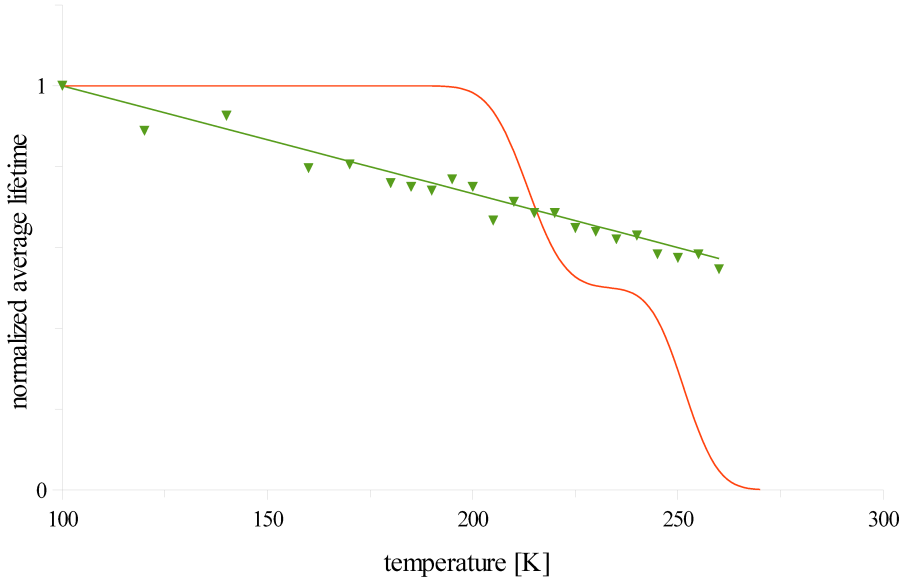

ture range of the first quenching step in Zn-HbA, a slight step is detected at around 240 K. At approximately 265 K, near the melting point of ice, almost complete quenching occurs. The slight quenching step at around 240 K is comparable with results of proton NMR relaxation experiments in the 500 µs time range, and is attributed to the activation of hydrogen motions in structured water regions around the components of aqueous buffers [138, 137]. Thus we identify this step with the mobilization of structured water around the porphyrin molecules and the buffer components. This mobilization can be accounted for the increase in the diffusion coefficient of quenchers, and thus for the decrease in lifetime. The quenching experiment was also performed on Zn-PP dissolved in DMSO, the result is strikingly different, as shown in Figure 6. This solvent was selected because it *does not have any phase transition* in the studied temperature range. Although the intrinsic lifetime was strongly quenched by the sulfur of DMSO (as can be seen in the extremely short lifetime value in Table 2), the signal was measurable up to 274 K. A gradual quenching effect without any steps was observed corresponding to a matrix without a phase transition in the studied range. This also shows, that without the protein matrix, the low-temperature (first) step observed in the quenching experiment with Zn-HbA is absent. Comparison with NMR data suggests that when the dynamics of the matrix (protons of the

Figure 7: Normalized average lifetime data of partly deoxygenated Zn-HbA (orange curve, triangles). For comparison the curves of normal Zn-HbA (red) and Pd-CP (blue) are also shown.

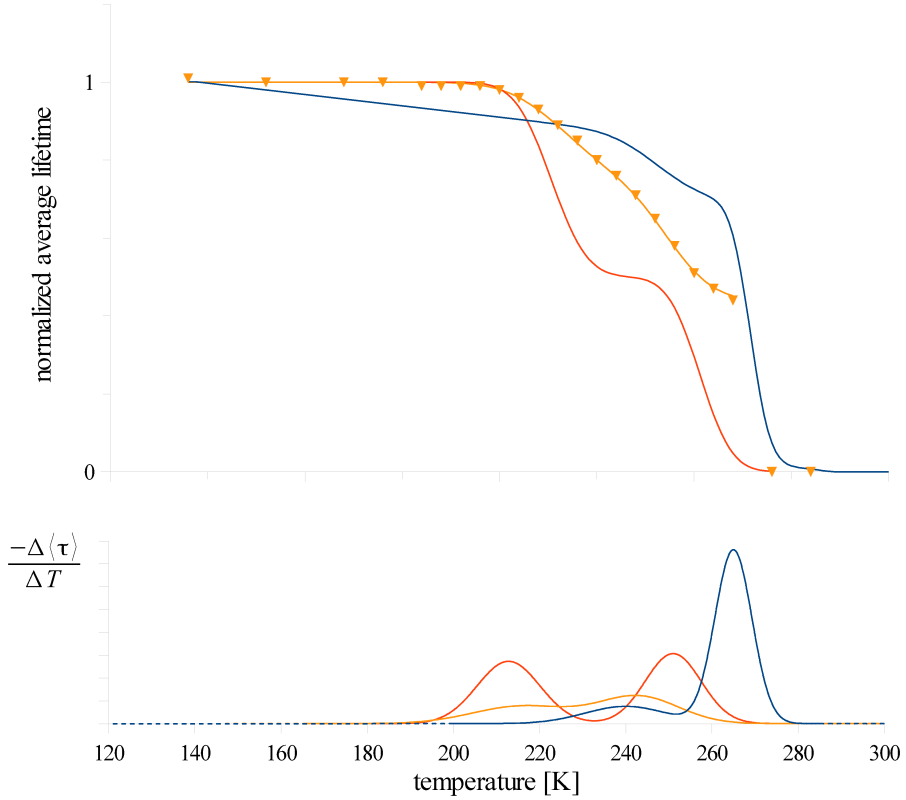

hydration layer) coordinated to a molecule dissolved in aqueous solution (i.e. one chromophore) becomes activated, a phosphorescence quenching effect may be observed. Therefore we conclude that the low-temperature step in the quenching experiment on Zn-HbA should be attributed to the activation of motions in the protein matrix around the chromophore. The NMR data also suggest that the second step in the HbA data, which overlaps with the transitions seen in the data of Pd-CP in HEPES correlates with the activation of the hydration layer around the protein.

1.3.2.1 *The role of collisions with O_2 molecules in the quenching effect.*

The role of collisions with O_2 molecules in the quenching effect can be studied by comparing the data obtained on the fully air-saturated sample with those of the partially deoxygenated sample in the case of Zn-HbA, as shown in Figure 7. The comparison indicates that partial depletion al-

most completely eliminates the low-temperature quenching step[7], while the second step remains detectable. It has to be noted however, that the very small remains of the first step still occur at the same temperature as in the O_2-rich samples. It is also important, that in this sample, *total quenching occurs only around the thawing temperature of ice*. These observations show not only that the low-temperature step detected in oxygen saturated protein samples is related to activated motions in the protein, but also that these motions are permissive of oxygen diffusion. In both the protein and the aqueous matrix, the diffusion of oxygen requires the activation of large-scale motions[39, 157]. *The results indicate that the activation temperature of such motions of the protein (possibly forming a unified dynamic unit with its hydration layer) and of the matrix are clearly distinguishable, and that of the protein is lower.*

1.3.2.2 *Activation of millisecond motions in the protein and in the solvent may not be separated in the presence of glycerol.*

It has been suggested that large scale motions - e.g. those allowing for a "hopping"-like movement of small molecules in the surrounding matrix, or allowing the uptake or release of such ligands – are "slaved" to two kinds of fluctuations around the protein matrix: to the α-fluctuations in the solvent environment through long-range dipole-dipole interactions, while their internal local vibrations follow the behavior of the β-fluctuations of their hydration shell[35]. The experimental techniques underlying these models often involved optical spectroscopy at low temperature using the standard method of adding cryosolvent (glycerol) in quite high percentages (up to even 90%) to the aqueous buffer of the protein solution to avoid light scattering, to extend the measurable range of kinetic parameters, and to avoid the possible structural effects of crystalline ice formation during cooling. To test the effect of cryosolvents, the phosphorescence quenching experiment was repeated on Zn-HbA in the presence of 60% (v/v) glycerol as shown in Figure 8. Glycerol changes both quenching steps, shifting their characteristic temperature ranges closer to each other. The increase in the temperature of the first step (from 213 K to 220 K) we attribute to the effect of increased viscosity on protein dynamics [3]. The lowered temperature of the second step (to 240 K) is comparable to the phase transition point of concentrated glycerol/water mixtures (-34.7 °C $\approx$ 238 K for 60% (w/w) glycerol content). The two-step fea-

7 The derivative curves are normalized to their area under the curve. Without this normalization the derivative curve of the partially deoxygenated sample would not be seen in the common figure.

Figure 8: Normalized average lifetime of Zn-HbA in 60% v/v glycerol mixture (black symbols and curves). For comparison Zn-HbA under the usual conditions is also shown with red.

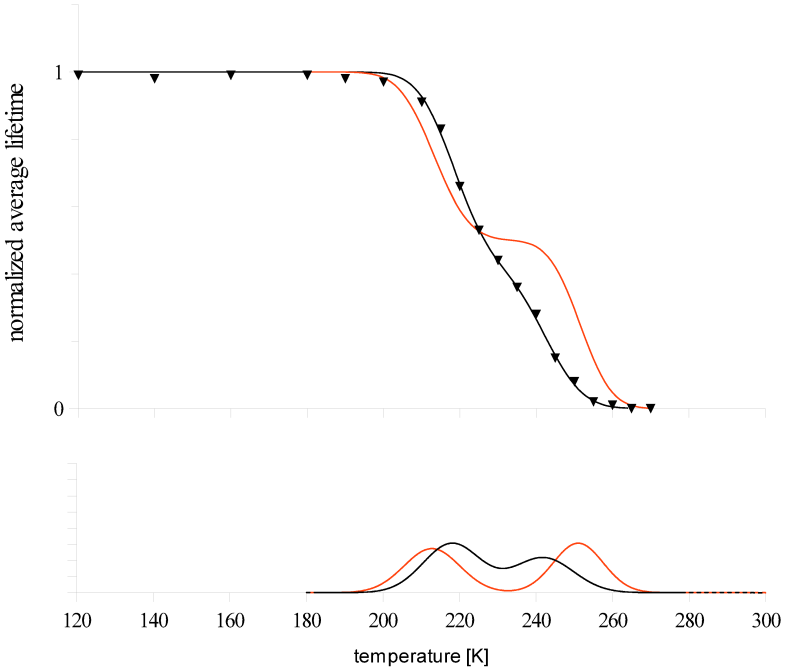

ture of the quenching effect becomes observable only in the derivative representation, whereas in the lifetime vs. temperature function, the two steps fuse into a single step, easily attributable to the activation of motions in the solvent, which is of glassy nature in the case of high glycerol content. In such a case the slaving of large-scale protein dynamics to α-fluctuations of the solvent above Tg[34] [8] (now ~ 210 K) may be a good approximation, since the Tg value of the protein and that of the glassy solvent almost overlap with each other. *The relation of protein dynamics and solvent dynamics remains hidden under these conditions.* There is another important outcome of the glycerol effect: the shift of the activation temperature of protein dynamics directly proves that it is sensitive to the structure and the dynamic nature of its immediate environment. The ability of high glycerol concentrations (>65%) to cause even protein denaturation (as can be observed in several cases, although not always,

8 Tg is the glass-transition temperature. Should the observed effect be a glass-transition similar to the α- and β-fluctuations described in the cited articles, then Tg in our case should be the transition temperature, approximately 210 K.

and some proteins are less sensitive than others) is another point which should not be overlooked.

1.3.2.3 *The same protein dynamics is observed either by porphyrin or by tryptophan phosphorescence.*

To prove that the observed dynamics monitored by Zn-PP in the ß subunits is not the property of the heme environment, but is characteristic of the whole protein, I have measured the dynamics activation also based on the Trp phosphorescence of Zn-HbA. The protein contains six Trp residues. The Trp lifetimes were relatively short[80] even at low temperatures (see Table 2) due to self-quenching and energy transfer to the hemes[117], but could be determined with acceptable precision. The Trp

Figure 9: Normalized average lifetime of the Trp residues in Zn-HbA (blue curve and symbols). The error is also shown, since it is larger than 5%. For comparison the data of Zn-PP in Zn-HbA is also shown (red curves).

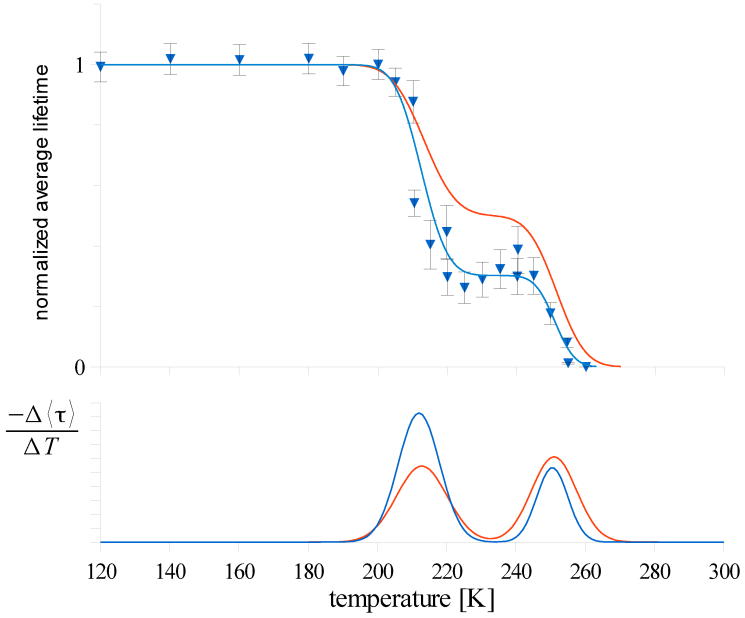

lifetime data compared with the data of Zn-PP are shown in Figure 9. both first quenching steps are very similar in the two kinds of monitoring, indicating that the effect reflects the global behavior of the Zn-HbA matrix. *The perfect overlap in the temperature scale proves, that the dynamical activation of the protein matrix is not a local phenomenon around the chromophores, but instead a dynamical transition of the whole protein molecule.* The differences in the step sizes are caused by differences in the oxygen diffusion

Figure 10: Normalized average lifetime of Myoglobin (dark green line and symbols). For comparison the Trp data of Zn-HbA is also shown. For clarity only the error bars of Mb data are shown on the graph.

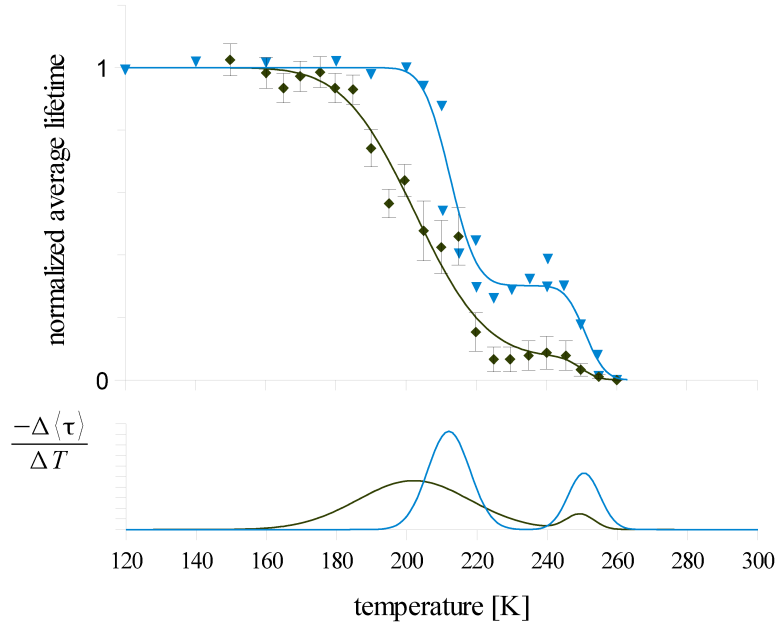

pathways in the protein matrix to the site of the different chromophores (heme or Trp), and differences in the quenching efficiency as well.

1.3.2.4 *The first quenching step is specific for the protein.*

The use of Trp phosphorescence allowed us to compare the phosphorescence quenching effect in two different proteins. We selected human Mb having two Trp-s for comparison, dissolved in the same buffer as HbA. The first phase of lifetime decrease is significantly different in the two distinct proteins, whereas the second quenching step becomes activated at nearly identical temperatures for both proteins as can be seen in Figure 10. *Thus, the first step in the thermal activation of quenching is characteristic and specific for the global millisecond dynamics of the protein under study.*

1.4 A SIMPLE MODEL

Before further analyzing the data, it is important to summarize briefly the results presented so far. I will also present the simple thermodynamic model, which can be used to describe the observed effect.

From the results section presented before, three conclusions can be derived:

1. The observed transition is reproducible if the cooling is sufficiently fast

2. *The transition can only be observed reliably if there is no glass-forming substance (such as glycerol or similar anti-freeze agents) present in the system.*

3. The transition is specific for the protein, and also global for a given protein molecule (i.e. it does not depend significantly on the nature, and position of the chromophore probe used to monitor the transition). As a working hypotheses it can be assumed, that the oxygen molecules present in the system are mainly responsible for the quenching of phosphorescence, and they act as "test-molecules": If there is sufficient dynamical activation in the protein molecule, then the diffusion becomes greatly enhanced, which leads to an increase of the quenching efficiency, and a corresponding drop in the average lifetime.

Several experimental and theoretical works deal with the so called "glass-transition", the thermal activation of proteins at cryogenic temperatures. Several experimental techniques have been applied to study the phenomenon, mostly optical absorption, neutron scattering and Mössbauer spectroscopy[108, 97, 42, 41, 40, 39, 35, 34, 27, 28]. Recently NMR has also been used to monitor the protons of water molecules[138, 137, 78]. I have already cited some of the most recent relevant articles, and it is important to decide, if the observed dynamical transition is of the same nature as described in these articles, or something different. There is a specific feature of the glass-transition, which can be used for additional comparison beyond the difference between the samples containing none and 60% glycerol. The glass-transition as measured with these techniques is usually a relatively broad transition on the temperature scale, as can be seen, e.g., in Figure. 4 of [35], and is usually represented in an Arrhenius-type of diagram. In Figure 11 an overlay is shown, with the quenching rate constants ($k_q = 1/\langle\tau\rangle - k_o$) of Zn-HbA (red) and the Zn-PP/DMSO

Figure 11: Arrhenius plot of the Zn-HbA data (red) and Zn-PP/DMSO data (green) overlay-ed with Fig.4 from [35]. BA,DA and "exit" represent various rate constants measured in Mb, while α and β represent the two types of fluctuations.

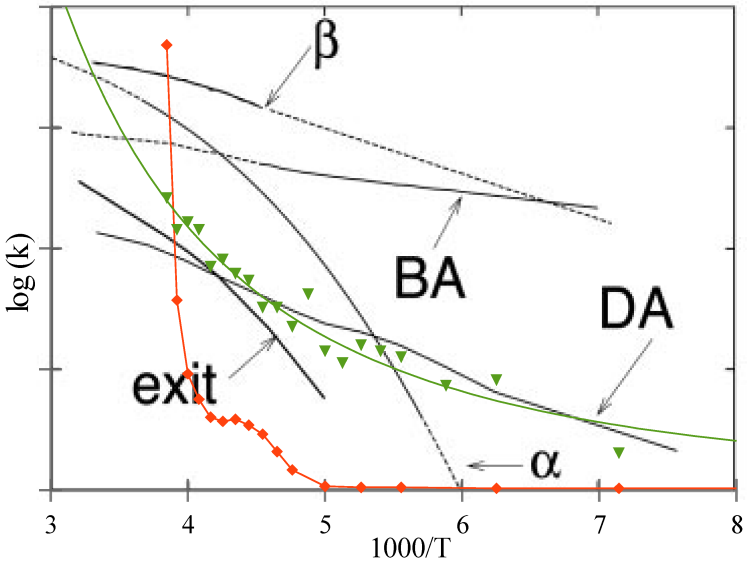

(green). It can be seen that while the Zn-PP/DMSO data-set somewhat resembles the glass-transition data of Figure 4. of [35], the Zn-HbA data is strikingly different. It is important to note, that the timescales obviously play a major role in the observed effects, and with the experimental method of phosphorescence quenching I am only monitoring a specific time-window of a few hundreds of microseconds up to seconds. Other techniques such as neutron-scattering and Mössbauer spectroscopy are sensitive to processes of a totally different time-scale. This may also lead to the very different nature of the observations. While it can not be totally excluded that the transition of the protein is related to the glass-transition phenomenon (since a similar transition temperature of approximately 210 K was observed in some cases in Mb and hemoglobin [81, 97]) observed previously, the very different behavior on the temperature scale may justify the effort of building a simple model which can account for the observed effect.

First, I will present the simplest possible qualitative description, and then a quantitative model will be presented.

1.4.1 *Qualitative model of the thermal activation of millisecond protein dynamics.*

Proton NMR studies in the ~500 μs time-window of motions in bovine serum albumin (BSA) in a temperature range similar to the one investigated in this study yielded data for the proportion of mobilized water protons in the hydration layer around the protein, in water regions coordinated to the buffer components and in icy structures of the buffer, selectively[138, 137]. The cooling and warming protocol in these studies was very similar to our method. No mobile water molecules were observed below 220 K, the mobilization of the hydration layer around BSA became activated above this temperature, detected as an abrupt increase in the number of mobile protons. When the temperature was further increased, mobilization of the structured water around the buffer components was first observed as a separate phenomenon on the temperature scale, and then upon warming further, the melting of the bulk icy matrix followed. These data provide strong support for the idea that the activation of large-scale protein dynamics seen in our experiments is coupled to the activation of dynamics in its surrounding hydration layer. A very simple qualitative model of the thermal activation of millisecond range of motions in our protein samples is outlined in Figure 12. Oxygen molecules are shown as red dots, their diffusion ability is represented with double-ended arrows. The protein is shown as a simple pictogram, the chromophores are shown as blue squares. As a simplification not all of the two Zn-PP-s and six Trp-s are shown, but only four general "chromophores", to emphasize that the model is not dependent either on the number, or on the position of the chromophores inside the protein under study. The boundary of the protein is marked with a thick line, this also represents the protein - coordinated water molecules of the hydration shell. "State 1" in this model is the frozen state, in which molecular oxygen [9] is approximately equally "immobile" (thus having a negligible diffusion coefficient) in the bulk solvent, in the hydration layer of the protein and inside the protein matrix. It can be hypothesized that during the first, low-temperature step of phosphorescence quenching, motions within the protein (and maybe also in its closely coupled boundary of the hydration shell) become activated. This leads to a dynamic state of increased, but still limited oxygen diffusion in the coupled system ("State 2"). When the temperature is further elevated, oxygen diffusion becomes activated also

9 Or any other diffusable quencher, I will only represent oxygen later in the discussion, but it can be applied to any other quencher as well.

Figure 12: Qualitative model of the dynamic transition. Zn-HbA data are shown in red, the pictograms represent three different states as discussed in 1.4.1.

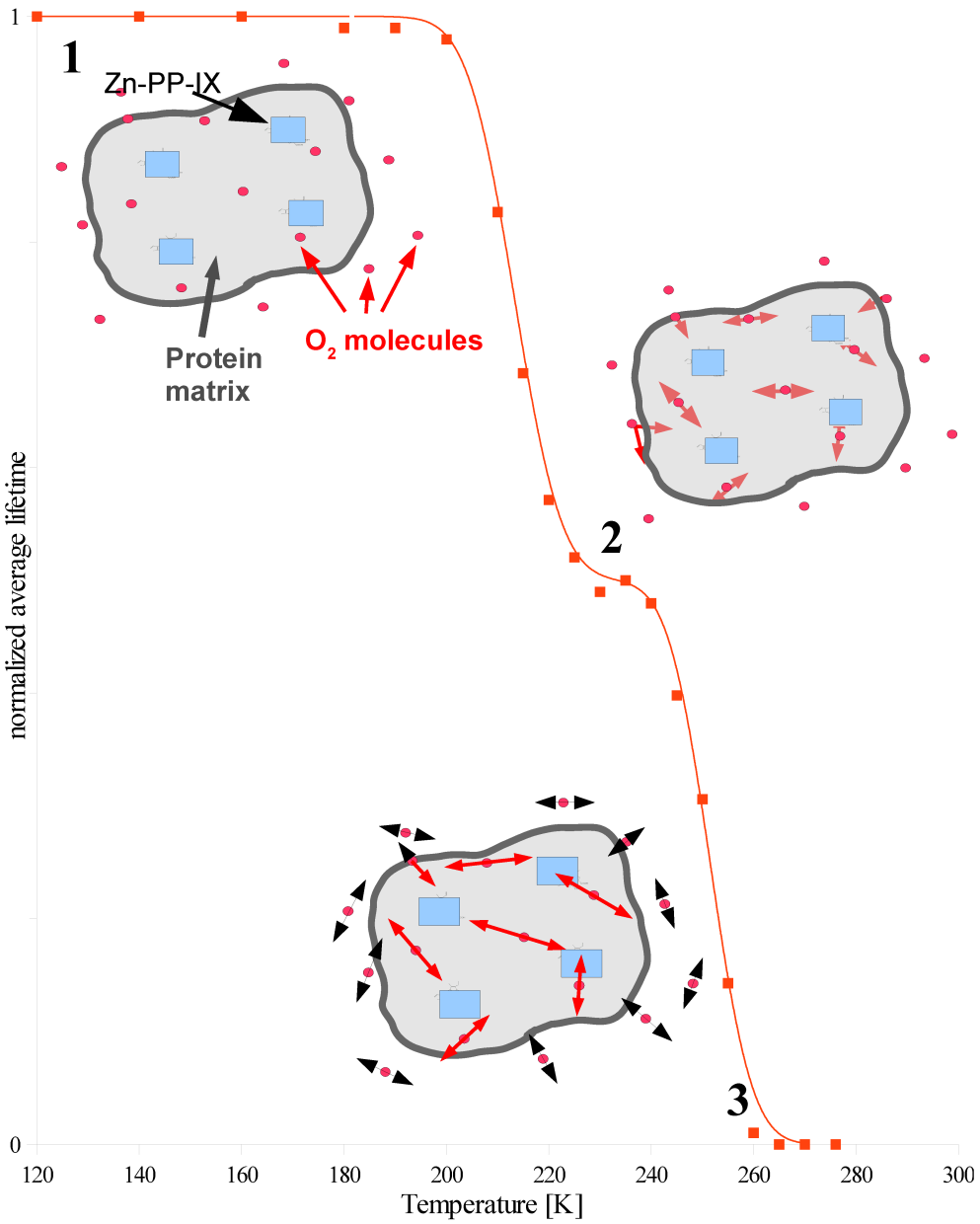

in the bulk matrix, causing a further increase in the quenching efficiency through an increase of diffusion-coefficient of the quencher, allowed by the increased dynamics of the bulk solvent matrix, which results in a final reduction of the phosphorescence lifetime below the detection limit of our instrumentation ("State 3"). This latter activation of the matrix is surely related to the glass-transition, while the activation of the hydration shell may be influenced by both the protein, and the bulk solvent.
The second transition is very complex, involving a coupling of the hydration shell to the bulk solvent, and also the glass-transition. It is also not specific for the protein, as can be seen in the comparison of Mb and Zn-HbA in Figure 10. It is more interesting to focus on the first transition, which seems to be specific for the protein, and according to the proposed simple model only involves the protein itself[10]. Therefore the presented qualitative model will only focus on this first transition from "State 1" to "State 2" in Figure 12.

1.4.2 *Quantitative model of the first transition*

The presented simple thermodynamic model ignores the details of molecular mechanisms and assumes that "State 2" corresponds to activated collective dynamics in the protein. It is considered as a *single particle* in the sample from a thermodynamic point of view. At a certain temperature the individual particles fluctuate between energy states and the probability to find a single particle in its m^{th} micro-state with E_m energy is P_m. We suppose that P_m is proportional to the respective Boltzmann factor:

"protein" is the protein molecule + the tightly coordinated water molecules

$$P_m \sim e^{-\frac{E_m}{kT}} \tag{6}$$

10 Of course the hydration shell can not be neglected, and it may induce a coupling to the solvent also during this first phase. However, as apparent from the data, this additional effect does not modify the transition significantly, and as a first approximation it's influence can be neglected. Therefore I will assume from now on, that the first transition is specific, and confined to the protein molecule. However the term "protein" must be extended: water molecules being tightly coordinated to the surface of the molecule have to be included to the "molecule", since their dynamics is essentially "tied" to the dynamics of the relatively large protein to which they are coordinated. These additional water molecules may significantly influence the transition in the case of very small proteins, but the systems included in this thesis are all relatively large, and thus this modification can be assumed to be very small relative to the effects arising from the protein molecule itself.

We suppose that the particles are identical, independent, and in the frozen state of the environment (during the first transition) they are distinguishable. This assumption is supported by the fact that during the rapid cooling process each protein is "trapped" in an individual conformational state. Thus on the basis of ergodicity, the distribution of energy, *P(E)*, is given as:

$$P(E) \sim \Omega(E) \cdot e^{-\frac{E}{kT}} = e^{-\frac{E - TS}{kT}} \tag{7}$$

where $\Omega(E)$ is the number of micro-states which have E energy. Since the entropy is given as $S = k\ ln\Omega$, where k is the Boltzmann constant, one may further develop the equation into the final form of Equation (7). In equilibrium states this formula can give the respective equilibrium values of the physical quantities. In the model we suppose two energy states: "1": frozen with a long average lifetime, τ_o (= intrinsic lifetime), "2": (higher energy state) with activated quenching that leads to an average lifetime τ_d, decreased by a factor of K_d where $\tau_d = \tau_o / K_d$. If the number of molecules in the two states "1" and "2" are N_o and N_d, respectively, the average lifetime of the ensemble can be calculated in this model as:

$$< \tau >= \frac{\sum_{i=1}^{n} N_i \tau_i}{\sum_{i=1}^{n} N_i} = \frac{N_0 \tau_0 + N_d \tau_d}{N_0 + N_d} = n_0 \tau_0 + n_d \tau_d \tag{8}$$

where n_o and n_d are the relative number of particles without and with activated dynamics, respectively. It is important to note, that Equation (8) expresses the same average lifetime as Equation (4). For the comparison of data obtained on different chromophores and proteins it was useful to normalize the average lifetime data:

$$\frac{< \tau >}{\tau_0} = n_0 + n_d \frac{\tau_d}{\tau_0} = n_0 + \frac{n_d}{K_d} \tag{9}$$

Since every measurement was carried out in thermal equilibrium[11], we may use Equation (7) to determine the expected value of the relative number of particles (n) in a given state. Thus it follows:

$$\frac{n_d}{n_0} = e^{-\frac{\Delta E + T\Delta S}{RT}} \tag{10}$$

Here ΔE and ΔS are the (molar) energy and entropy differences between the frozen and thermally activated states of the particle. Taking into account that the number of particles is constant ($n_o + n_d = 1$), and substituting the expressions for n_o and n_d into Equation (9), we obtain

$$\left(\frac{<\tau>}{\tau_0}\right)(T) = \frac{1 + \frac{1}{K_d} \cdot e^{-\frac{\Delta E + T\Delta S}{RT}}}{1 + e^{-\frac{\Delta E + T\Delta S}{RT}}} \tag{11}$$

which yields the temperature dependence of the relative average lifetime, which can be directly fitted to the average lifetime data obtained from the measurements by Equation (4). The parameters of the fitted curves derived from the derivative representation (transition midpoint temperature (T_{MP}) and maximum slope value (Sl_{MP}) are obtained as:

$$T_{MP} = \frac{\Delta E}{\Delta S} \qquad Sl_{MP} = \frac{\Delta S}{4RT_{MP}}\left(\frac{1}{K_d} - 1\right) \tag{12}$$

In the figures the solid lines fitted to the data points correspond to Equation (11) in the case of the first step. The model clearly fits the experimental data very well, and the fitting thus yields the thermodynamic parameters of the function. The thermodynamic parameters concerning the first step are shown in Table 3.

1.4.3 *Analysis of the thermodynamic parameters*

The magnitude of the energy difference in Table 3 is comparable to the energy of a few hydrogen bonds. The entropy change is comparable to the denaturation entropy of about 2 - 5 amino acid residues[69]. These

11 At least close enough to thermal equilibrium so, that non-equilibrium processes should not influence the results significantly.

Table 3: Thermodynamic parameters of fitting to the first transition step: ΔE (energy change), ΔS (entropy change), T_{MP} (midpoint temperature), and K_d (= τ_o / τ_d) , ± s.d.

sample	ΔE [kJ/mol]	ΔS J/mol·K	T_{MP} [K]	K_d
Zn-HbA (Zn-PP)	113.4 ± 4.4	532 ± 22	213.1 ± 0.3	2.0 ± 0.1
Zn-HbA (Trp)	93.0 ± 13.8	435 ± 76	213.9 ± 5.6	4.0 ± 0.7
Mb (Trp)	36.2 ± 6.0	182 ± 37	198.7 ± 4.9	10.6 ± 1.7

literature support the effort of building up a view of the thermally activated quenching mechanism. Collisions with O_2 molecules may involve an average "hop-distance" (mean free path) of a length of a few (2 - 5) residues. Thus, collisional quenching is made possible by a limited - and likely anisotropic - diffusion process inside the protein similarly to ligand diffusion in Mb (see e.g. [21, 25, 136]), by "hopping" through transiently opening spaces, which are created transiently by the global dynamics of the structure. The very simple two-state thermodynamic model fits the experimental data and yields realistic parameters[12].

There is significant difference in the thermal activation of quenching between Zn-HbA and Mb as seen in Figure 10, also manifested in the thermodynamic parameters. Apparently, the conditions in Mb significantly increase the probability of activated quenching based both on the energy- and entropy-difference values (they are smaller than in Zn-HbA). In addition, the significantly lower activation temperature (T_{MP}) in Mb implies that in this case the energy-difference is relatively less significant than the entropy-difference between the activated and non-activated states as can be seen from Equation (12). The increased K_d points to a greater efficiency of quenching in Mb. It is difficult to establish a detailed molecular basis that explains the difference in the activation of millisecond dynamics between Mb and Zn-HbA. The experiment itself is only capable of monitoring quenching, but can not distinguish between different quenching events. The thermodynamic model that yields the compared

12 That the model yields realistic parameters does not *prove* that is "true", but it does indicate, that it *might* even be true as well. We have to remember the message of the citation from the Bible: "we see through a mirror" during all our lives, and this is especially true in science. Every result, law is considered as a "working hypothesis" as long nothing contradicts it. Then, if a contradicting experimental result is found and confirmed, the hypothesis has to be re-thought. What I am presenting here is a working hypothesis, which is at least self-consistent, and also consistent with the experimental data.

parameters describes both cases as ensembles of independently fluctuating molecules, where each protein is treated as a "particle", as described. Thus monomeric Mb molecules are compared to tetrameric Zn-HbA. A first look at the enormous number of data concerning the cooperative behavior of hemoglobin subunits in oxygen binding would suggest that they should evidently form a dynamically coupled unit. A closer look, however, yields very little direct information on the details of this dynamic coupling, e.g. on how the presence of the interfaces between the subunits would influence the overall dynamics, whether there is a size effect involved, etc. Reported results of molecular dynamics simulation are based on techniques that address different questions[154]. Dissociation studies suggest that the separation of the tetramer into dimers requires less energy than dissociation into monomers[105], thus this contact seems to be looser, which may also affect the strength of dimer-dimer dynamic coupling. Although studies by the Ackers group on the cooperative behavior of HbA formed of asymmetrically mutated dimers lead to the conclusion that the dimers behave "autonomously" in the cooperative oxygen binding effect[1], one would expect more evidence for declaring the dimers to be dynamically uncoupled units in HbA. If this were the case, however, then the dynamic difference between Mb and HbA could be related to the very interesting dynamic role of the hydration layer in the case of Mb versus that of the subunit interface partially bordering HbA dimers.

Nevertheless, it can be stated, that possibly relevant thermodynamic parameters can be calculated from the experimental data with the help of the simple thermodynamic model presented in this section. The next interesting question is, if these parameters correlate with biological function, if these activation - energy and - entropy values have biological significance. This question can be at least partly answered, if one compares the dynamical transition of Zn-HbA under conditions reflecting various different states of its biological function.

2

BIOLOGICAL SIGNIFICANCE

2.1 ALLOSTERIC EFFECTORS

Hemoglobin is a tetrameric protein, which plays a vital role in the transport of oxygen. It consists of two dimers of and subunits that reversibly bind and release oxygen[104]. A simple view is presented in Figure 13, some important structural elements are highlighted in the figure. The description of this cooperative phenomenon has been most frequently derived from the (MWC) two-state allosteric model[89] that attributes cooperativity to a rapid equilibrium between two conformations of distinct oxygen affinity of the whole tetramer. These distinct states are the fully unliganded T-state and the fully ligated R-state. Szabo and Karplus[131] modified the two-state model incorporating the stereo-chemical mechanism suggested by Perutz[101] for the T $\rightarrow$ R switch, and introduced ligation-induced tertiary changes within the T-state. In this extended model (MWC-SK), it was proposed that cooperativity still works through a ligation-induced shift in the equilibrium of states T and R, but the model attributed importance in the conformational switch to certain changes at the inter- and intra-subunit interfaces. Upon ligation in the T-state, the network of inter-subunit interactions become perturbed, some (e.g. salt bridges) become broken up to release the characteristic strain of the T-state. The mechanism involves a rotation of one dimer with respect to the other[8], thus reaching the more relaxed R-state, as depicted in Figure 14 . It has been widely reported that some molecules, referred to as heterotropic allosteric effectors - such as Cl^- ions, inositol hexaphosphate (IHP), Bezafibrate (BZF), or 2,3-diphospho-glycerate (DPG) - considerably lower the oxygen affinity (and thus shift the oxygen binding curve to the right, as shown in Figure 15) of the T-state upon binding to HbA but not to the heme[1][46, 75, 82, 102]. The binding of these effectors is very different, and there is still controversy in the literature how and where they exactly bind, especially Cl^- and BZF are not well understood, while it is known that IHP and DPG bind primarily through electrostatic interactions into the central cavity[5, 65, 106]. The modulation of the oxygen dis-

1 Hence the name *allosteric* effectors: they influence the function of the protein without directly binding to- or in the vicinity of the active site.

Figure 13: Atomistic crystal structure of hemoglobin (T-state, bound to inositol hexaphosphate). The individual subunits are each colored differently for clarity, the Zn-PP substitution of the heme groups in the β-subunits is marked with green, two of the six Trp-s are marked with red, the inter-dimeric interface region is emphasized with a brown line.

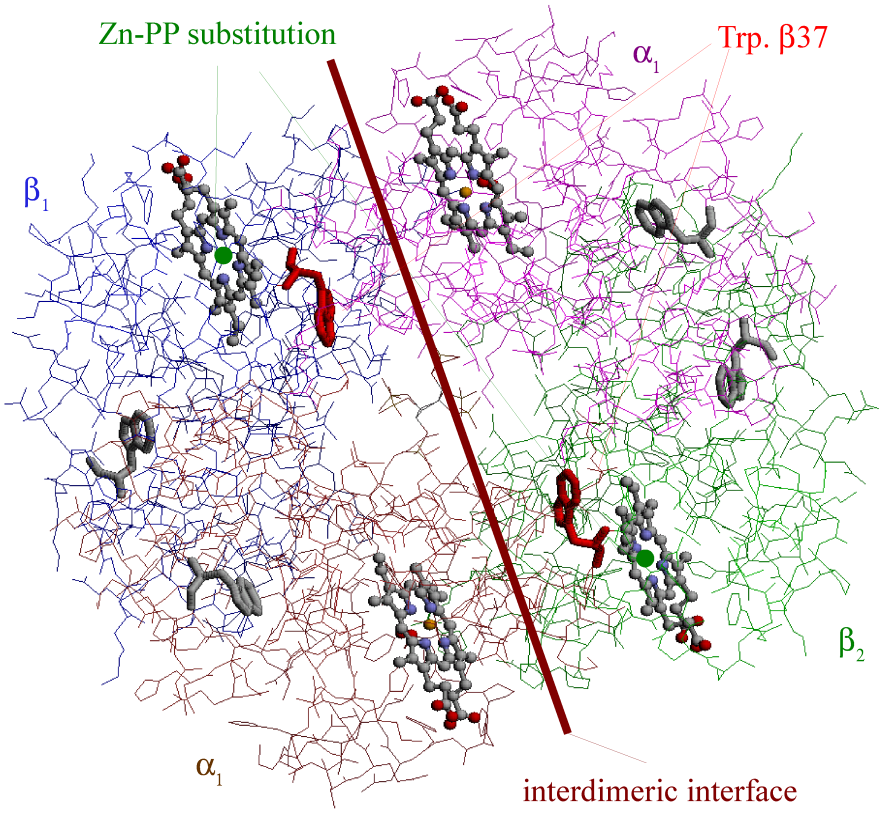

sociation curves by allosteric effectors is addressed in the extended MWC-SK model by the assumption that allosteric effectors bind specifically to the somewhat larger central cavity of the T-state and stabilize this conformation. This shifts the R $\rightleftharpoons$ T equilibrium in favor of the T-state and consequently lowers the overall affinity to oxygen[103, 102]. The well known Bohr effect and results reported for Cl^-, also influencing the oxygen affinity of the T-state[52, 119], show that, in a broader sense, H^+ and Cl^- can also be considered as being members of the family of allosteric effectors. Extended studies on the effect of allosteric effectors, however, indicated that they not only bind to the T-state but also to the R-state[48, 144]. The modulation of the oxygen association constants (K_T and K_R) in both states was shown to occur at a much broader scale than previously known (65-fold change in K_T and 2000-fold change in K_R; see [142, 155] for details). These data initiated the reformulation of the earlier models for the allosteric action of heterotropic effectors. The recently proposed "global allostery model"[155] supposes that the effectors can bind to both the T- and R-states and that effectors induce direct *tertiary* conformational changes[2]. These tertiary effects then lead to the detected changes in oxygen association[155, 142]. Until now, no structural data have been published for the complex of R-state human HbA with allosteric effectors; the only available structure is that of horse HbA complexed to CO[121]. Recently, however, a docking and molecular dynamics simulation study[73] proposed models for the structure of HbA bound with the allosteric effectors DPG, IHP, and 2-{4-{(3,5-dichlorophenylcarbamoyl)- {methyl}-phenoxy}-2-methylpropionoc acid. These results supported the model allowing for binding of effectors also in the R-state and proposed primary binding sites in the central cavity of the R-state tetramer, and thus supporting the global allostery model described above.

If the proposed global allostery model is "true", then the - though maybe subtle - tertiary conformational changes caused by the binding of allosteric effectors could also influence the global dynamics of the HbA molecule. If so, then this modified dynamics may result in a different activation energy (ΔE) and activation entropy (ΔS) values, which can then be detected by the method presented in the previous section. We have

2 Earlier models, including among others the MWC-SK, and its further extensions, supposed a change of the interfaces between the subunits, which is a quaternary effect, but not a change in the tertiary structures of the subunits themselves. This assumption is supported by the fact, that no significant structural changes can be seen in- and in the surrounding of the heme groups upon the binding of allosteric effectors. (Although the change upon the R $\rightleftharpoons$ T transition very large, but it is not the direct effect of the binding of the effectors.)

chosen four different effectors to test this hypothesis: Cl^-, IHP, DPG and BZF, based on the literature, and our previous work[117, 72], the magnitude of their effect approximately follows this order: Cl^-< IHP ≈ DPG < BZF.
In the next section I will present and discuss the data obtained with the new optical method.

2.2 EFFECTORS AND THE TRANSITION

As discussed, if the binding of heterotropic allosteric effectors influences the dynamical state of the hemoglobin tetramer, then this should appear in the change of the activation of this dynamics as well. With the optical method presented in this thesis, however, a special type of dynamics is monitored, namely only those motions, which have a characteristic time-window of approximately 10^{-5} ... 1 seconds. If there are changes in these motions due to the binding of these effectors, then the temperature dependence of the phosphorescence quenching may also be different in each case, and different from the state without these effectors. The main goal is *not* to provide details of the mechanism of action of these allosteric effectors, since the method is not capable of providing spacial - structural information. Rather, my goal is to provide a "test-case" of the method with these data: if differences can be detected between various effectors, and between the effector-bound and the "stripped" (without any allosteric effector bound) samples, it can further support the idea, that the activation- energy and entropy values provided by the new method may indeed have meaningful biological relevance.

the term "stripped" is widely used in the HbA literature to indicate the absence of allosteric effectors, therefore I will use it throughout the thesis in this sense as well.

2.2.1 *Activation of global dynamics in the presence of allosteric effectors.*

The next few figures present the data obtained on samples

bound to different allosteric effectors: Cl^- in Figure 16, IHP in Figure 17, DPG in Figure 18 and BZF in Figure 19. The average lifetime data are shown in Table 4 together with the concentrations in which the effectors were used. These concentrations were selected to match those used in previous studies (for eg. [155, 141, 142] and references there) in the literature. Cl^- ions were added to the samples in the form of NaCl. The samples were also checked with absorption spectroscopy, and spectra were compared to the data available in the literature. No significant differences above noise level were found in any samples.

Figure 14: Schematic representation of the rotation of the two dimers with respect to each other during the transition between the two states of R and T.

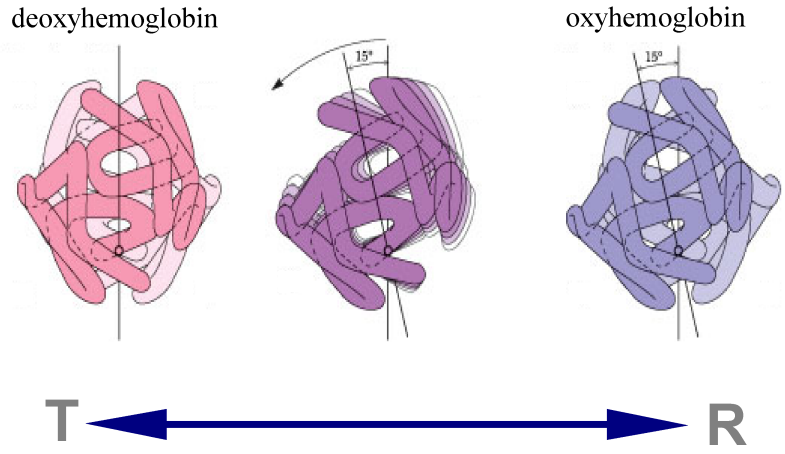

Table 4: Average phosphorescence lifetime of Zn-HbA bound to allosteric effectors. For comparison the data of stripped Zn-HbA is also shown in this table.

sample	<τ> at 10K [ms] ± s.d.
Zn-HbA stripped	28.7 ± 0.6
Zn-HbA + 100 mM Cl^-	28.9 ± 0.8
Zn-HbA + 2 mM IHP	29.0 ± 0.8
Zn-HbA + 2 mM DPG	27.6 ± 1.1
Zn-HbA + 10 mM BZF	28.0 ± 0.9

Figure 15: Oxygen binding curve of hemoglobin. The curve shows the oxygen saturation curve of the whole tetrameric molecule, thus 100% saturation is equivalent to the total binding of 4 oxygen molecules. The shifting of the curve to the right (decreased binding affinity) is caused by allosteric effectors, and is shown with an arrow. In the bottom of the figure the structure of three different allosteric effectors are also shown.

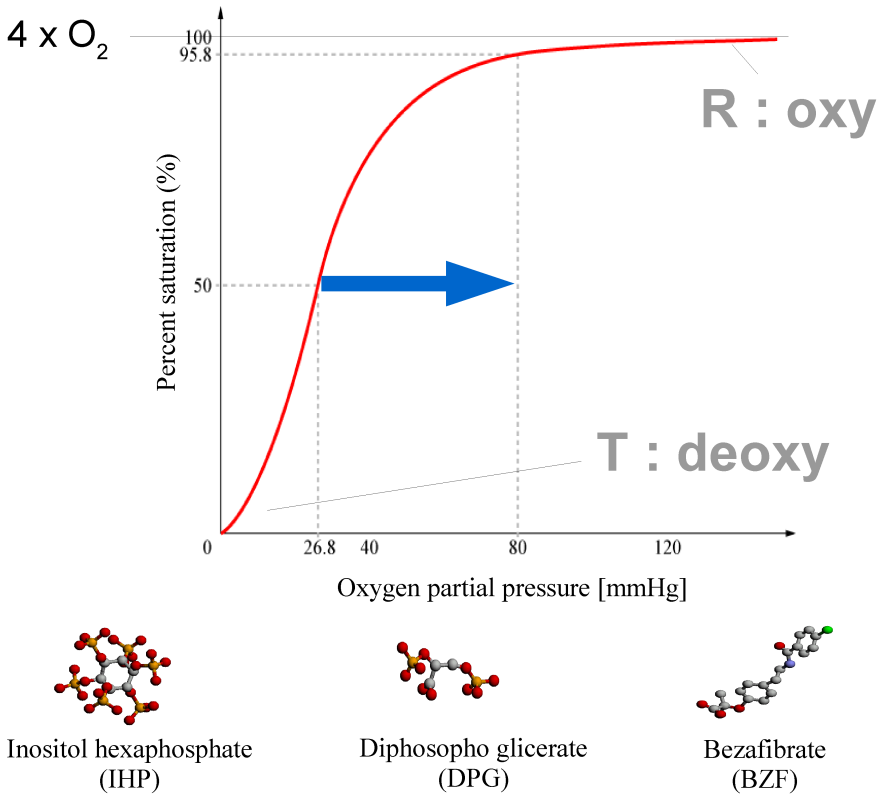

Figure 16: Normalized average lifetime of Zn-HbA bound to Cl^-(purple curve and diamonds). For comparison stripped Zn-HbA is also shown with red. The negative derivative functions are also shown in the bottom graph.

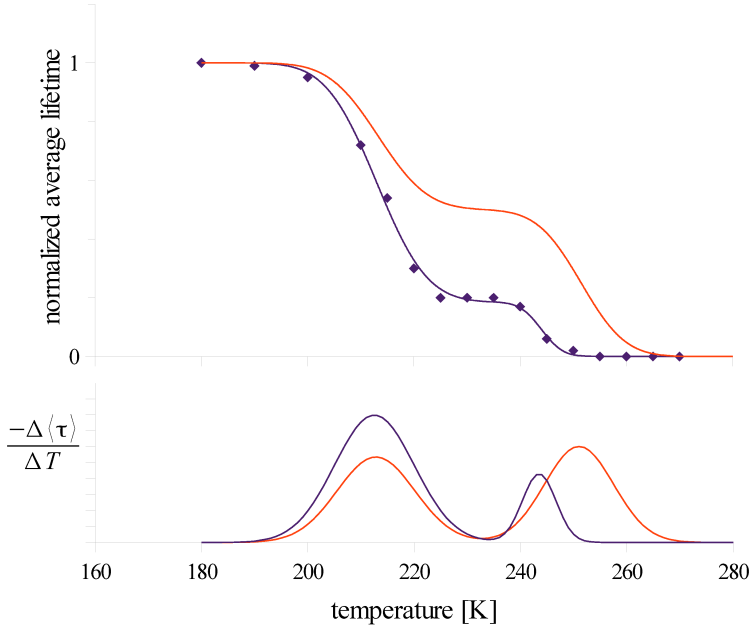

It can be seen, that the binding of allosteric effectors modifies the curves, and significantly change the first transition. The magnitude of the change follows the order of Cl^-< IHP ≈ DPG < BZF. While the binding of Cl^-, IHP and DPG cause a relatively small shift of the transition on the temperature scale, BZF causes a large shift accompanied by an also significant broadening of the transition. The change of the second transition is not as clear. While the differences of the transition points on the temperature scale in the derivative representation may seem significant, the cases of DPG and IHP have to be treated with caution: as can be seen, during the first transition the drop of the lifetime is very large. As apparent from Equation (5) the drop in the lifetime is accompanied by the same drop in the intensity. This intensity reduction after the first transition - as can also be seen in Table 5 comparing the K_d data - causes the signal/noise ratio to also significantly decrease, which makes the lifetime determination less certain (the relative error is much higher in these cases than average, reaching up to 15 ... 20 %). The increased error then causes an uncertainty in the fitting of the sigmoid function to the second transition, which manifests itself as an uncertainty in the second "peak" of the derivative functions.

Figure 17: Normalized average lifetime of Zn-HbA bound to IHP (blue curve and triangles). For comparison stripped Zn-HbA is also shown with red. The negative derivative functions are also shown in the bottom graph.

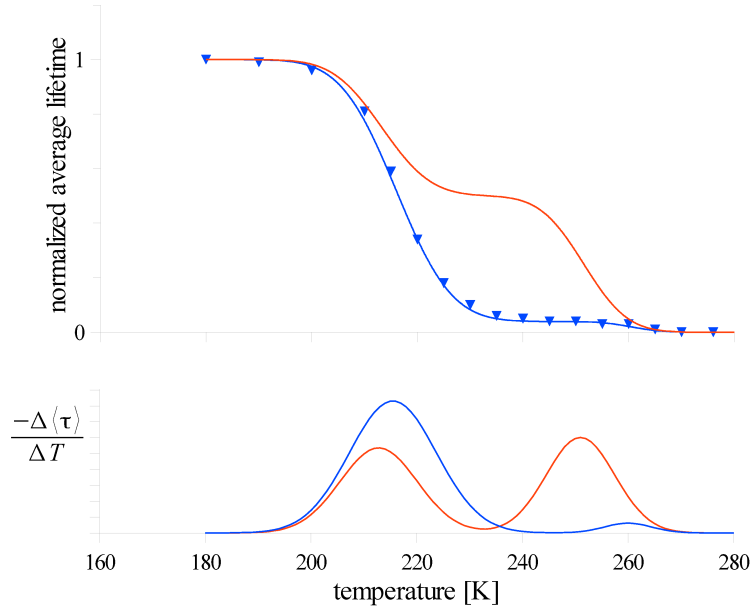

2.2.2 *Analysis of the differences caused by allosteric effectors*

The thermodynamic parameters calculated from the fitting of Equation (11) to the data are shown in Table 5. Changes in the second transition may not be relevant due to the factors described before, however, they can also arise from the perturbation of the hydration shell caused by the millimolar concentration of "foreign" molecules compared to the stripped case. While the time-scales and the systems are very different, the importance of the environment is emphasized in the literature of glass-transition in proteins (see for eg. [96]). In the analysis of the dynamical transition (1.4) it was shown that the second step includes the coupling of the protein to the bulk solvent as a major effect. This can not be excluded from the analysis of the differences caused by allosteric effectors. Most notably, this effect is evident in the case of Cl^-, which sample involved the addition of 100mM NaCl to the 100mM HEPES buffer. This effectively doubles the molarity of the solvent, and acts as an anti-freeze agent[3]. This can

3 Addition of salt is widely used to avoid freezing of water, or at least considerably lower the freezing-point. A corresponding decrease of the melting-point is also evident in this case.

Figure 18: Normalized average lifetime of Zn-HbA bound to DPG (orange curve and triangles). For comparison stripped Zn-HbA is also shown with red. The negative derivative functions are also shown in the bottom graph.

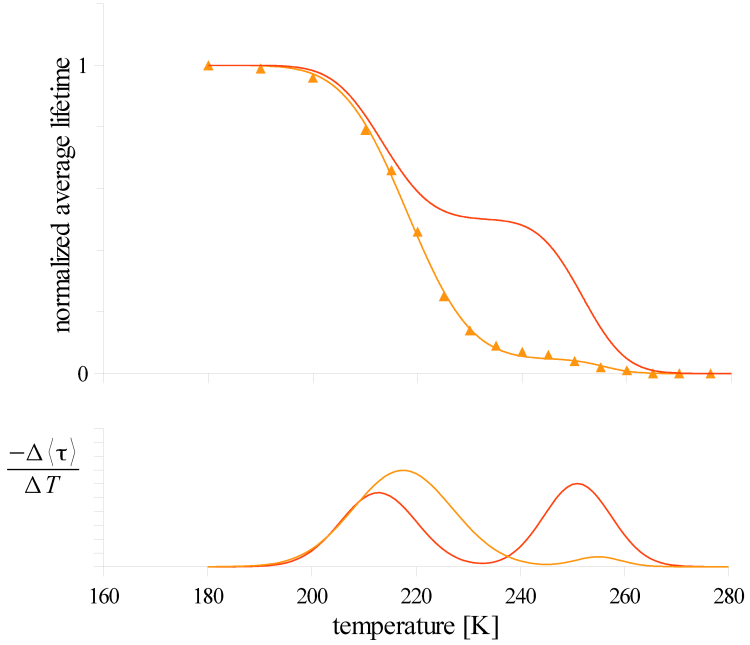

Table 5: Thermodynamic parameters of the first transition in different Zn-HbA samples. For comparison the data from Table 3 of the stripped from (and calculated from Zn-PP lifetimes) are also shown ± s.d.

sample	ΔE [kJ/mol]	ΔS J/mol·K	T_{MP} [K]	K_d
Zn-HbA stripped	113.4 ± 4.4	532 ± 22	213.1 ± 0.3	2.0 ± 0.1
Zn-HbA +100mM Cl^-	97.7 ± 5.6	456 ± 29	214.2 ± 0.7	5.33 ± 0.43
Zn-HbA + 2 mM DPG	71.5 ± 3.7	327 ± 27	218.5 ± 0.6	29.38 ± 3.03
Zn-HbA + 2mM IHP	77.4 ± 3.5	358 ± 24	216.4 ± 0.4	31.46 ± 2.85
Zn-HbA + 10mM BZF	42.3 ± 1.7	187 ± 10	225.9 ± 2.5	17.85 ± 1.96

Figure 19: Normalized average lifetime of Zn-HbA bound to BZF (dark grey curve and triangles). For comparison stripped Zn-HbA is also shown with red. The negative derivative functions are also shown in the bottom graph.

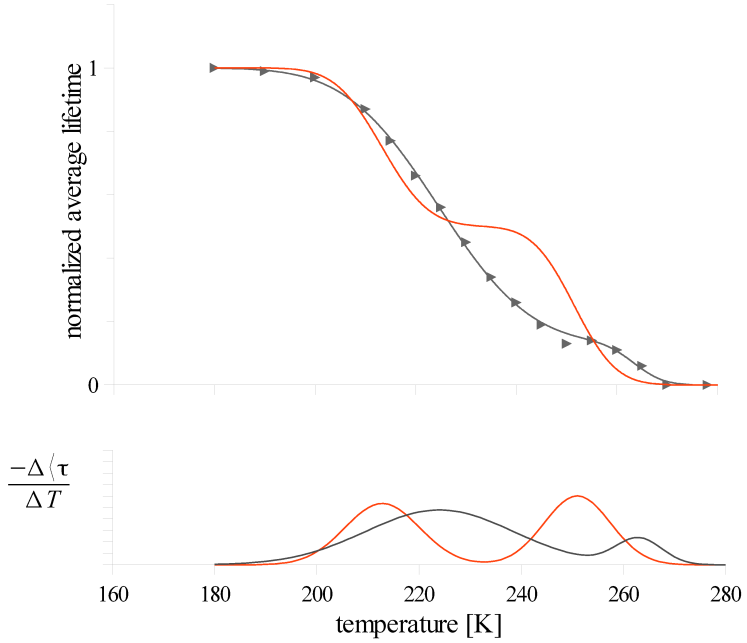

account for the observed shift of the second transition by almost -10 K, since due to the decreased melting point the state "3" on Figure 12 will be reached at a lower temperature.

The first transition was shown to be specific for the protein, therefore it is of greater importance in the search for biological significance of the results available from the new method. In Figure 20 the curves are shown in a common figure to aid comparison of the first transitions. To emphasize the fact that the second transition is of less importance, it is shown in pale colors. The activation energies and entropies also change significantly upon the addition of allosteric effectors. Both the activation energy- and entropy- values are significantly smaller than in the stripped case, Cl^- ions having a relatively moderate effect, while DPG and IHP decrease these values by about 30%, and BZF by more than 50%. The magnitude of the *change* in the ΔE and ΔS values corresponds to the effector *strength*: Cl^- < DPG ≈ IHP < BZF. This shows that the special type of dynamics monitored by the quenching experiment can be more easily activated in the hemoglobin+effector complexes. This may indicate a "softening" of the structure caused by the effectors, which may correlate with the decreased dissociation volume of the tetrameric structure found

Figure 20: Comparison of the first transition of Zn-HbA under various conditions: stripped (red), with added Cl^-(purple), with added DPG (orange) and added BZF (dark grey). The respective derivative functions are also shown in the bottom. To emphasize the importance of the first transition, the second half of the curves are shown in pale colors.

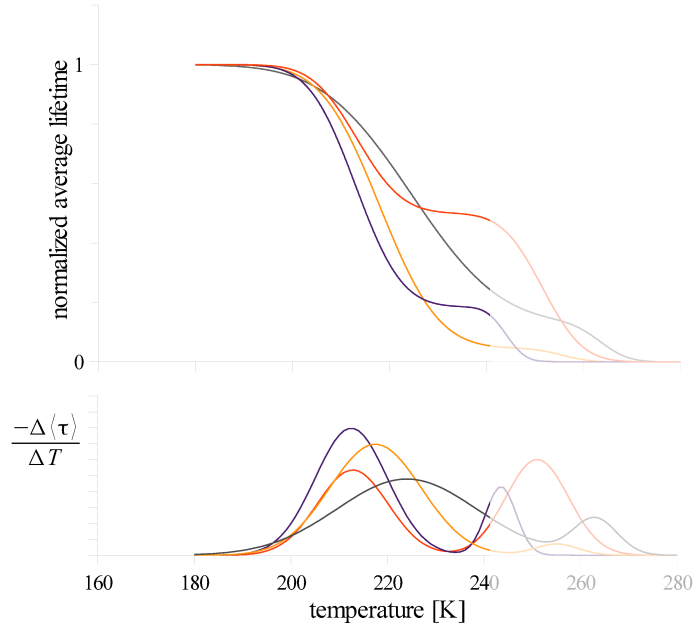

in our pressure tuning experiments[117, 72].

The change in the K_d values indicate also that there is a change in the diffusion coefficients of the quenchers inside the protein, and addition of the allosteric effectors generally increases the diffusion rate. This also indicates some kind of "softening", however regarding the molecular details no solid inference can be drawn from these data. It can also be seen, that the relative drop in the activation entropy values is larger than the relative drop in the activation energy values, thus the activation of the dynamics becomes proportionally more "energy-intensive", and the ratio of the released entropy is smaller. This accounts for the increase in the transition temperature (T_{MP}).

Of course, taking into account other experimental data (pressure tuning and fluorescence line narrowing, as will be shown in the next sections), possibly interesting speculations can be made, and I will attempt to present some of them in chapter 5. In short, most probably the pathways of the quenchers are changed by the addition of allosteric effectors, due to a realignment of the dynamic fluctuation patterns of the structure. This realignment then may play a role in transmitting information through the interfaces between the monomeric subunits, and may also

serve as an information "pathway" through the entire structure. This way allosteric effectors may influence the function of hemoglobin (and possibly other allosteric proteins may function in a similar way) not only through static structural changes, but also through influence on the dynamic global movement patterns of the entire structure of the protein. These are of course speculations only, the data do not allow for more than to observe the changes in the activation parameters of the ms ... s - timescale global dynamics.
It can however, be stated, that the new optical method presented in this thesis supplies activation - energy and - entropy data of a special kind of global, slow dynamics of the protein which correlates with it's biological function in a sense, that any biologically significant changes in the protein's function also manifests in changes of these activation parameters.

This dynamics is not identical to the dynamics of the same time-scales at room temperature, since the boundary of the protein is bound to a solid matrix during the first transition. However, this limited dynamics is still representative for the protein, and reflects in some way it's dynamics under physiological conditions. The exact differences between this limited dynamics and the dynamics under physiological conditions can not be inferred to with this technique unfortunately[4].

The results presented in the next sections are better understood in a retrospective way, therefore they are presented in the light of the results of the new method.

In the next sections I will present results of other experiments (pressure-perturbation, and fluorescence line narrowing) done on hemoglobin previously during my PhD-work. These data can be put in an interesting context knowing that there is a change in the global dynamics of hemoglobin by the addition of allosteric effectors, than without this result.

4 Maybe NMR, or other site-selective method will be able to add data to these questions, however the time-scale of ms ... s is still hardly accessible.

3

CHANGES AT THE INTERFACES - PRESSURE PERTURBATION

3.1 INTRODUCTION TO PRESSURE PERTURBATION STUDIES

In this section results of a pressure-perturbation study are presented. These results can be related to the results presented in the previous section. High pressure is known to have distinct effects on proteins [58] depending on the applied pressure range. Typically, 0.5 ... 1 GPa is needed to denature a protein, by squeezing water into the interior [125]. Lower pressure causes elastic deformations, the extent of which are characteristic of the compressibility [71, 36] of the protein. Because pressure is an intrinsic thermodynamic parameter, pressure can shift thermodynamic equilibria of various kinds, including conformational transitions of proteins [9]. One such equilibrium that is typically perturbed by pressure is oligomer dissociation. Pressures in the range of 100 ... 200 MPa have been shown to be able to affect the quaternary structure of the proteins without affecting their secondary and tertiary structure [124, 123]. Previous pressure experiments performed on HbA [105, 90, 2] showed that pressure tuning affects various optical properties (e.g. light scattering, absorption, fluorescence emission, and CD-spectra) of the sample. In a detailed study [105] it was shown that applying pressure at pH 7 and 10^{-6}... 10^{-4} M protein concentration will shift the tetramer $\rightleftharpoons$ dimer equilibrium in favor of the dimers, and at pH 9, the observed dimer $\rightleftharpoons$ monomer equilibrium will be shifted in favor of the monomers. No systematic study applying pressure perturbation was conducted to observe the effect of various allosteric effectors on the subunit interfaces in HbA. It was our goal to compare the effect of allosteric effectors on the tetramer $\rightleftharpoons$ dimer equilibrium in the T- and R-states by applying high hydrostatic pressure and steady-state fluorescence techniques. Based on literature data [64, 112], we have used the intrinsic fluorescence of the tryptophan residues as a marker of changes at the interface region. Measurements under high hydrostatic pressure were, however, not feasible on deoxyhemoglobin, because the sample holder inside the pressure cell cannot be isolated in a gas-tight manner from the pressure transmitter fluid (water) in the device. To overcome this difficulty (and for its multiple chromophores), we

Due to space-restrictions this is only a very short introduction to pressure-tuning, interested readers are directed to the cited references for details about the theory and methodology.

used Zn-HbA to mimic the structure of the T-state. Oxygen equilibrium studies and x-ray crystallography have shown that this derivative, as a five-coordinated metal hybrid of HbA, can be considered analogous to T-state HbA, although not being perfectly the same [98, 120, 18]. The use of zinc substitution is supported by results that show a low energetic cost compared with other (for e.g. cobalt) metal substitutions [64]. This indicates that the conformation is relatively close to the native form. It can be considered questionable, however, for which of the T-state subpopulations the analogy holds. The conformation within being "T" was shown to be slightly tunable by environmental conditions, for example by sol-gel encapsulation [112, 113]. This tunability was also found within zinc hybrids rendering the CO-ligated form the least tense among a variety of ligated forms and external conditions [111]. Literature data, however, show that the zinc hybrids in general have lower oxygen affinity than deoxy-HbA [87]. Based on this we considered Zn-HbA form, which may be the least tense among the zinc hybrids, a sufficiently good model for the native T-state. Oxygen saturated, non-hybrid HbA was used to study the R-state, it is termed "oxy-HbA " in this thesis.

3.2 Method of pressure perturbation

3.2.1 *Fluorescence Emission Spectra under High Pressure*

A high pressure cell with sapphire windows was mounted in a spectrofluorometer , as seen in Figure 21. The figure shows the current setup, in which a custom-modified spectrometer is used. Data presented in this section was acquired with the use of a previous setup, in which the high-pressure cell was mounted in a Fluorolog-3 spectrometer. That setup had a lower efficiency, since the optics of the spectrometer did not match the numerical aperture of the cell. To improve the signal-level, I have redesigned the system, and built it around a Hitachi spectrometer, which was modified to adapt it to the optics and geometry of the pressure cell. The optical path is also shown in the figure (excitation path in light blue, emission path in light green), together with the added optical elements. Two Ø 6.3 mm focusing lenses are fit into the window-plugs of the cell, to focus / parallelize the beam, other lenses are used to obtain a matched numerical aperture to the monochromators. High pressure was created by a manually driven piston pump (Nova Swiss, Effretikon, Switzerland), and pressure was monitored with a pressure transducer (DMS-580.4018

Figure 21: The current high pressure setup. Drawing of the high-pressure cell, image of the modified spectrometer, and of the whole setup. Light paths are shown in blue / light green for excitation / emission respectively, the used quartz cuvette is also shown with its stopper.

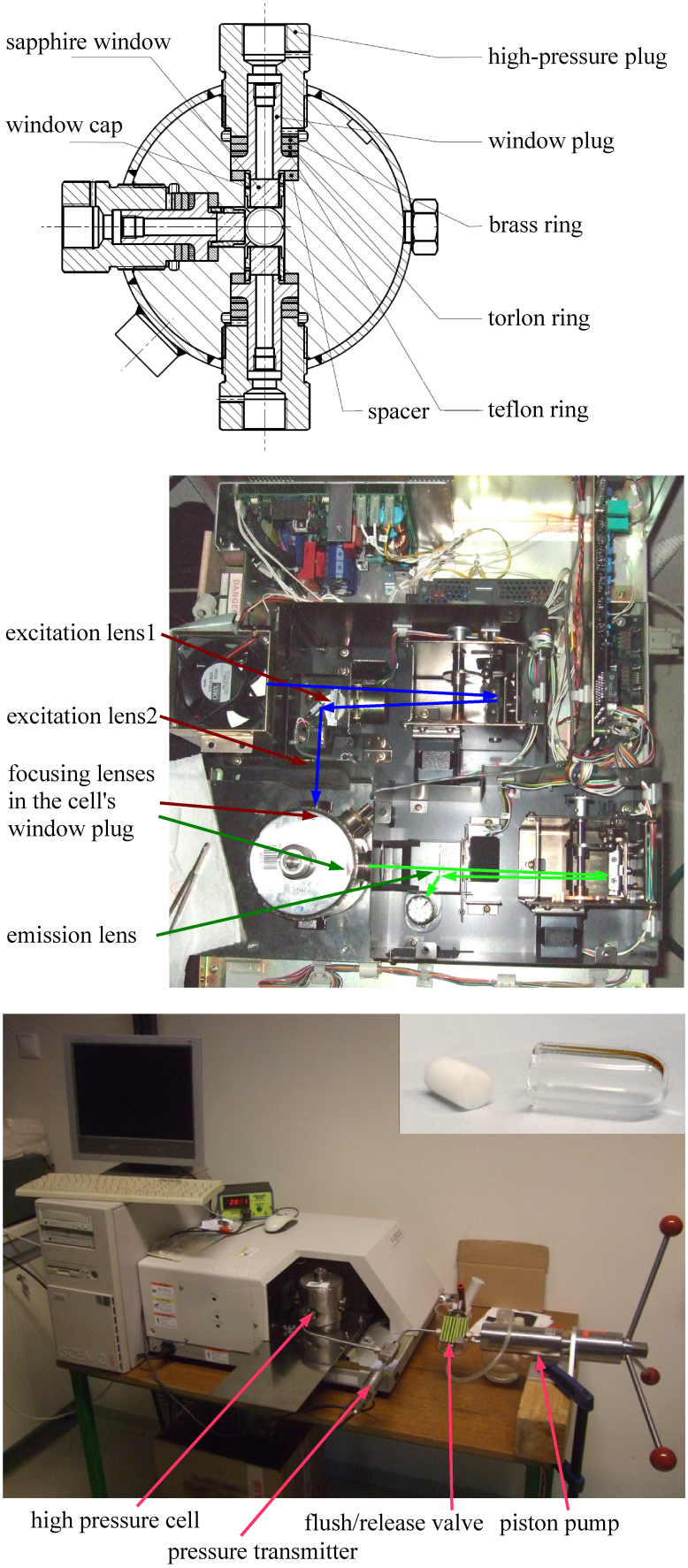

Nova Swiss, Effretikon, Switzerland) equipped with a digital meter, with an accuracy of 10 bar. The sample was allowed to equilibrate at each pressure for 3 minutes. Repeated spectra at the same hydrostatic pressure did not show detectable differences after this time, therefore it could be concluded that equilibrium was reached. Spectra were acquired by counting the detected photons for 1s at each wavelength, with slits of the monochromators adjusted at 5 nm excitation and 2 nm emission bandpass. The temperature was maintained by a thermostat at 20 °C and was directly controlled in the sample with a special thermometer rated for 7000 bar maximum pressure. The HbA sample was injected into a quartz tube (UV-fused silica) with a 2.4-mm inner diameter with 1.3-mm wall thickness and 19-mm height. The sample volume was 110 µl. This tube was covered with a rubber stopper and placed into the pressure cell. The pressure transmitter fluid was water. Spectral shift under pressurization was determined based on either the maximum position of the emission band determined by a Savitzky-Golay algorithm[114].
It was important to control the state of the protein under high pressure. We wanted to avoid any secondary or significant tertiary structural changes during the experiments. Therefore it was important to determine the "safe" pressure range. Two methods are especially suited for these controls: UV-VIS absorption spectroscopy - as already mentioned - is highly sensitive to tertiary structural changes to the environment of the chromophores, and FTIR spectroscopy, which is a useful tool to estimate secondary structural elements.

3.2.2 *Absorption Spectra at High Pressure*

The high pressure cell was mounted in a Cary 4E UV-visible spectrophotometer (Varian Inc, Palo Alto, CA) and kept at 20 °C. Spectra were acquired at a scan rate of 1 nm/s, using the full height slit mode, allowing for 1 nm bandpass. Control spectra before pressurization were acquired in the quartz tube, covered with a rubber stopper, and placed centered in the light beam.

3.2.3 *FTIR Spectroscopy Under Pressure*

The infrared spectra - to control possible changes in the secondary structure of the protein caused by high pressure - were obtained with a Bruker IFS66 FTIR spectrometer equipped with a broad band MCT solid-state de-

tector cooled with liquid nitrogen. During data acquisition, 256 interferograms were summed at a resolution of 2 cm^{-1}. High pressure was generated in a diamond anvil cell (Diacell Products, Leicester, UK), where the pressure was built up by means of a screw mechanism, which pressed the two diamonds against each other. The sample was held in the boring of a steel plate (gasket) between the diamonds. Sample volume was approximately 50 nl. Barium sulfate was used as an internal pressure standard in all cases[153]. All experiments were performed at 20 °C, and at a protein concentration of 800 µM. The broad band of water around 3350 cm^{-1} was used to control that the solvent is still in the fluid phase even at the highest pressure used in the experiments. No crystallization was observed in the experiments reported here. The overlapping components of the amide I/I band were resolved by Fourier self-deconvolution[70], which decreases the width of the component lines of the amide band. The optimal parameters were determined from the analysis of the power spectrum[127]. A resolution enhancement factor[70] of 1.5 was reached by using a Lorentzian band shape of 20 cm^{-1} bandwidth. The deconvoluted spectra were then fitted with gaussian functions, and the peak position of the band characteristic for α-helical structure was determined.

3.3 PRESSURE PERTURBATION RESULTS

Oxy-Hb and Zn-HbA samples corresponding to the R- and T-analogue state HbA, respectively, were studied in stripped condition as reference and then bound to various allosteric effectors. The effect of allosteric effectors was monitored by registering the conformational perturbation effect of high pressure using fluorescence emission and absorption spectroscopy. For the interpretation of the results it was important to compare the results of HbA to a similar, but monomeric protein, Mb.

I will only show data of Zn-HbA in the stripped condition, the spectra and their shifts were similar also in the cases of added allosteric effectors.

3.3.1 *Control experiments*

It was important to exclude the possibility of denaturation or any significant tertiary structural changes during the pressure perturbation experiment. As mentioned before, absorption spectroscopy is a useful tool to monitor any of these events. The results obtained by FTIR spectroscopy are shown in Figure 22, the spectra are shifted along the absorbance-axis for clarity. The blue lines show the FTIR spectrum of HbA at ambient pressure, the light-blue line is the deconvoluted spectrum, and dashed

Figure 22: FTIR spectra of HbA and Mb at ambient pressure (blue lines), at 325 MPa (red line) and at 900 MPa (black line). The position of the position of the amide-I peak of α-helical content at various pressures are also shown for HbA (squares) and Mb (triangles) together with their s.d.

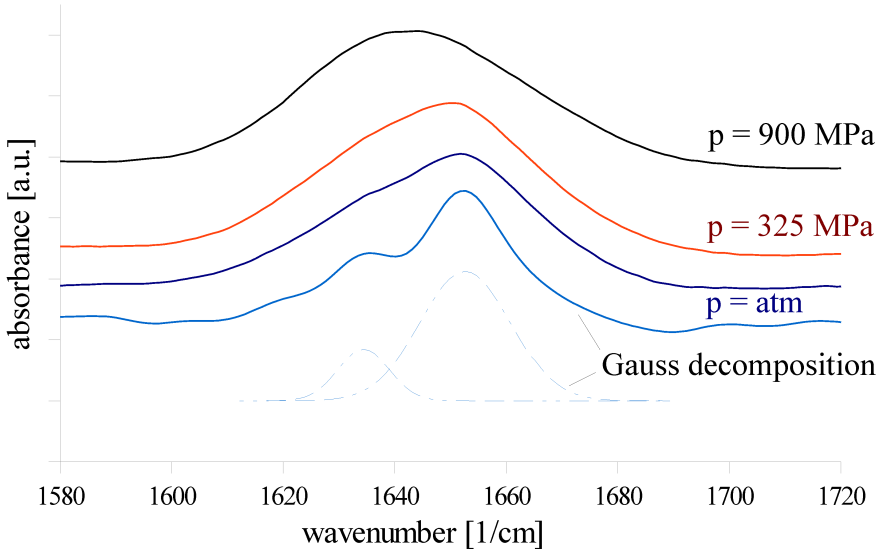

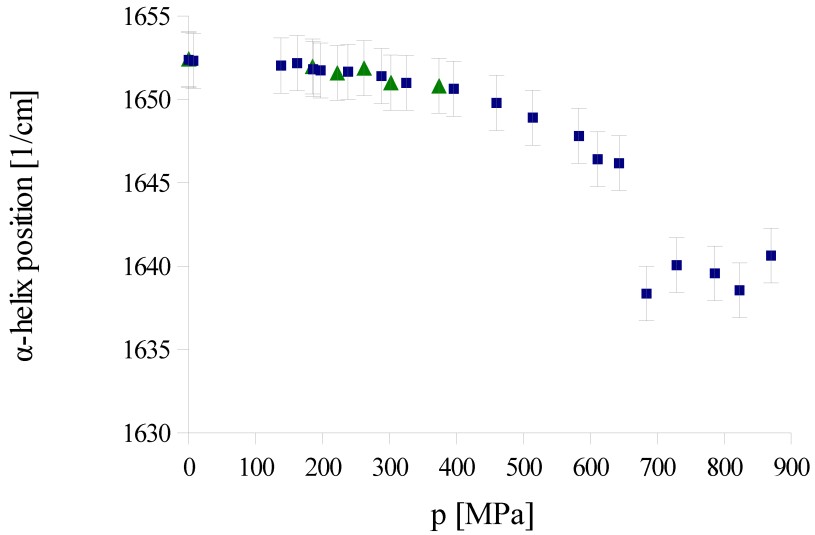

Figure 23: Absorption spectra of HbA at ambient pressure (blue line) and at 350 MPa (red line). Inset shows the absorption maximum of the Soret-band around 409 nm at various pressure levels.

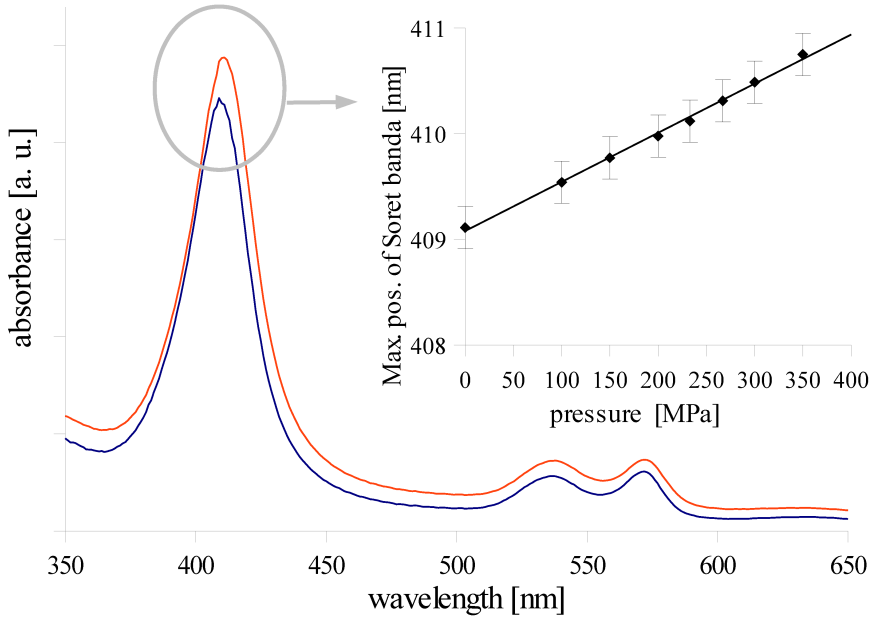

lines show the Gaussian-fitting, to obtain the peak position corresponding to the α-helices in the protein. It can be seen that the FTIR-spectrum corresponding to 3.25 kbar (325MPa) does not differ significantly from the spectrum at ambient pressure, thus up to this hydrostatic pressure no significant secondary-structural changes can be seen. The position of the amide-I band corresponding to the α-helical content of the protein is also shown at various pressure values for HbA (squares) and Mb (triangles). It can be seen, that there is a very slight shift of the amide band at the beginning, which can be attributed to elastic compression of the entire structure, and then above 4 kbar the slope increases, and a phase transition follows. To avoid any onset of a phase transition, we have chosen 3.5 kbar as the upper limit of the applied hydrostatic pressure for any subsequent experiments.

To further test against any tertiary structural changes, we have obtained UV-VIS absorption, and fluorescence emission spectra. The absorption spectrum of HbA at ambient pressure (blue line) and at 3.5 kbar (red line) are shown in Figure 23, the inset shows the absorption maximum of the Soret-band around 409 nm at various pressures. A slight, linear shift can be seen, which corresponds to shifts usually seen in the case of elastic compression of the structure. Similar shift was observed, e.g., in

Figure 24: Fluorescence emission spectra of Zn-HbA at ambient pressure (blue line) and at 350 MPa (red line). Inset in the figure shows the peak position of the Q-band of Zn-PP at various pressure levels. Excitation was at 290 nm wavelength.

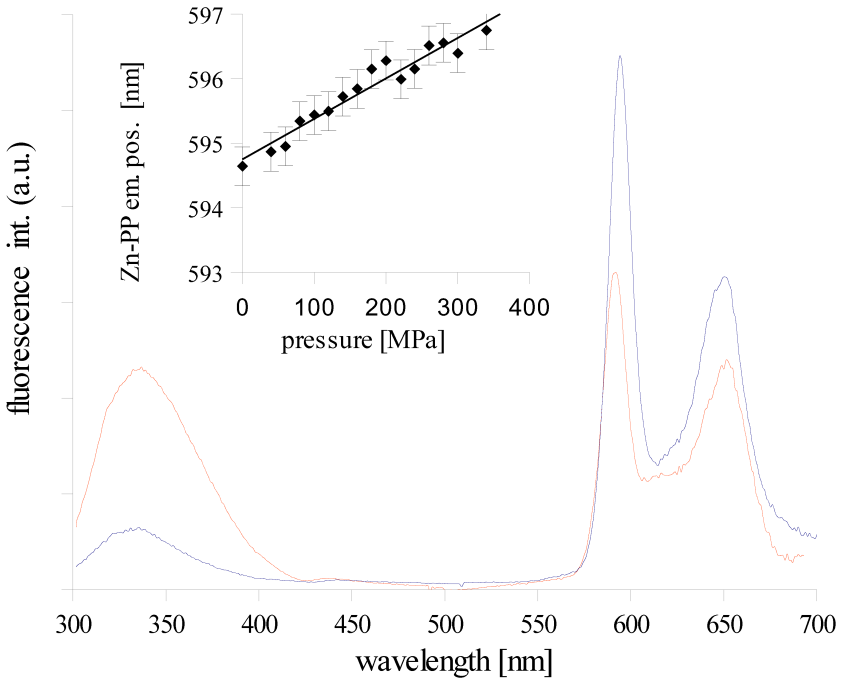

the case of cytochromes under pressure[67]. The Zn-HbA sample having two different chromophores at different places in the structure enabled us to further test the effect of hydrostatic pressure in this range.

The fluorescence emission of Zn-HbA is shown in Figure 24. It can be seen, that the changes in the Trp emission region (around 340nm) are significantly different from the change at the Q-band region of the Zn-PP emission (around 595nm). The spectrum was acquired with an excitation wavelength of 290 ± 2.5 nm (thus 290 nm with 5nm bandpass). The Trp fluorescence is seen around 340 nm, while the fluorescence emission of Zn-PP is also visible due to Förster-type energy-transfer from the Trp-s to the Zn-PP-s[49] (and to the two other heme groups as well). It can also be seen as a slight "dip" around 408 nm in the Trp emission spectrum. This could be further confirmed by registering the excitation spectrum of Zn-HbA at an emission wavelength of 595 nm, it had both the characteristic excitation spectrum of Zn-PP, and an additional peak at 290nm corresponding to the excitation maximum of Trp as can be seen in Figure 25.

Figure 25: Excitation spectrum of Zn-PP in Zn-HbA.

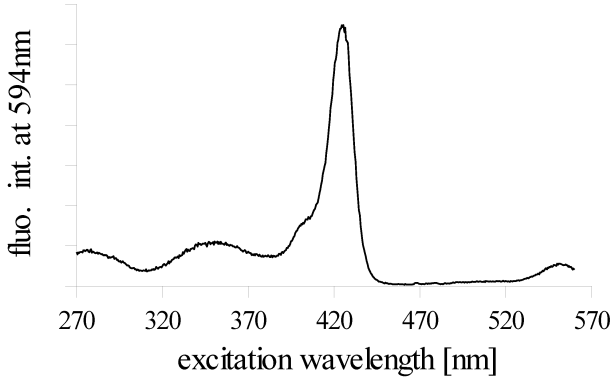

3.3.2 *Transitions seen in the Trp fluorescence*

The Trp fluorescence emission is distinct from the behavior of the Zn-PP. It also shows a shift of the emission maximum position, and it is accompanied by a large intensity increase, as can be seen in Figure 24, and in the case of non-hybrid oxy-HbA shown in Figure 26. . These changes are *not linear* however, as can be seen in Figure 27. This non-linearity is in sharp contrast to the perfectly linear behavior of Zn-PP in Zn-HbA, or the Trp in Mb, and shows a transition, which is not present in other data. It is also a striking difference, that the Trp emission intensity *decreases* in Mb together with the linear red-shift of the spectrum, while in HbA there is an *intensity increase* both in Zn-HbA and oxy-HbA. Before reaching any further conclusions, and discussing the results, it is important to rule out possible denaturation of the structure, as a cause for this different behavior. Most of the control experiments target this goal, I will summarize here the rationale for excluding denaturation.

This could be part of the discussion, but it may be better to have it here, there are other points to discuss later.

3.3.3 *Transition seen in HbA is not caused by denaturation*

3.3.3.1 *The 100 ... 200 MPa pressure range is very low.*

compared with the typical pressures needed for protein unfolding. It was shown previously that myoglobin is pressure-stable up to 650 MPa [58, 128, 83]. Data presented for Mb also show no signs of any significant structural change. Recently a denaturation pressure of 400 MPa was reported for the isolated subunits of HbA[53], but the observed 100 ... 200

Figure 26: Trp fluorescence emission of oxy-HbA at ambient pressure (blue line) and 3.5 kbar (red line). The inset shows the normalized emission spectra to emphasis the spectral shift accompanying the intensity increase.

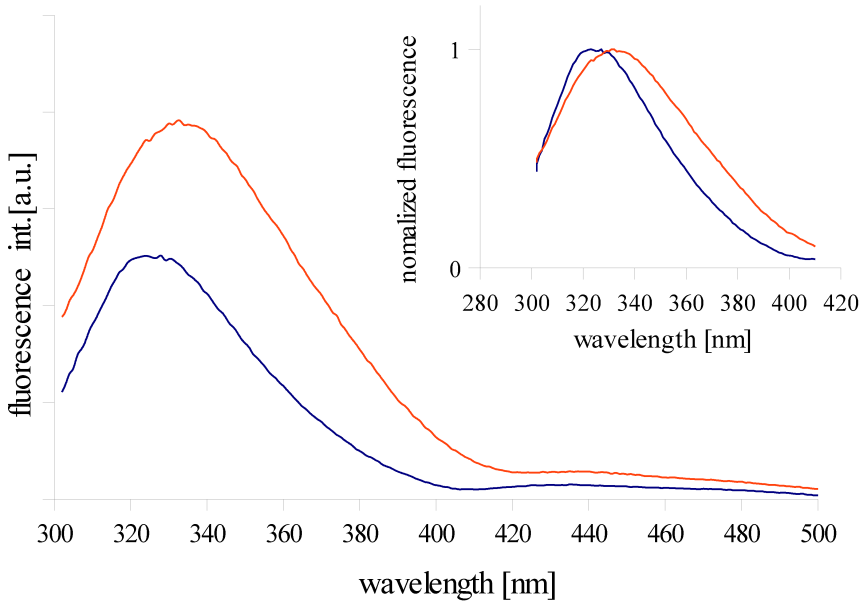

MPa transition pressure range - as seen in Table 6 - is significantly lower, and thus it is not reasonable to expect denaturation at this lower level of pressure.

3.3.3.2 *Absorption spectrum at 350 MPa.*

At this pressure the Trp emission is already red-shifted with respect to the initial emission spectrum. No significant changes, except a slight red shift, can be seen in the Q-band and in the Soret region. Denaturation of the protein would be clearly seen in the absorption spectrum, as can be seen, e.g., in the slow-cooled sample Figure 4. Also, as observed in the Q-band region, no change in the spin state or in the coordination state of the heme occurs in the pressure range used. The small linear shift of the Soret-peak in the absorbance spectrum in Figure 23, and the Q-band emission-peak (around 595 nm) of Zn-PP in Figure 24 can be explained by the change of the electronic transition energy due to applying high pressure that decreases the distance between the chromophore and the interacting units (atomic groups). This change of the electronic transition energy is supposed to be proportional to the solvent shift at atmospheric pressure. If the interaction of the chromophore with the atomic groups of the protein matrix is dominated by one kind of interaction with a potential energy of $1/R^n$ distance dependence, one observes a linear shift

Figure 27: Fluorescence emission of Zn-HbA at various pressure levels. The top figure shows the maximum position of the emission, the bottom figure shows the emission intensity at the maximum. Insets in both figures show the respective data for Mb.

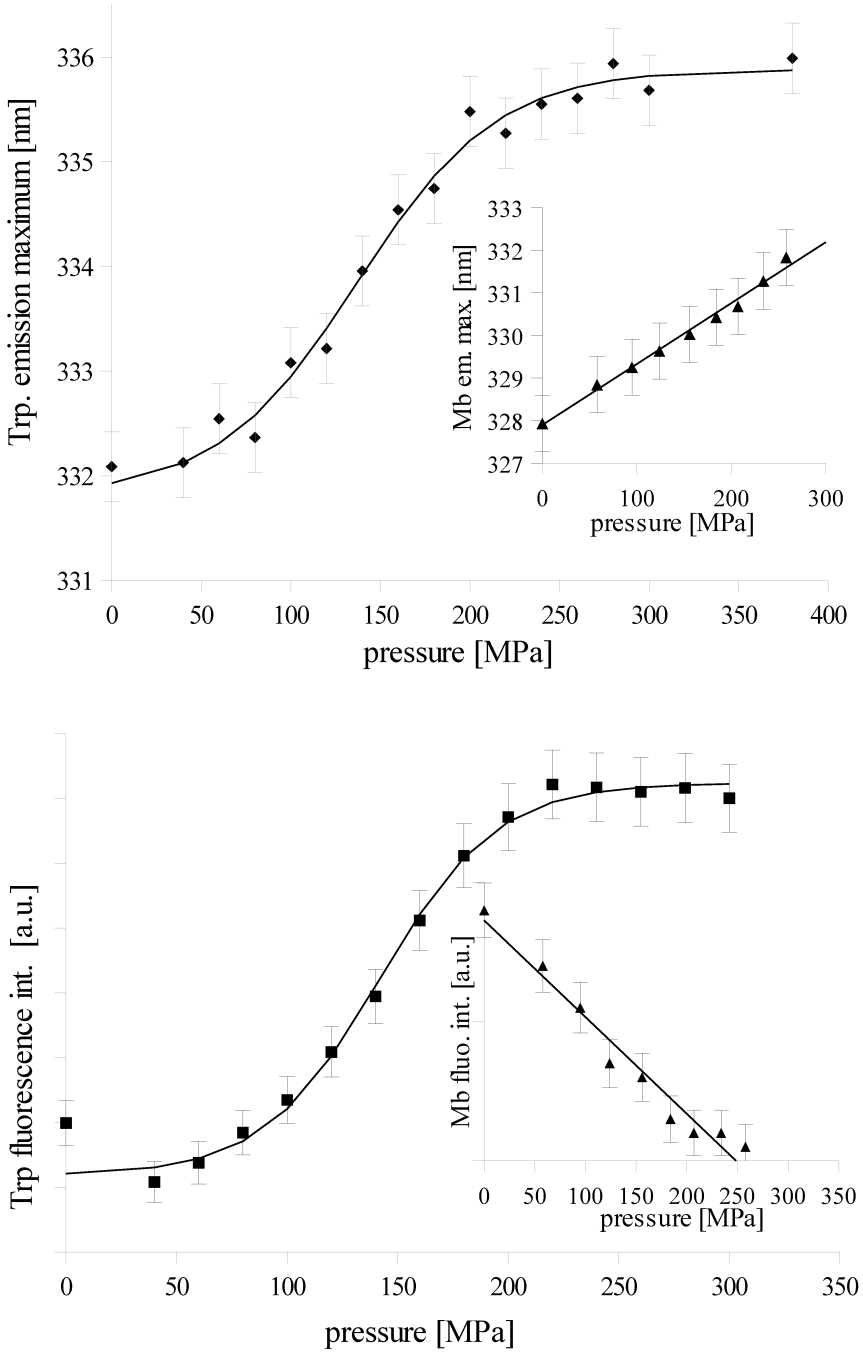

of the transition energy as a function of pressure [74, 158, 157]. The observed linear red shift has also been reported for other heme proteins [128, 67], and shows that the structure of the heme pocket in general was not affected, and we only see an overall elastic effect.

3.3.3.3 *This pressure range typically affects intermolecular interactions.*

It is well known that pressures of this range typically affect intermolecular interactions and cause the dissociation of oligomers[124, 123]. An earlier HbA fluorescence study [105] found reduced molecular volumes calculated from the fluorescence lifetime and anisotropy of a covalently attached fluorescent label 5-dimethylaminonaphthalene-1-sulfonyl chloride (dansyl chloride) under pressures up to 250 MPa. The authors interpreted these changes in terms of dissociation and not denaturation.

3.3.3.4 *Changes are not due to altered oxygen binding.*

Besides conformational changes induced by pressure, we have to consider the possibility of deoxygenation because of pressure. This, however, would lead to almost a magnitude stronger shift of the Soret band (an almost 20nm red-shift of the Soret band would occur upon deoxygenation) than the shift observed. Thus, we can rule out pressure-induced deoxygenation in this pressure range.

3.3.3.5 *FTIR spectroscopy.*

FTIR spectra do not show significant changes in the amide-I band position (characteristic for α-helical structure) up to 350 MPa, as can be seen in Figure 22. Because HbA is a predominantly α-helical structure, this rules out unfolding of any helices in this pressure range. To demonstrate pressure - induced unfolding, the FTIR spectrum acquired at 900 MPa is also shown which clearly shows an unfolded state. This spectrum is, however, very different from the ones corresponding to the lower pressure range.

3.3.3.6 *Comparison with Mb.*

Mb is a monomeric heme protein, and its tertiary structure closely resembles the structure of a HbA subunit, therefore it can be considered as a good model of a single HbA monomer. In the same pressure-range Mb behaves strikingly different however than HbA: both the shift of the maximum position and the intensity change are strictly linear. It has been reported in the literature how pressure itself influences the fluorescence

spectrum of Trp in tris(hydroxymethyl)aminomethane buffer, in the presence of alcohol or glycerol, and when it was incorporated in a small peptide[110]. In all cases a linear, continuous red shift induced by pressure was observed. This effect - attributed to the increase of water density and dielectric constant under pressure - would cause a shift of 1 ... 2 nm in the pressure range used here. The shift of the maximum position in our measurements is in this range, although somewhat larger, which can be attributed to the presence of the protein matrix. It is interesting to note that this red shift is comparable with the shift of the fluorescence maximum position of Zn-PP, showing the presence of the same elastic compression in HbA. None of the transition-like features of HbA appear in the fluorescence of myoglobin. It should also be considered that an elastic compression, which shortens the heme-Trp distance, would itself decrease the intensity of the Trp fluorescence because of an increase in energy transfer. This latter effect is expected to occur also in HbA but is overwhelmed by another effect, which can be attributed to pressure-induced dissociation of the tetramer.

3.4 DISCUSSION OF THE PRESSURE PERTURBATION RESULTS

The observed transition in the Trp fluorescence data of HbA, as seen in Figure 27 is of sigmoidal shape. The point corresponding to the half-transition, $p_{1/2}$ is distinct under different conditions, such as protein concentration, or the presence of allosteric effectors, both in the case of oxy-HbA, and Zn-HbA. The $p_{1/2}$data are shown in Table 6, the s.d. of the $p_{1/2}$ values is 3 ... 5 MPa. The $p_{1/2}$data are all in the 100 ... 200 MPa range, and the presence of allosteric effectors significantly modify these values. In the case of Zn-HbA the transition pressure decreases, while in oxy-HbA it increases.

3.4.1 *The transition is related to dissociation.*

As already mentioned, this transition can be interpreted as a pressure-induced dissociation of the tetrameric structure into two monomers. This interpretation is supported by the following rationale:

3.4.1.1 *Trp-s in the interface region.*

The HbA tetramer has six Trp residues, one in each α- and two in each β-subunits. It was realized a long time ago that Trp fluorescence could

Table 6: Mid-transition pressure values ($p_{½}$) of oxy-HbA and Zn-HbA under different conditions.

Hb type	concentration [mM]	added effector (with conc.)	$p_{½}$ [MPa]
Zn-HbA	0.68	none (stripped)	200
	0.23		160
	0.02		135
	0.06		140
	0.06	100 mM Cl^-	113
	0.06	2 mM DPG	94
	0.06	2 mM IHP	72
	0.06	10 mM BZF	165
oxy-Hb	7.7	none (stripped)	225
	0.77		157
	0.06		100
	0.06	100 mM Cl^-	137
	0.06	2 mM IHP	144
	0.06	10 mM BZF	170

be used to monitor conformational changes i.e. T $\rightleftharpoons$ R transition, and this sensitivity of the signal was assigned mostly to Trps β37 which are located at the $\alpha_1\beta_2$ and $\alpha_2\beta_1$ subunit interfaces[61, 62, 60]. In resonance Raman spectra obtained by UV excitation the contribution assigned to these Trp residues can be separately analyzed and used to monitor local structural changes in the interface region [112, 113]. In a fluorescence study, the sensitivity of the signal to structural changes relies significantly on the conditions for quenching by Förster-type energy transfer to the hemes. The Trps in HbA are within short distances from one or more hemes of the structure, thus the distance requirements of energy transfer are fulfilled (data can be seen in [117, 72]). This also explains that the fluorescence of Zn-PP can be excited through Trp excitation at 290 nm as seen in Figure 24. The energy transfer is also indirectly detectable through the relatively low quantum-yield of the Trp fluorescence. Energy transfer could also be tracked down indirectly by the low quantum yield of Trp emission in HbA. The β37 Trp is the Trp closest to the neighboring α subunit heme (Trp $\beta_1$37 to the α_2 heme, and Trp $\beta_2$37 to the α_1 heme). This distance is liable to become easily perturbed by changes at the inter-dimeric interface. It should be noted however, that Trp $\alpha_1$14 , Trp $\beta_1$15 and Trp $\beta_1$37 are within a short distance of their respective intra subunit heme group (the same holds for Trp $\alpha_2$14 , Trp $\beta_2$15 and Trp $\beta_2$37), thus are also subject to energy transfer to their heme groups, but since this heme is part of their respective subunits, a possible dimer-dimer separation should not perturb this type of energy transfer significantly. Furthermore, Trps α14 and β15 are far away from the interface, a change at the interface region should not perturb their fluorescence properties significantly. Based on the distance data, one can suppose that the fluorescence of Trps β37 will be sensitive to dimerization.

3.4.1.2 *Red shift of the Trp emission.*

Red shift is usually assigned to a local environment of increasing polarity, as in the case of exposure to water[107, 149], however, changes in the electric field and in the dipole moments around the Trp residue can also result in the shift of the Trp emission spectrum[107]. Since pressure-induced unfolding is ruled out, significant electric field or dipole moment changes in Trp surroundings can only be due to exposure to water. The Trps β37 are somewhat buried in the tetramer, but become solvent exposed in the dimer form. Thus a tetramer-dimer transition and a consequent water exposure could explain the observed red shift.

Figure 28: Concentration - dependence of the $p_{1/2}$data in oxy-Hb (squares) and Zn-HbA (diamonds).

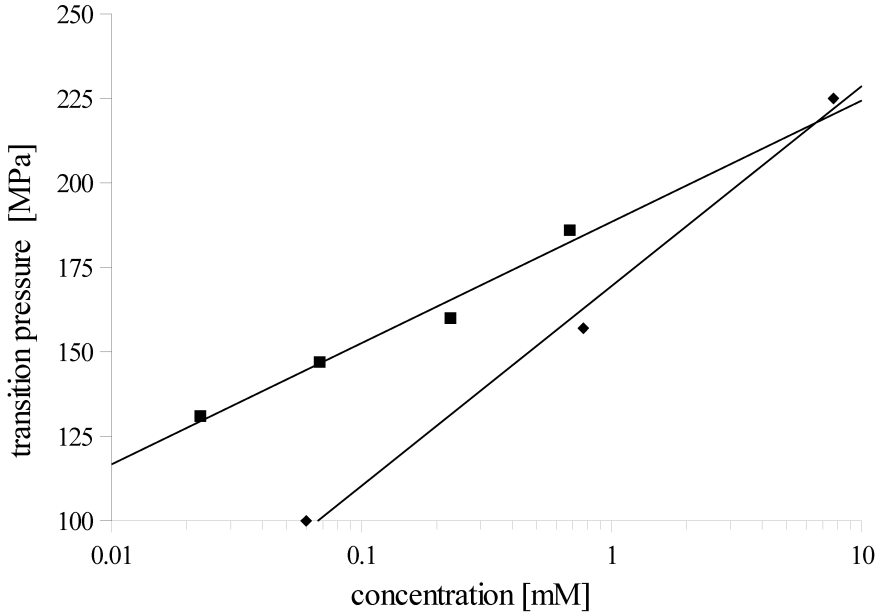

3.4.1.3 *Intensity increase during the transition.*

Besides the red shift, the intensity of the fluorescence emission is *increasing* during the pressurization. This can be attributed to - and is consistent with a *decrease* in the efficiency of the energy transfer to the heme groups of the neighboring dimer due to the tetramer dissociation. This effect would mostly influence Trps β37. Published energy transfer rates [49] indicate, that these Trps are the only ones having energy transfer rates to a heme in the adjacent dimer comparable to the heme in their own monomer (cf. Table 5. in [49]). The known strong dependence of energy transfer efficiency on the donor-acceptor separation explains the significant quantum yield effect. This argument is further supported by literature data, available for Trp fluorescence lifetime of HbA [50]. The ratio of a long component of the Trp lifetimes was shown to increase with pressure, and was attributed to pressure induced changes in the quaternary structure. In the case of the multimeric Hb of Lumbricus terrestis, a similar change in Trp fluorescence was also observed[62]

3.4.1.4 *Concentration dependence*

The concentration dependence of the transition pressure is shown in Figure 28, it clearly supports the tetramer $\rightleftharpoons$ dimer transition model : dissociation reactions are known to depend strongly on the concentration

of the initial molecule, while this dependence would not be expected for unfolding or denaturation reactions. Also, if the observed effect would be due to a possible shift in the ratio of possible different sub-populations in the T state[1], a concentration dependence would not be expected. Besides the pressure-induced red shift and intensity increase in Trp fluorescence, also a significant broadening in the Trp emission band can be observed. This can be attributed to an increased heterogeneity in the fluorescent Trps when dimerization takes place. The broad initial (atmospheric) Trp emission spectrum reflects also to an initial heterogeneity of the fluorescent Trps, which can be partially also attributed to the existence of conformational sub-populations.

3.4.1.5 *Pressure induced dissociation is well known*

High pressure dissociates protein oligomers by squeezing water molecules into the voids. This model was experimentally verified by H/D exchange experiments[135]. Theoretically this is also expected since *ordered water molecules have a smaller volume than those in the bulk solution*, and thus based on the LeChatelier-Braun principle, the disintegration is favorable under increasing pressure. High pressure induced dimerization - and also monomerization - of HbA have been previously demonstrated based on fluorescence labeling and anisotropy measurements [105][2].
Based on these considerations, it is very likely that the observed changes in Trp fluorescence under high pressure report on the change of the tetramer $\rightleftharpoons$ dimer equilibrium. In the next section I will present a simple model, which relates these changes to the observed changes in the emission spectra.

3.4.2 *A simple model of the pressure-induced dissociation*

First we define a parameter α for the degree of dimer formation such, that $\alpha = 0$ represents the fully tetrameric state, and $\alpha = 1$ represents the total dissociation, i.e. the fully dimeric state. Thus the concentration of

1 The T-state population is known to be a sum of multiple conformational sub-populations, this is referred to as the "plasticity" in the T-state. This is more pronounced in hybrid hemoglobins than in the native deoxy HbA [111, 112, 113, 87].

2 These data are, however not fully comparable with our results, since differences in the experimental conditions (different buffers, pH, and sample preparation methods) are known to influence the stability of the HbA tetramer. We used pH7.4 where HbA is primarily in the tetrameric form. Also, there was no attempt in [105] to calculate dissociation constants from the data.

the tetramer *[T]* and dimer *[D]* forms can be expressed with α, and the total protein concentration C_o:

$$[T] = (1-\alpha)C_0 \qquad [D] = 2\alpha C_0 \tag{13}$$

The dissociation constant K_d can then be expressed as:

$$K_d = \frac{[D]^2}{[T]} = \frac{4\alpha^2 C_0}{1-\alpha} \tag{14}$$

Manipulating Equation (14) to solve for α and discarding the negative solution yields:

$$\alpha = \frac{\sqrt{K_d^2 + 16K_d C_0} - K_d}{8C_0} \tag{15}$$

Where K_d is a function of pressure and dissociation - volume (ΔV) according the thermodynamic equilibrium:

$$K_d = K_{d0}\, e^{\frac{-p\Delta V}{RT}} \tag{16}$$

Through Equation (16) α is also a function of pressure, and K_d is equivalent to the dissociation constant measured with conventional methods at atmospheric pressure (K_{do}). Substituting Equation (16) into Equation (15) yields a sigmoid-like function:

$$\alpha = \frac{\sqrt{K_{d0}^2\, e^{2\frac{-p\Delta V}{RT}} + 16C_0 K_{d0}\, e^{\frac{-p\Delta V}{RT}}} - K_{d0}\, e^{\frac{-p\Delta V}{RT}}}{8C_0} \tag{17}$$

Taking into account that the spectrum in the first-order approximation is a linear function of α, e.g., the maximum position of the Trp emission peak may be approximated with:

$$\lambda_{max} = \lambda_0 + \alpha \cdot \Delta\lambda \tag{18}$$

Table 7: K_{do} and ΔV data of oxy-HbA and Zn-HbA under various conditions, and at 60μM concentration. The relative error of the data is approximately 5%.

Hb type	effector and concentration	K_{do} [$\cdot 10^{-6}$ M]	ΔV [mL/mol]
oxy-HbA	none (stripped)	1.41	-99.5
	100 mM Cl^-	1.22	-83.2
	2 mM IHP	0.47	-97.7
Zn-HbA	none (stripped)	0.44	-105.3
	100 mM Cl^-	0.78	-106.6
	2 mM DPG	2.06	-103.6
	2 mM IHP	12.9	-83.4

where λ_o is the emission maximum position on the wavelength scale at atmospheric pressure, and $\Delta\lambda$ is the total spectral shift. This approximation can be combined with Equation (17) to yield:

$$\lambda_{max} = \lambda_0 + \frac{\sqrt{K_{d0}^2 e^{2\frac{-p\Delta V}{RT}} + 16C_0K_{d0}e^{\frac{-p\Delta V}{RT}}} - K_{d0}e^{\frac{-p\Delta V}{RT}}}{8C_0} \cdot \Delta\lambda \quad (19)$$

This function can then directly be fitted to the data shown in Figure 27, to yield the parameters K_{do} and ΔV. The data obtained with this model are shown in Table 7.[3] The $p_{½}$ values can be related to this model, they are the pressure values corresponding to $\alpha = ½$.

In fact the solid lines in Figure 27 are curves obtained by fitting Equation (19) to the data

The data show that allosteric effectors distinctly influence the dissociation constant (K_{do}), and the dissociation-volume (ΔV) in oxy-HbA and Zn-HbA.

3 The data of BZF are missing from the table. This is due to the fact, that BZF has its own fluorescence emission, and it interferes with the Trp signal. The half-dissociation pressure $p_{½}$ can be reliably obtained, but the fitting of Equation (19) can not be performed. This, and further remarks on BZF fluorescence data is discussed in detail in [117]. It has to be also noted, that the fitting of Equation (19) is an ill-conditioned problem, and thus the uncertainty of the values (estimated by the s.d. of the fitting to be approximately 5%) may be somewhat larger than the s.d. values coming from the fitting process. Therefore the use of $p_{½}$ is also worthwhile.

3.4.3 *Analysis of the data*

The dissociation model can be further verified, if we express the concentration-dependence of the $p_{½}$ values, by solving Equation (17) for α, and then substituting α = ½ yields a logarithmic function, which is the same as shown in Figure 28.

$$p_{\alpha=1/2} = \frac{RT}{\Delta V} \cdot \log\left(\frac{K_0}{2C_0}\right) \tag{20}$$

There are many points, which can be discussed to relate the results to other data in the literature. This can be read in [117], I will present only the main points here.

A HbA solution is always a dynamic mixture of tetramers and dimers, however the dimer concentration is usually very low. The dimer-tetramer equilibrium was extensively studied along with the kinetics of the dissociation [4, 6, 152, 12, 23, 59]. Under our conditions the dimer ratio is estimated to be less than 1% in the R state of oxy-HbA , and less than 0.1% in the T state (Zn-HbA). Physiological conditions (high protein concentration, close to neutral pH) shift the equilibrium towards the tetrameric form. Considering the data for the R state, the determined dissociation constants (K_{do}) agree well with previous reports on R state HbA[6], where tetramer to dimer dissociation constants were measured in the case of stripped human oxy-HbA, and also in the case of the IHP-complexed HbA, *the values agree within experimental error*. This again very strongly supports the presented simple model, and the interpretation behind it. many other dissociation constants were not measured in the literature before, primarily due to experimental limitations (e.g., the dilution method would also dilute the effector, while other methods may influence the oxygen binding, and thus artificially shift the equilibrium).
It is important to note, that in both cases the $K_{do}$and ΔV data strongly depend on the presence of allosteric effectors. This further supports the global allostery model. In the original argumentation for that model was based on the strong modulation of oxygen-binding (association constants K_R and K_T) in both R- and T- states of HbA by these effectors. It is interesting to see, if the changes in the K_{do} values can account for the observed modulation of the association constants. This we can do for the R state based on characteristic half oxygen-saturation (P_{50}) values from the literature [6], P_{50}= 0.4 mmHg for the dimer form and 1.78 mmHg for the tetramer. As an approximation, we can assume that the proportion of the dimers is low enough (less than 1%), such that the measured P_{50} values can be considered in a first approximation as a linear combination of the tetramer- and dimer - P_{50} values. Since from K_{do} we know the propor-

Figure 29: Summary of the changes in equilibria caused by allosteric effectors

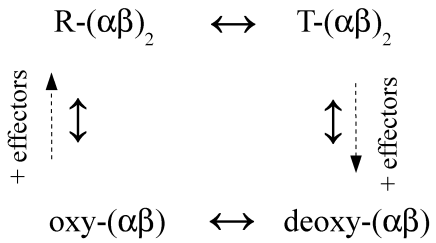

tion of the dimers, we can estimate the change in P_{50} caused *only* by a change in the tetramer $\rightleftharpoons$ dimer equilibrium. Under our experimental conditions (i.e. 60µM total HbA concentration, and pH 7.4) and for the IHP binding to oxy-HbA as an example, we obtain a 10% increase in P_{50} as an estimate. In the literature, the *reported changes in P_{50} are more than a magnitude higher* [155]as an effect of binding IHP, that is, *changes in the dissociation constants can not account for the total effect of allosteric effectors on oxygen binding. This again supports the idea, that changes in K_{do} and ΔV are accompanied by subtle, but important changes in the overall structure and dynamics of the entire tetramer.*
Finally, the changes in the equilibria caused by allosteric effectors are summarized in Figure 29.

Double ended arrows represent the equilibria, and dashed arrows show the influence of allosteric effectors. *The changes in these equilibria are most probably a direct consequence of tertiary structural changes propagating from the effector binding sites to the dimer interfaces in both quaternary states.*[4]

4 There are more possible speculations, but these will be presented in chapter 5. In short, most probably the changes caused by allosteric effectors are being indirectly monitored by the dissociation parameters, and the primary change may be in the dynamics, which will then affect the overall interface tightness, and strength.

4

RELATION TO COMPRESSIBILITY

4.1 INTRODUCTION TO FLUORESCENCE LINE NARROWING

Fluorescence line narrowing (FLN) is a high resolution technique[100], which is often used to study the vibronic energy map of a given chromophore. It requires cryogenic temperature, to decrease the vibrational coupling to the matrix, and also to increase the Debye - Waller factor (and also reduce temperature-broadening), and narrow laser excitation to achieve resolved fluorescence emission spectra. Since at low (approximately 10K) temperature there are very few thermally induced excitations, and conformational transitions can almost totally be excluded, the excitation by a narrow - bandwidth laser source excites only certain sub-populations (in the electronic transition-energy) of the chromophore. This is emphasized in Figure 30, where in the upper figure panel "A" shows a number of chromophores being randomly distributed on the energy-scale. Every molecule has a distinct (0,0) $\rightarrow$ (1,0) electronic transition energy, since it is perturbed by the protein matrix, and every protein molecule of the ensemble has a somewhat different 3D structure, which is then reflected in a distribution of the transition energies around a mean value (as the structures are distributed around the "average" structure). We can order these molecules according to their (0,0) $\rightarrow$ (1,0) electronic transition energies, as seen in panel "B". As a first approximation, it can be supposed that in every chromophore the (0,0) $\rightarrow$ (1,0) transition energy is perturbed by its protein environment, but within a given electronic band the energies are not changed with respect to each other, thus all the (1,0) $\rightarrow$ (1,i) energies are the same in all chromophores[1], thus the lines in panel "B" are parallel. As a model, the distribution of the (0,0) $\rightarrow$ (1,0) transition energies are assumed to be Gaussian, but it can be any other distribution as well. The bottom figure shows the situation during a narrow-band laser excitation. A laser with ε_g energy and $\Delta\varepsilon_g$ bandwidth (shown on the right as an arrow, and black horizontal line through the distribution-map) is resonantly exciting some sub-populations of ΔN_p

This is a very basic introduction to the use of FLN, interested readers are directed to excellent review articles [37, 91, 134, 36]

1 This means that only the electronic states of the chromophore are perturbed by the surrounding protein matrix. If this is not the case, then it only adds another correction-factor, but it does not change the main theory

Figure 30: Demonstration of the FLN technique. Upper figure shows the ordering of molecules on the energy-scale, bottom figure shows the fluorescence emission by a narrow-band excitation. See text for details. Figure reprinted with permission from [68]

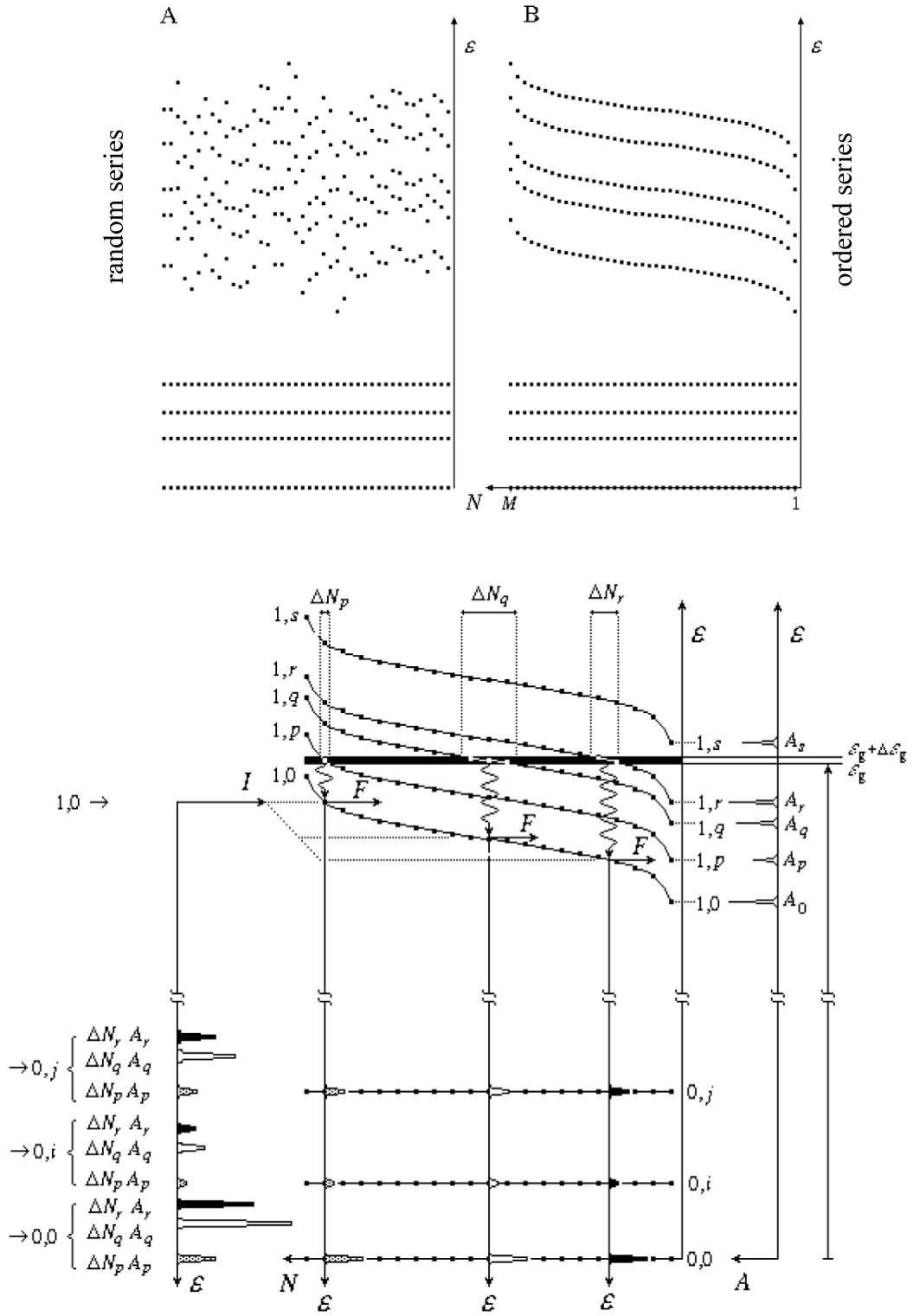

Figure 31: Comparison of room-temperature emission spectrum (blue line) and FLN resolved emission spectrum (red line) of Zn-HbA.

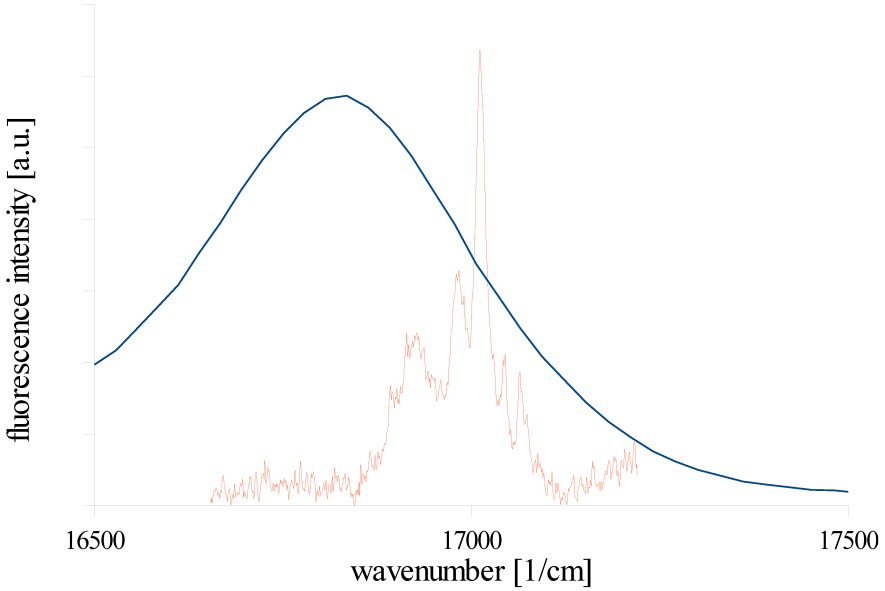

, ΔN_q and ΔN_rsizes. Each sub-population has a different absorption quantum-yield, and also a distinct emission quantum-yield. On the F - ε scales the individual emissions of the sub-populations are shown, while on the left side I - ε graph shows the composite emission spectrum which can be recorded with the instrument. This recorded emission spectrum is distinct from the room-temperature conventional fluorescence emission spectrum. In a conventional fluorescence experiment the excitation is broad-band relative to the FLN: in FLN the bandwidth is approximately 20 GHz in our experiment, while at about 400 nm excitation wavelength the 5 nm bandpass is equivalent to approximately 10^4 GHz. This causes practically all sub-population to be excited at room temperature, and also the sub-populations freely inter-convert during the experiment. The vibrations of the chromophores are also thermally excited, all these factors lead to a broad emission peak. A comparison is shown in Figure 31, the conventional spectrum is the same as in Figure 24, but only the part overlapping the FLN experiment is shown, converted, and corrected[66] to wavenumber scale.

As can be seen, the FLN spectrum is resolved, it contains sharp emission lines resulting from resonant vibronic excitations, superimposed on a background of broad bands, which are also present due to emissions from non-resonant phonon-coupled excitations[37, 43] . The spectra taken under the fine tuning of the excitation frequency allow for determining the vibrational levels of the electronically excited state, and the inhomo-

geneous distribution function (IDF) as follows. It is long known, that by shifting the excitation laser energy (ε_g) the observed sharp peaks of the resolved spectrum also shift with the same energy difference as the excitation laser as seen in Figure 33. This can be explained by looking at the bottom of Figure 30. Let us assume, that we are exciting on the $q^{\text{-th}}$ curve, thus ΔN_q number of chromophores are excited from the (1,q) vibronic line, which has an A_q absorption quantum-yield. By shifting ε_g to a new value, within the same distribution (thus we do not leave the $q^{\text{-th}}$ curve corresponding to A_q), ΔN_q will change according to the overlap of the laser line-width and the $q^{\text{-th}}$ distribution function. The emission energy of the peak corresponding to this $q^{\text{-th}}$ curve will be always shifted with respect to the ε_g laser energy by the (1,q) $\rightarrow$ (1,0) energy difference [2]. Since the laser is exciting in most cases not only one vibronic line, e.g., "q" but mostly several others at the same time (in the figure "p" and "r" too) multiple sharp peaks can be seen in the spectrum at different position, and they all shift parallel with the shifting of the laser. Since the intensity of the peak is proportional to ΔN_q at a given laser energy, it is important to note, that $\Delta N_q$is not only graphically the overlap of the $q^{\text{-th}}$ distribution with the laser line-width, but also the derivative function of the $N_q(\varepsilon)$ distribution function. If we plot the amplitudes of the peaks in a given series, then the ratio of the peak heights $\omega_p(\varepsilon)$ is proportional directly to this derivative function, which is the IDF itself. Thus:

$$\omega_q(\epsilon) = A_q \cdot \Delta N(\epsilon) \qquad \Delta N(\epsilon) = k \cdot \frac{\Delta N}{\Delta \epsilon} \cdot \Delta \epsilon_g \tag{21}$$

As can be seen in Equation (21) the IDF ($\Delta N/\Delta\varepsilon$) differs only by a constant from $\omega_p(\varepsilon)$, the normalized peak-height function. Since this is true for every peak-series, to reliably determine the IDF of a given sample, it is important to simultaneously track every series, and then fit the "peak-height" distributions together.

While the individual vibronic distributions themselves are also reporting on the environment of the chromophore[3], it is more interesting to relate the IDF to the dynamics of the system. According to the fluctuation-dissipation theorem of statistical physics [76] the volume fluctuations $< V$

2 which is constant in a first approximation. If not, then it can be seen as a non-linear, non parallel shift of the emission peak with respect to the laser energy shift.

3 And thus changes in the vibronic energy map would report on changes in the surrounding protein structure. It can also be estimated that the "range of sensitivity" is a few Å, since the solvent shift of a given chromophore in a given protein is caused by electrostatic and dispersive interactions[13] which both fall off by R^{-n}.

- $< V >>$ of a system - arising from conformational dynamics in a protein - can be characterized by its compressibility (χ):

$$< V - < V >>= \sqrt{\kappa k T < V >} \tag{22}$$

where V is the volume of the protein, k is the Boltzmann - constant and brackets denote averaging. Since the volume fluctuation is proportional to the square - root of the compressibility, determining the compressibility at higher pressures than physiological can also reveal important aspects of protein dynamics. The volume fluctuations will still be not too large to destroy the structure, if denaturation due to pressure can be circumvented. A cryogenic method is well suited to this task, since in the frozen state denaturation is not expected to occur,even at very high pressures, because the boundary of the protein is firmly bound to a solid matrix. This inhibits any large-scale conformational change, thus prevents the denaturation of the protein.
As can be seen from the room-temperature data in Figure 24 the broad emission shifts with pressure. A similar shift by pressurization of the IDF determined by FLN can also be observed. The compressibility can be calculated from this shift of the IDF, as described in detail in [126]. In short, the shift of a given spectral line from ν_o to ν_p under pressure is proportional to the solvent shift (ν_o- ν_{vac}) of the environment, where ν_{vac} is the vacuum frequency, the wavenumber, where the given chromophore in a hypothetical situation - of being in the absence of environmental interactions, but with unchanged conformation - would absorb light. In a linear approximation and supposing that the effect of the environment can be described with a potential proportional to R^{-6} distance dependence, the model leads to the formula[74]:

$$\nu_p - \nu_0 = 2(\nu_0 - \nu_{vac})\kappa p \tag{23}$$

This model was used successfully to describe pressure induced shift of the optical transitions in glassy matrices, and also in proteins [43, 158, 157]. In the case of the shift of the IDF, one has to consider not a single spectral line - as being the case in Equation (23), but a distribution of the solvent shift values. If we assume a normal distribution, or a sum of normal distributions, then it can be calculated that:

$$\nu_{0p} = \nu_{00} + 2\kappa p \cdot (\nu_{00} - \nu_{vac}) \qquad \sigma_p = (1 + 2\kappa p)\sigma \tag{24}$$

where the extra "0"-s in the indices emphasizes the fact that this corresponds to the center of the normal distribution, and σ is the width of the normal distribution. If the IDF can be approximated by a normal distribution, then Equation (24) also holds for the IDF[4]. It can be seen, that the shift of the IDF is also accompanied by a broadening if the pressure is increased. The slope of both the broadening and the shift on the energy scale is proportional to the compressibility, and thus to the volume fluctuation of the system. In the next section data obtained from Zn-HbA under different conditions is presented, and discussed.

4.2 COMPRESSIBILITY RESULTS

The experimental setup was the following:
For the FLN experiment we used a Coherent 899-01 ring dye laser pumped by an Coherent Innova 307 Ar-ion laser. The dye used for excitation was Rhodamine 560 or 590 (Exciton Laser Dyes). The spectral width of the laser line was 0.5 cm^{-1},the output power was 0.3 ... 0.6 mW/mm^2. Fluorescence emission was collected at approximately 35° angle relative to excitation and focused into a THR 1000 monochromator (Jobin-Yvon). For detection a CCD camera (WR CCD-4679 DV401-BV, Andor Technology) cooled to -65°C was used, mounted at the exit slit of the monochromator. Integration time was 20 ... 60 s for each spectrum. The sample was maintained at 10 K inside a diamond anvil cell with a closed cycle M22 cryostat (Cryophysics SA) equipped with a Model-330 auto-tuning temperature controller (Lake Shore Inc). Pressure inside the cryostat was 10^{-2}mbar, it was monitored with a model AGD-101-L Pirani-gauge (Edwards High Vacuum International), and a vacuum was generated with a rotary vacuum pump (model RV5, Edwards High Vacuum International). The concentration of Zn-HbA was 60µM in 50% v/v glycerol:buffer solution mixture (buffered to pH7.4 with 100mM HEPES). Pressure was adjusted with helium gas in the special low-temperature diamond anvil cell (Diacell Products). This cell of 40 nl volume allows for applying pressures in the range of 0 ... 2 GPa. A ruby chip frozen into the sample was used for the pressure determination[38], which also made it possible to check the temperature inside the cell [151]. The accuracy of the pressure values measured at low temperatures was typically 0.2 kbar. The schematic representation of the experimental setup is shown in Figure 32.

4 If the IDF can be approximated by the sum of normal distributions, then each Gaussian component will have its own shift and broadening.

Figure 32: Schematic representation of the FLN experimental setup. The bottom left picture shows the photograph of the diamond cell mounted on the cold-finger of the cryostat, the small mirror is used to direct the excitation light (green line) to the sample, while the big mirror is placed into the setup for photographic purposes, only to show the other side of the cell. The upper right picture shows the setup with the cryostat closed and operating.

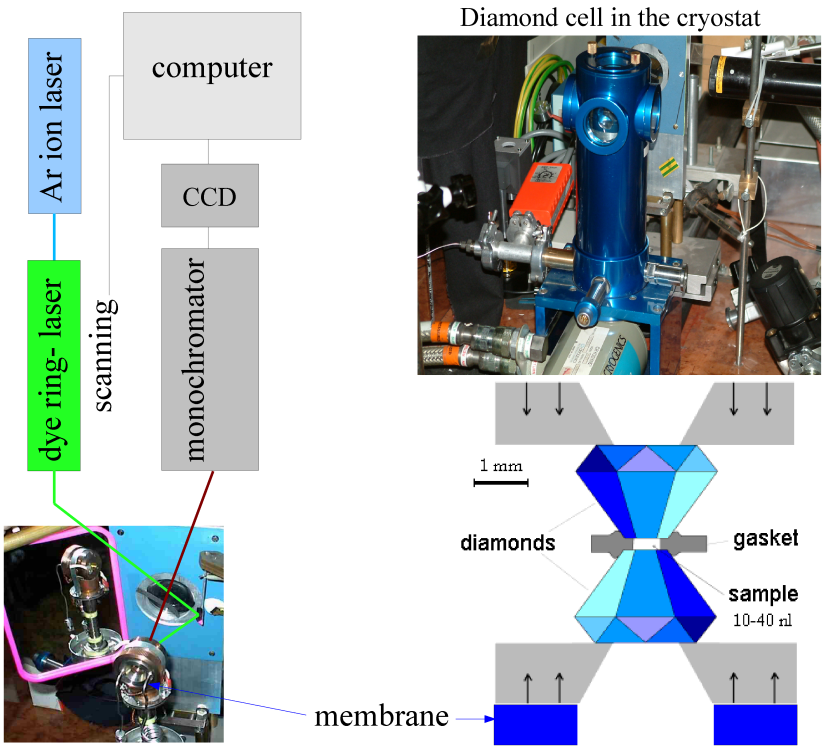

As discussed in the introduction, the IDF can be calculated by following a single peak of the resolved emission spectrum, and determining the amplitudes at each excitation laser energy. The IDF can then be determined from any of these series, but most reliably from all series together.

As can be seen in Figure 33 already in a few spectra many peaks can be found, and they all have to tracked individually, and "peak-heights" have to be determined. It is also important to subtract the non-resonant, phonon - coupled, excitation - background. I have written a software package ("IdfFit" [5]) to automate this task. The software is custom-designed to also allow for the wavenumber - calibration of the CCD camera attached to the monochromator in the experimental setup, and it outputs

5 For a more detailed description see Appendix Section §B.2.

Figure 33: A sample series of resolved spectra. The sample is Zn-HbA + 100 mM NaCl at 1.4 kbar. The spectra are shifted along the intensity axis for clarity. The excitation laser scanned the range of 17840 cm^{-1} ... 18214 cm^{-1}.

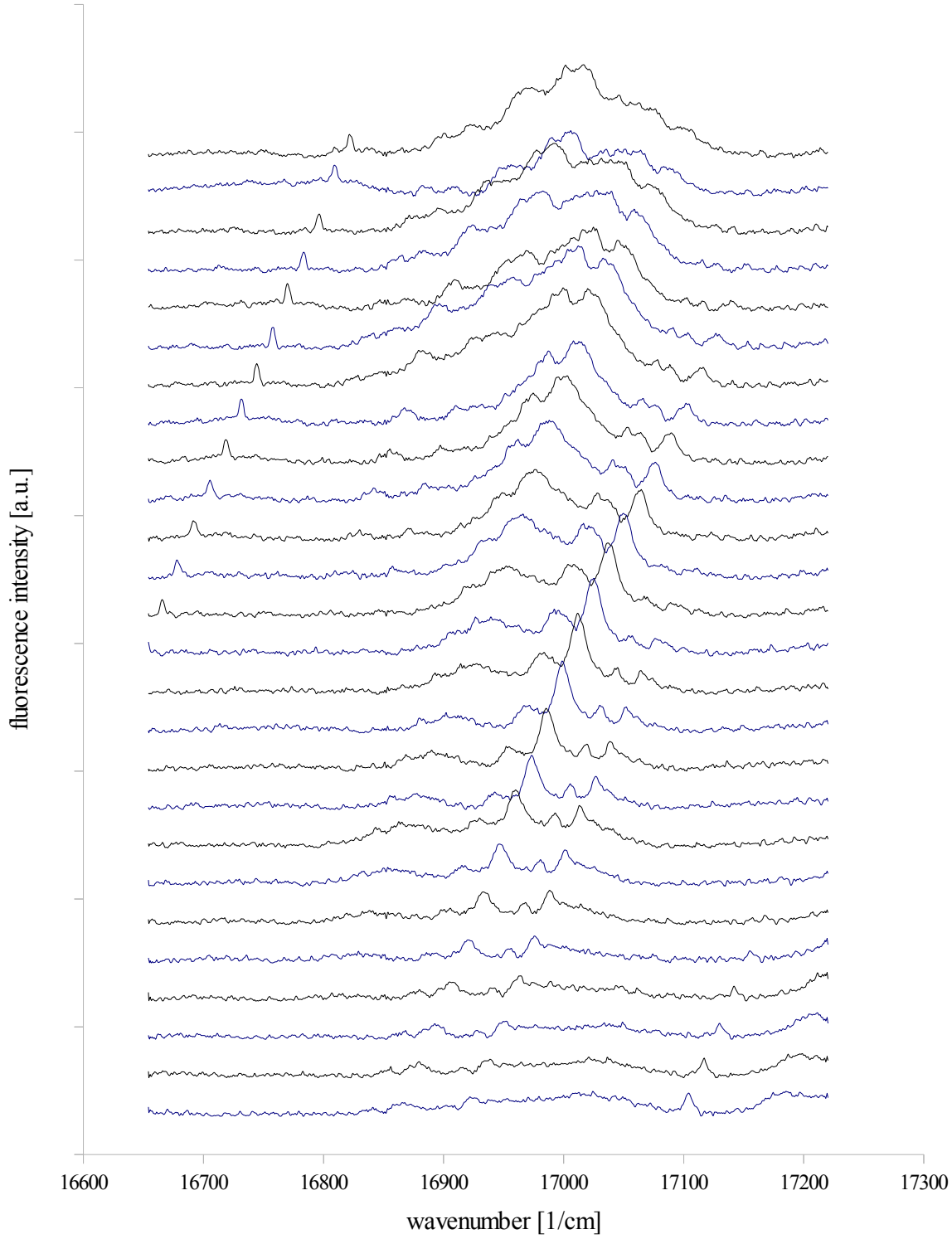

Figure 34: The IDF of Zn-HbA + 100mM NaCl at 1.4 kbar. The figure shows the raw output of the IdfFit program as an illustration of the calculation of the IDF. The program also reports the parameters of a Gaussian fitting to the data.

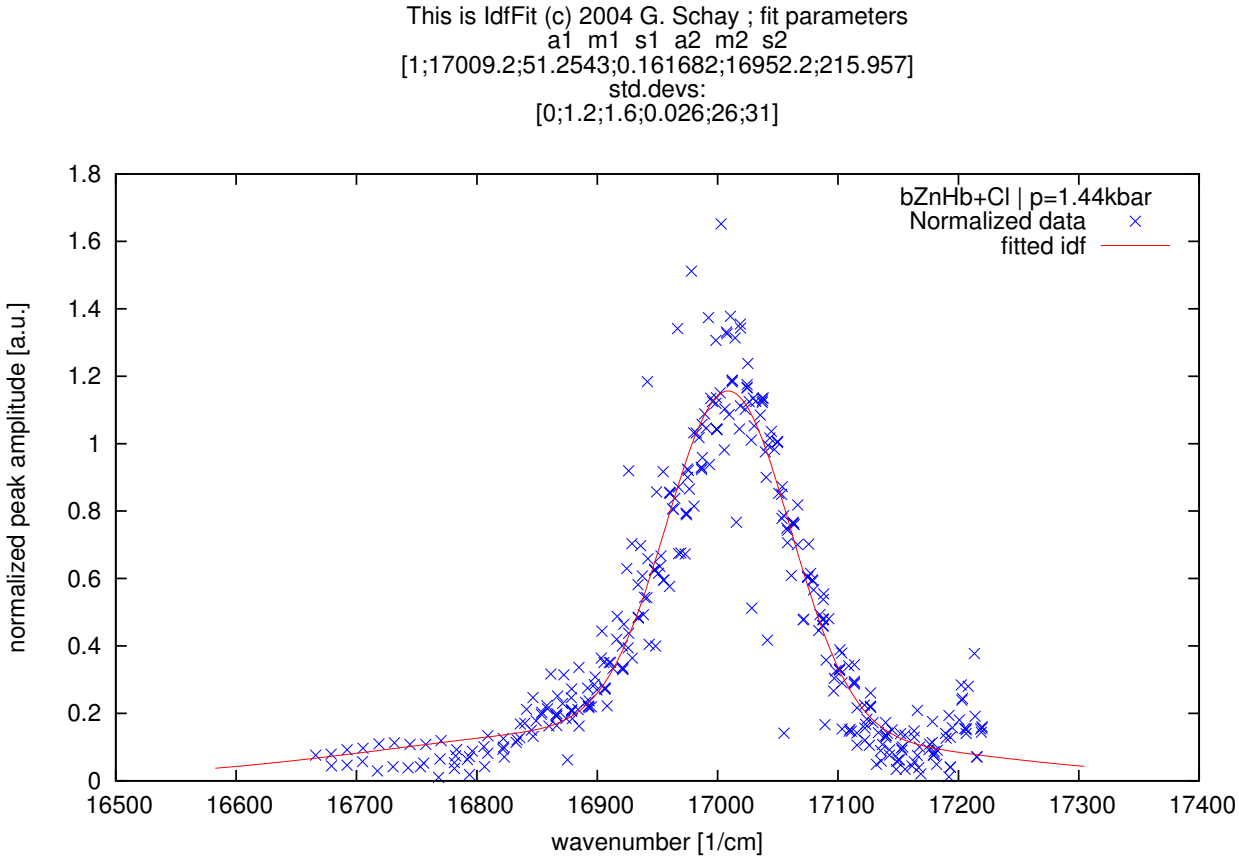

both the IDF, and a tracking-report of each peak-series. Typically 120 ... 160 spectra were recorded and processed at each pressure level, Figure 33 shows only a fraction of these for clarity. An example IDF calculated from this spectral series is shown in Figure 34. As can be seen, the main component of the IDF is a single normal distribution, thus Equation (24) can be used to estimate the compressibility[6]. The IDF also shifts with increasing pressure, as shown in Figure 35. As apparent from the figure, the center of the IDF on the energy (wavenumber) scale shifts with pressure, and a simultaneous broadening can also be seen.

6 The program reports the s.d. in percent, see the error bars in Figure 36 for the absolute values.

Figure 35: Shifting of the IDF due to increasing hydrostatic pressure. As an example the IDF-s of Zn-HbA + 100 mM NaCl is shown, and for clarity the individual data-points are omitted, and the IDF-s are shifted along the vertical axis. The pressure levels in kbar units, corresponding to each curve, are shown in the top of the figure. The shift of the IDF-s is not proportional to the pressure increase.

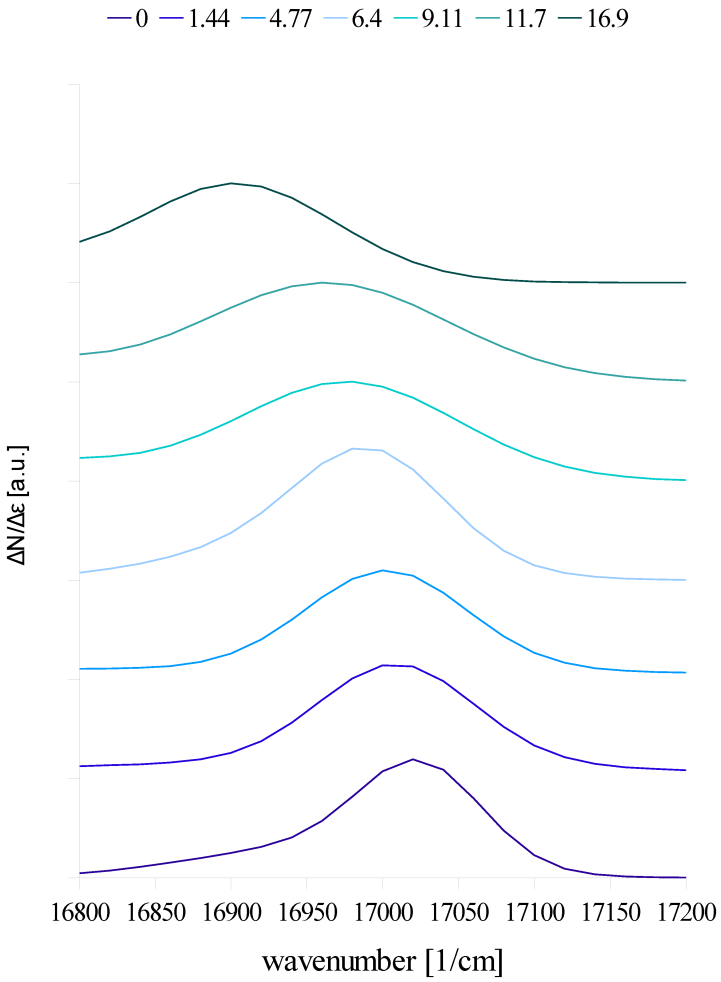

Figure 36: IDF position and width values (with s.d.) for various Zn-HbA samples under pressure.

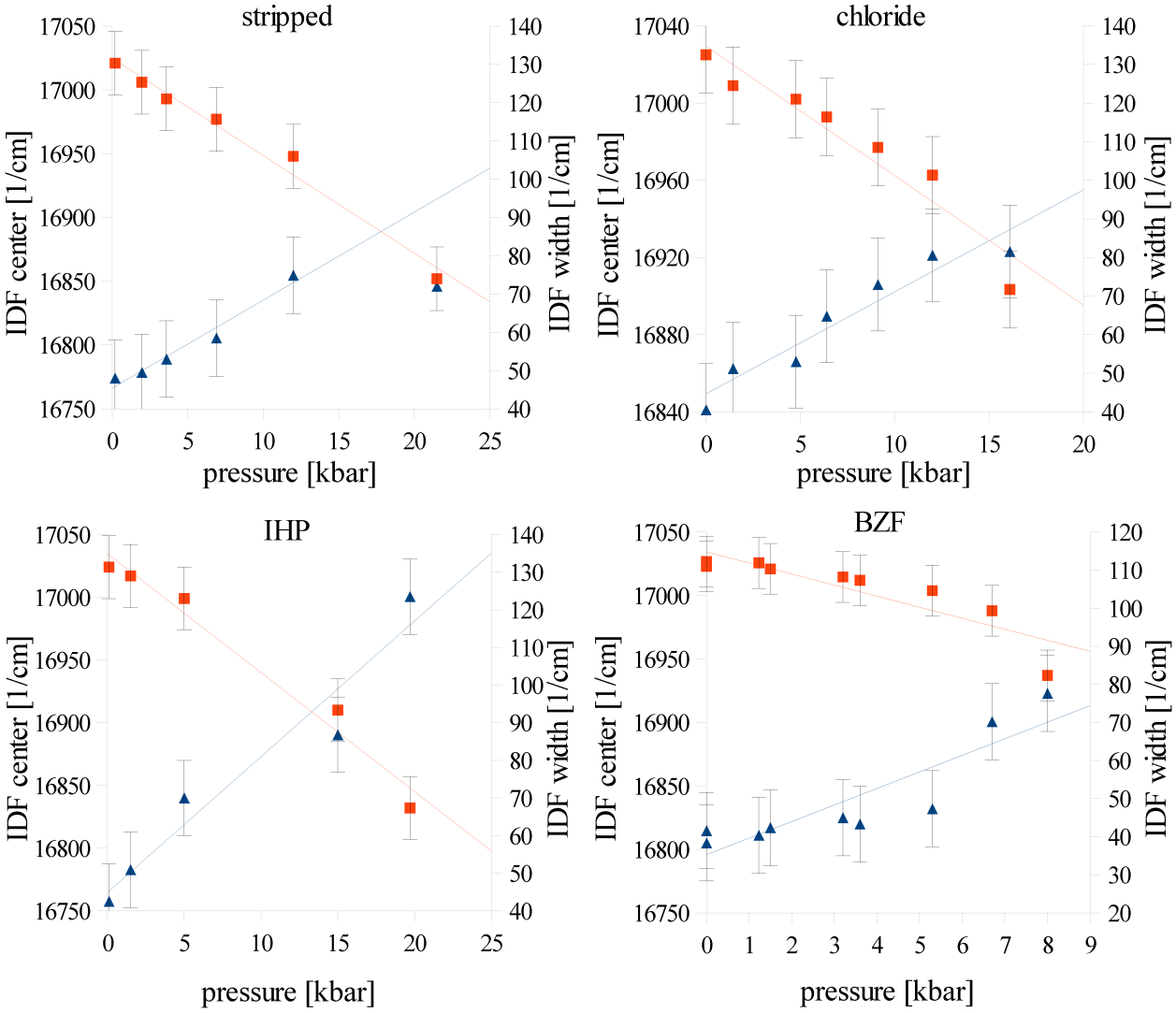

The FLN experiment was performed on Zn-HbA in the stripped condition, with 100 mM Cl^-, 2 mM IHP and 10mM BZF. The shift of the IDF center positions on the energy scale, and the width of the IDF at various pressure levels are shown in Figure 36. It can be seen that the shift of the IDF fits relatively well to the linear model predicted by Equation (24), although at pressure values above approximately 15 kbar deviations may be found (e.g., in the BZF figure, the position of the last point at high pressure is an outlier, most probably due to some change around the chromophore), and the elastic compression model may not hold at very high pressure values. It can also be seen that the slope behaves in a similar manner, the shift being linear up to about 15 kbar. This indicates, that

by raising the pressure over this limit, a possibly local structural change happens around the chromophore.

4.3 DISCUSSION OF COMPRESSIBILITY

The deviation from linearity at very high pressure values may arise from local non - isotropic changes in the structure around the chromophore. This may involve a slight rearrangement of side-chains, which can lead to a change in the interactions between the chromophore and the protein matrix. This change is reversible, since we have always recorded an absorption spectrum also after the FLN experiment, and no significant changes were found in any samples. Although a slight change can not be excluded, significant rearrangements certainly do not take place.
The lines in Figure 36 indicate a linear regression to the data, the parameters of the regression are listed in Table 8. As apparent from the table, there is a slight change in the slope of the IDF - center-position vs. pressure data upon the addition of allosteric effectors. This change is almost within the error, and in the case of BZF the direction of the change is inverse with respect to the change caused by chloride or IHP. It can also be seen, that the center of the IDF at atmospheric pressure (ν_o) does not depend significantly on the presence of allosteric effectors. This may indicate, that the effectors do not cause a significant reorganization of the protein structure around the chromophore, at least not in the sensitivity-range of this method (which is a few Å). This is also seen in Figure 37. The same conclusion can be drawn from the broadening data, the slope is positive, as expected, but the change caused by allosteric effectors is almost within the s.d. range. Since the vacuum-frequency (ν_{vac}) is not known for Zn-PP in Zn-HbA, therefore the compressibility values can not be calculated, but *it is not the absolute value of the compressibility, which is important in the interpretation of the data, but more the change caused by allosteric effectors*. The presence of only a very small effect can be related to the previous results, but the relation is not straightforward, and also not ambiguous. Therefore my thoughts about a possible interpretation better fit in the speculations section of chapter 5

Figure 37: Overlay of the IDF shifts of Zn-HbA in the stripped (red, squares), with 100mM NaCl (green, triangles) and 10mM BZF (orange, triangles).

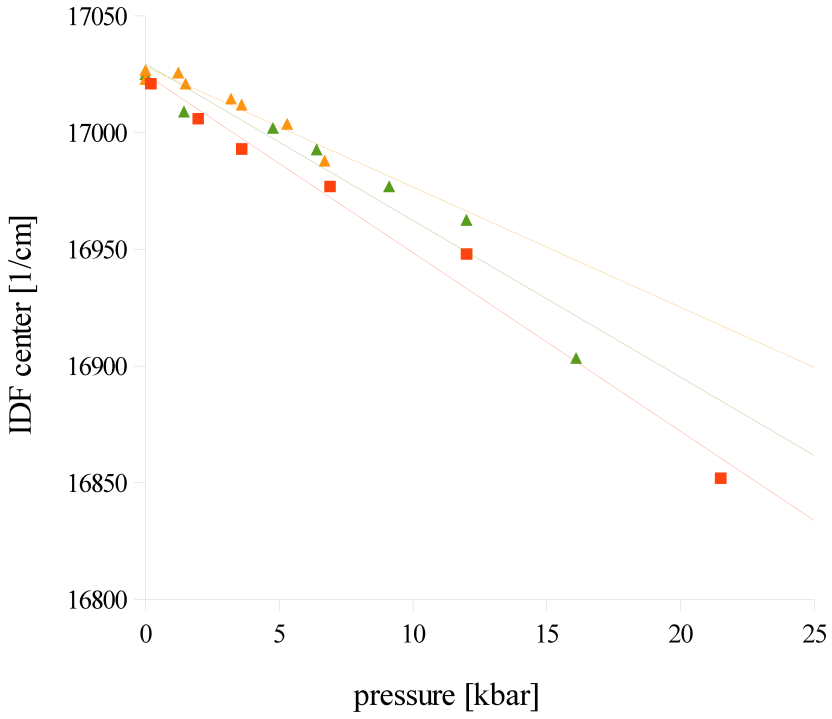

Table 8: Parameters of linear regression of the shift of the IDF data. Note, that the slope of the IDF-center ($d\nu_0/dp$) is proportional to the isothermal compressibility ($\varkappa$).

Zn-HbA sample	slope ($d\nu_0/dp$) [cm^{-1}/ kbar]	s.d.	$d\Delta\nu_0/dp$ [cm^{-1}/ kbar]	s.d.	ν_0 [cm^{-1}]	s.d.	$\Delta\nu_0$ [cm^{-1}]	s.d.
stripped	-7.7	± 0.5	2.3	± 0.2	17025	± 5.6	45.4	± 1.6
100mM Cl^-	-6.7	± 0.9	2.6	± 0.3	17029	± 7.9	44.7	± 3.1
2 mM IHP	-9.5	± 1.0	3.6	± 0.5	17034	± 10.7	44.9	± 6.1
10 mM BZF	-5.2	± 0.6	3.4	± 0.9	17028	± 2.2	36.9	± 3.4
10 mM BZF with last point	-8.7	± 1.8	4.3	± 0.9	17034	± 7.6	35.3	± 3.6

5

SUMMARY

Conclusions from the activation of the global dynamics:

- Thermodynamic parameters (activation - energy and - entropy) of the dynamical activation can be calculated, these are specific to the protein (see the difference between Zn-HbA and Mb).
- The protein's own internal, intrinsic, slow (ms ... s timescale) global dynamics can only be monitored in a solvent free from anti-freeze agents.
- The monitored dynamical activation is a global phenomenon of the entire protein molecule, since it does not depend on the type or position of the reporting chromophore.
- The activation parameters change significantly if allosteric effectors are added to Zn-HbA, and the change is in accordance with the efficiency of the effector in O_2 binding (stripped < chloride < IHP $\approx$ DPG < BZF).

Conclusions from the pressure perturbation study:

- The Trp fluorescence signal shows a sigmoidal transition, which can be attributed to the tetramer $\rightarrow$ dimer dissociation
- By fitting a simple model to the data the atmospheric dissociation constant, and the volume-change during dissociation can be calculated.
- These parameters again significantly change in both oxy-HbA and Zn-HbA upon the addition of allosteric effectors, again approximately in accordance with the efficiency of the effector.
- The change is in the opposite sense in oxy-HbA and Zn-HbA, in the latter case the inter - dimeric interface is becoming weakened by the addition of effectors, which is manifested in the increase of the dissociation constant.

Conclusions from the compressibility (or accurately, from the IDF-shifting) data:

- The shift of the IDF is linear with pressure.
- Slight deviations from the linearity can be found at pressure levels above 15 kbar, which may indicate a local reorganization of the protein structure above a certain pressure level.
- The changes in compressibility (thus in the broadening of the IDF and in the slope of the shifting of the center if the IDF) due to the addition of allosteric effectors is minuscule, and probably within the error range. However, the directions of the change are again in accordance with the efficiency of the effector, with the exception of BZF.

There are many parallel findings in these conclusions, most notably that all the calculated parameters seemingly depend on the presence, and type of allosteric effectors. This shows that there has to be a *global* change in the behavior of the protein. The global nature of the change arises most strongly from the results of the new phosphorescence method. It is of significance that *the activation parameters do not depend on the position of the chromophore inside the protein matrix.* The absence of significant changes in the room temperature absorption and fluorescence spectra, however, exclude the possibility of significant tertiary structural reorganization, at least around the Trps and Zn-PPs of the protein. It has to be noted, that both type of chromophores are in key positions not only for the tetramer $\rightarrow$ dimer dissociation, but also for the R $\rightleftharpoons$ T transition, and thus oxygen binding.

If we exclude the possibility of significant tertiary structural changes, than the significant variations in both the inter-dimeric interface binding-strength, and in the activation parameters of the global slow dynamics have to be explained in a different way. Let us take a look again at the activation parameters! *The calculated energy and entropy values are consistent with a fair sized, transiently opening cavity. This cavity is not static, it opens only for a very short time, and forms a passage for the quencher (oxygen) in the structure. This way the oxygen molecules can "hop around" in the protein matrix, with a step-size of the size of such a cavity.* Taking the denaturation entropy [69] of approximately 30 cal/(mole K residue), the observed entropy change is equal to the denaturation entropy of 2 ... 5 residues. The energy change is also in the order of a few H-bonds, thus the data are consistent with this idea. In Mb possibly similar "traps" were seen by crystallography experiments under Xe gas, or by transient Laue-crystallography, in which the hopping of CO in Mb was observed [136, 25, 130, 16, 15, 19]. In fact, local unfolding was also proposed as a

mechanism of ligand transfer in Mb [32], which is also consistent with the theory of transiently opening spaces.

The opening of the cavity is then probably made possible by the ongoing collective dynamics, which may behave analogous to a traveling compression-wave in a soft material, making some places softer and less dense, than the others. In the transiently softened parts of the protein a local cavity can open up making the passage and then rapidly collapse, thus trapping the small molecule in its new position. This causes a limited, and of course anisotropic diffusion, the apparent diffusion coefficient of which will be very sensitive to alterations in the global dynamics responsible for the softening - hardening of the matrix. In this framework, the addition of allosteric effectors - as an important (but not sole) effect - simply modifies these "wave-like" oscillations of the protein structure. It is also important to note, that these oscillations do not have to alter the average 3D structure[1], thus they would not be detectable by simple ensemble methods, such as conventional fluorescence spectroscopy. One can argue, that in the FLN experiment - in which the individual molecules are each trapped in their own conformation by the solid matrix - the changes in this global dynamics should be manifested. This is true, however if the changes in this dynamics are not large, then the conformational distribution at a given time-point, when the sample is frozen, may not differ very much from a sample under different conditions (added effector), and thus the IDFs determined in the FLN experiment may remain identical within experimental error. It has to be noted here, that the individual resolved spectra were somewhat different in each case. It is also a limitation, that the FLN technique requires a transparent sample, thus anti-freeze agent has to be added. This may further reduce the observed effect. A third consideration is also important: in the FLN experiment, at low temperature the Debye-Waller factor is close to 1, while at the temperature of the dynamical activation it is certainly much lower, since many vibrations are thermally excited. Thus, while at low temperature the zero-phonon lines play the major role in the determination of the IDFs, at the higher temperature of the dynamical activation the phonon-wings[68] take over the dominance. This change alone may very well account for the lack of a highly significant change in the shifting of the

1 Since every single molecule has its own global dynamics, and the statistical average may stay within experimental error, if this dynamics is not correlated. And since the molecules are not synchronized in terms of this dynamical fluctuation, the effects may cancel each other in the population averaging, if a quasi - static 3D structure is being determined. If dynamics is being monitored, then of course the changes will show-up.

IDFs[2]. This consideration raises the apparent controversy between the very significant changes in the interface-strength data obtained by room-temperature pressure perturbation, and the lack of any highly significant effect in the FLN experiment: at room temperature this slow global dynamics is already activated, and may play a significant role by influencing the interfaces as well. If these global oscillations include the interface region, ie. the amplitude of the oscillations in the interface region is large, then any changes in these oscillations could - even strongly - influence the interactions between the two dimer surfaces.

As a summary:

Global, slow dynamics may play an important role in the regulation of protein function. It may even play a major role in allostery. If we think about the global dynamics as some sort of collective oscillations of the structure, than a larger assembly like HbA may have many more types of these oscillations than a relatively small structure like Mb. Also, if a protein is small, a significant part of its structure is only a few Å-s away from the solvent, and solvent-effects may influence its dynamics more strongly. Thus it may not be "autonomous enough" to build up a sufficiently complex internal dynamics, which would allow for allosteric fine-tuning.

The generalized conclusion of the results on HbA dynamics would be proved if the elaborated phophorescence method would lead to similar results in other proteins. Until now the technique was applied for two other proteins: PGK and dUTP-ase in collaboration with Szabolcs Osváth and Beáta Vértessy. Results on these two systems are presented - due to space restrictions only shortly - in the next part of the thesis.

2 This consideration was an important driving-force in the developement of the phosphorescence method.

Part II

APPLICATION TO OTHER PROTEINS

GENERAL REMARKS TO THE APPLICATIONS

In this part two examples of the application of the new optical method are shown. The two proteins are distinct, phosphoglycerate kinase (PGK) is a monomeric protein, which has two relatively well separated domains, while deoxyuridine triphosphatase (dUTPase, DUT) is a homotrimer. They have a common feature though: the active site for catalysis is not part of only a single domain or monomer, but in the case of PGK both N- and C domains of the polypeptide chain play a role in the catalysis moving towards each other by a hinge - bending motion to form the catalytic site, and in the case of DUT each of the three catalytic sites is composed of parts belonging to all three subunits.
In both systems there is much knowledge already about the importance of dynamics in the function, therefore it is interesting to see if results obtained with this method correlate with previous knowledge, and are the results able to also possibly add to- or extend this knowledge. Due to space restrictions of this PhD thesis, I am not able to go into details in the literature survey, only the most important facts will be briefly summarized in both cases [3]. It also has to be noted, that these are still ongoing projects. In both cases the data already available enable the drawing of certain conclusions, but these conclusions probably need to be supported by additional experiments.

3 This is not a real limitation, since both molecules are chosen only from a pragmatical point of view, to show the possibility of applying the method and theory described in the previous part of the thesis. Thus, a more detailed literature survey (including the reaction mechanism, proposed models, etc.) would not add to the scope in any significant way, but would overflow the page limit of a PhD thesis.

6

PHOSPHOGLYCERATE KINASE

6.1 INTRODUCTION TO PGK

Yeast 3-phosphoglycerate kinase (PGK) is a typical two - domain hinge - bending enzyme with a conserved primary structure and tertiary fold including a well - structured inter-domain region[10, 150]. The two domains interact via a helical hinge and through the C terminal helix, which folds back to the N domain, and proved to be crucial for enzyme activity [150, 109]. The structure is shown in Figure 38. Contacts between the two domains are formed through hydrophobic interactions and hydrogen bonds in the folded structure [146]. There are two tryptophan residues in the wild-type yeast PGK that can serve as luminescent probes of the protein conformation [85, 24, 26]. Folding of fragments containing less than one complete structural domain is incomplete and not cooperative, but both individual full-length domains (N and C) fold into native-like structures[99, 63]. PGK therefore is a suitable model to study the mechanism of domain - domain interplay and its role in protein dynamics.
Mutants of histidine tagged PGK, histidine tagged N domain of PGK, and histidine tagged C domain of PGK were expressed as described earlier[92, 93]. His-affinity purification was done on Ni-NTA column (Qiagen), the purified protein was flash frozen in liquid nitrogen and stored at -80 °C until use. A model system based on the two-domain structure of PGK was constructed to study the role of domain interactions on the dynamics of PGK. The system consists of four mutants (N, C, N*C and C*N) that contain a *single* tryptophan residue. The four mutants are logically organized in two pairs. Both pairs contain one individual domain (either the N or the C terminal domain) and a corresponding mutant of the intact protein. Within the pair, the single tryptophan residues are placed at identical positions. This ensures that any changes in the dynamical activation between a given pair is not due to the Trp being at a different position, but rather due to the presence of -, and interaction with the other domain.

Figure 38: Schematic representation of the PGK structure, showing the hinge region as well. The domain abbreviations are shown in dark red color (N, C, N*C and C*N). The sequence differences between the engineered constructs is presented in the table below the structures. Figure reprinted from [94] with permission.

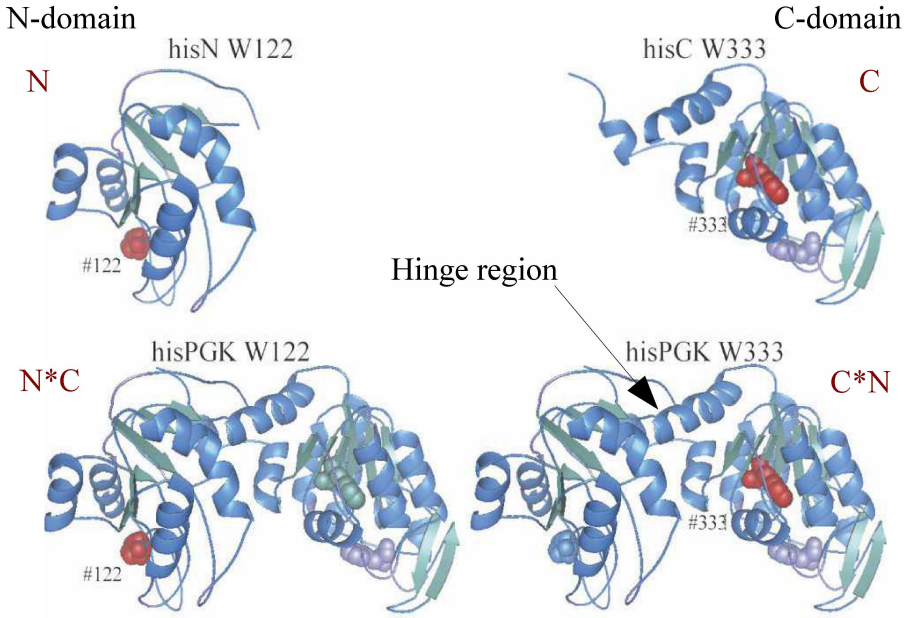

yPGK WT	hisN W122	hisPGK W122	hisC W333	hisPGK W333
full sequence	*residues 1-185*	full sequence	*residues 186-415*	full sequence
No his-tag	*his-tagged*	*his-tagged*	*his-tagged*	*his-tagged*
Y122	*W122*	*W122*		Y122
W308		*F308*	*F308*	*F308*
W333		*F333*	*F333*	W333

6.2 TRANSITIONS IN PGK

The experimental conditions were identical to the phosphorescence quenching experiment of Zn-HbA. I have used the established "fast-cooling" protocol, the sample contained 20µM of protein in a 20 mM potassium phosphate (pH 6.2) + 1 mM ethylenediaminetetraacetate buffer. The phosphorescence decay curves are shown in Figure 39. Since the signal/noise ratio was considerably lower as in Zn-HbA, I have tried a third evaluation which is similar to the MEM, but the distribution is bound to be a sum of gaussians in the decay-rate space. All evaluations lead to the same $<\tau>$ within error. This however shows that it is possible to assume a sum of gaussians in the decay-rate space which may correspond to a distribution of structures[1]. Similar to the procedure in the case of Zn-HbA the average lifetimes[2] can be calculated at each temperature. This is shown for all the four constructs in Figure 40. As can be seen the step corresponding to the dynamical transition is very different in the four cases. In the case of the N-domain a relatively sharp transition can be seen, while in the case of the C-domain a significant broadening with respect to the curve belonging to the N domain is apparent. This remains to be the case also in the C*N full length PGK, the broadening blends the end of the transition into the second transition corresponding to the softening of the surrounding matrix. A strikingly different curve is seen in the case of the N*C (ie. the Trp is in the N domain), the dynamical activation seems to be splitted into two steps. The first step coincides with the step seen in the N-domain alone, while a second step follows closely which lowers the average lifetime to the value seen in the case of the N-domain. This

1 This is work-in-progress, the custom-written iterative re-convolution software is currently being developed. Several more decays have to fitted with the software to compare the results with MEM distributions. It can be seen that the overall structure of a given pair of distributions are the same, however there are cases in which smaller peaks are missing from either of the two distributions. Since in the case of noisy data the classical MEM tends to over-estimate the width of a given peak in the distribution, it is "normal" that sometimes a single peak in the MEM is resolved into two peaks in the gaussian representation.

2 If we assume that there are distinct sub-populations, based on the MEM analysis, then $<\tau>$ represents an averaging of the structures. We could try to re-do the analysis presented here for each "sub-structure", but the assignement of the peaks in the MEM is not straightforward: as can be seen, everything changes during the transition. It is more probable, that the different peaks in the MEM correspond to very similar structures (at least in the N domain, which is known to fold into a well-defined 3D structure), but with quenchers trapped in distinct locations. These distinct quencher-positions are reflected in multiple liftime-groups resolved by the MEM.

Figure 39: Sample decays of the PGK N domain construct at various temperatures. The line represents the fit to the data as in Figure 2. Two kinds of distributions are shown: obtained by MEM (panels to the right) and by allowing only a sum of gaussian distributions in the decay-rate space (middle panels).

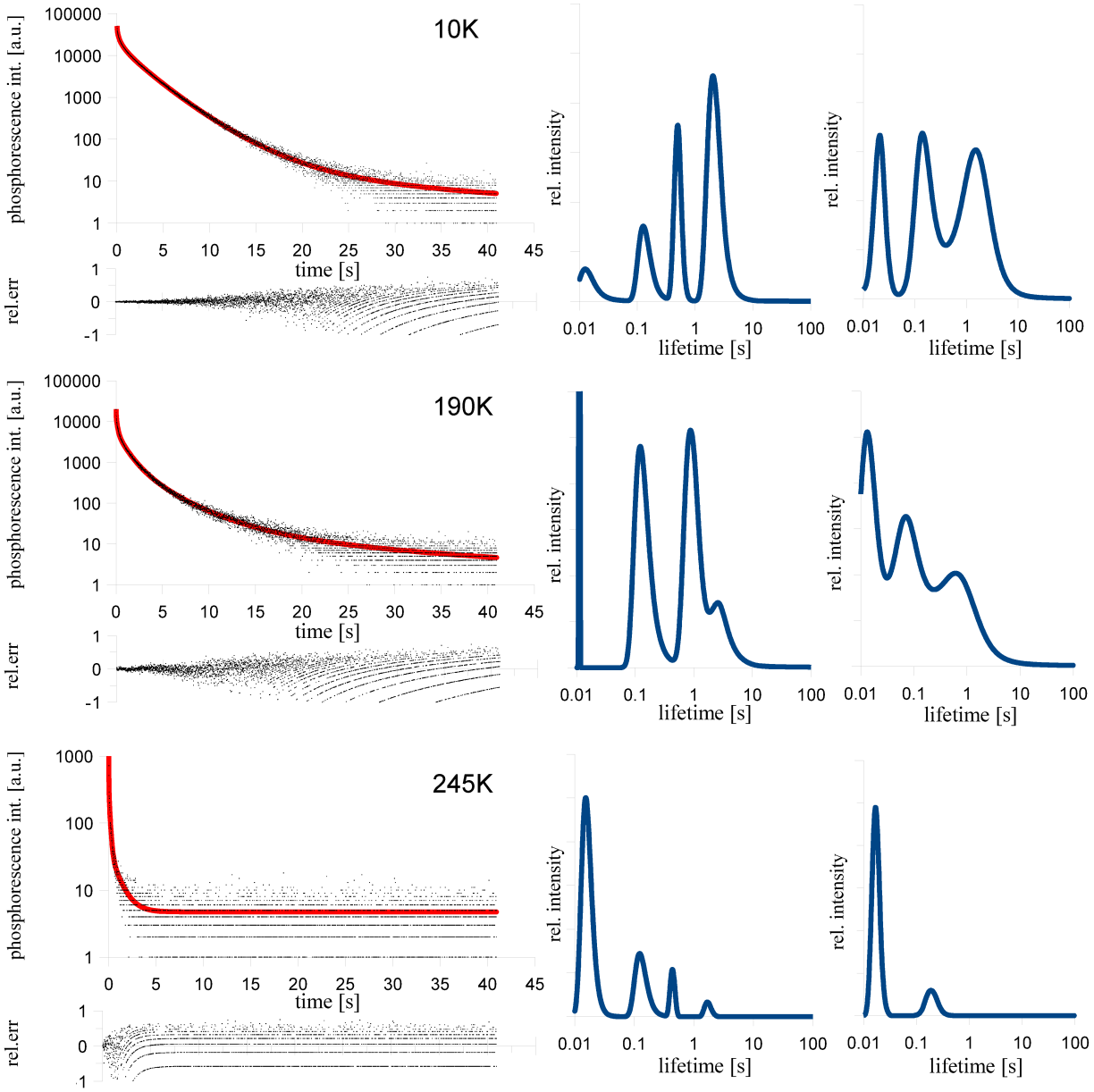

Figure 40: Average lifetime values of the four different PGK constructs at various temperatures. The solid lines are the fits to the dynamical transition. The error bars show the s.d. of the data.

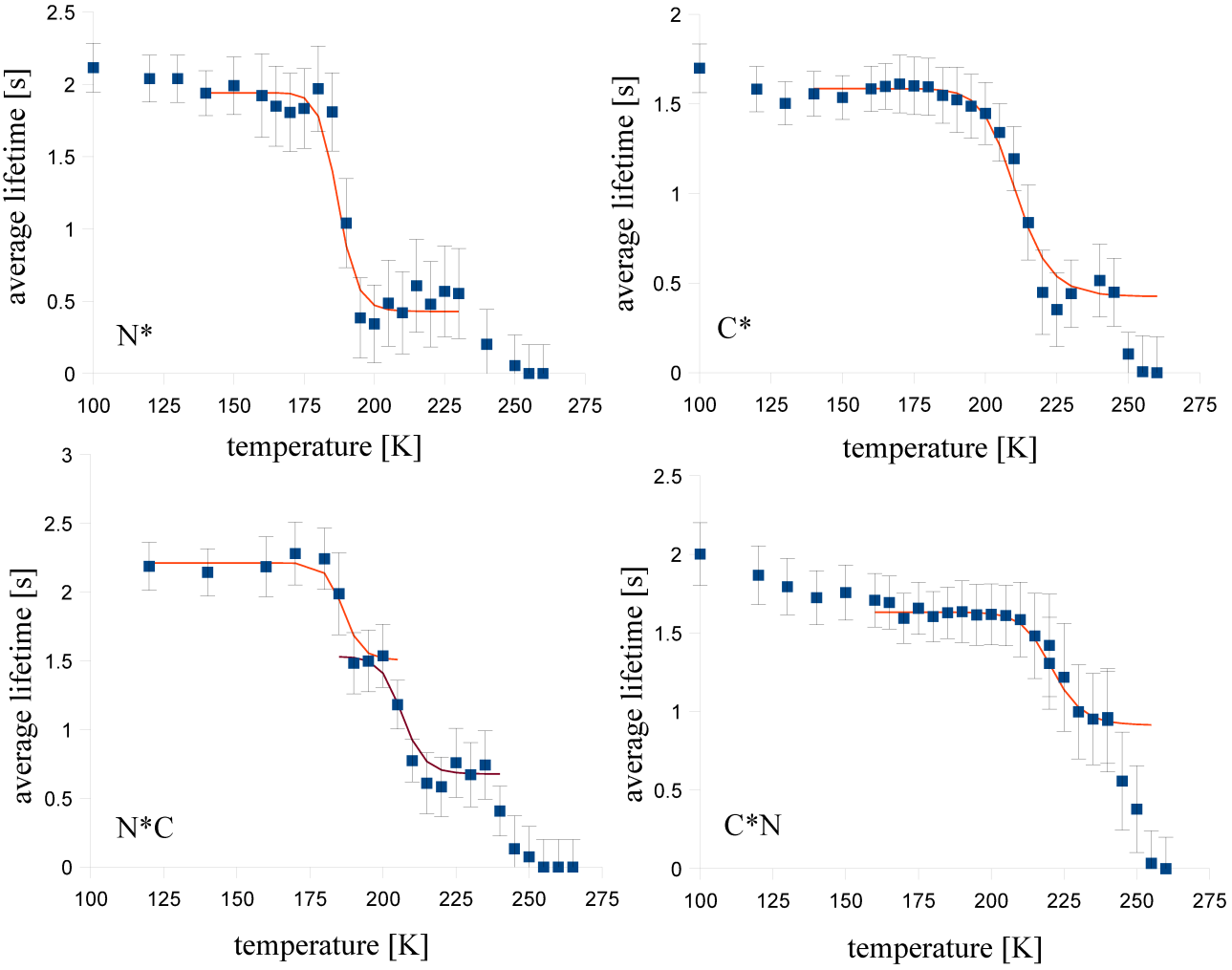

two-step behavior is distinct from the single, broad transition of the C*N construct. Since the differences between the curves are striking, I have omitted the derivative curves from the graph in Figure 40 for clarity[3].

6.3 INTER-DOMAIN INTERACTIONS IN THE DYNAMICAL TRANSITION

The results suggest that the two domains of PGK correspond to two dynamic units of the native state. Motion of the two dynamic units, however, is strongly coupled through domain - domain interactions. Interplay between the two domains has been shown earlier to be crucial for

3 The derivatives would not aid the conclusions in this case, but instead would just make the figure more complicated.

Table 9: Parameters of the dynamical activation of PGK constructs.

construct type	ΔE [kJ/mol]	ΔS [J/mol K]	K_d	T_{MP} [K]
N	84.1 ± 6.7	445 ± 36	4.7 ± 0.3	189 ± 5.1
C	61.7 ± 5.6	293 ± 26	3.7 ± 0.3	211 ± 9.7
N*C 1	92.1 ± 6.4	494 ± 35	1.5 ± 0.2	186 ± 4.1
N*C 2	(93.4 ± 6.5)	(452 ± 31)	2.3 ± 0.2	207 ± 3.9
C*N	74.5 ± 7.2	336 ± 24	1.8 ± 0.2	222 ± 10.8

enzyme function [146]. It can be seen that the interaction between the two domains has *asymmetric* effect on the activation of motion in the domains. This seems surprising based on the symmetric structure of the PGK and the apparently symmetric role of the domains in bringing the 1,3-diphospho glycerate and ADP together for phosphate transfer. The results of the dynamical activation, however, are in accord with earlier findings indicating that domain - domain interactions also have an asymmetric effect on the folding of the domains[94]. The parameters of the activation are listed in Table 9.

As apparent from the data, there is an asymmetry also in the activation parameters, the ΔE and ΔS values differ significantly in the case of C*N and N*C constructs, and resemble the difference of the N and C data. In both pairs (N , N*C) and (C , C*N) the activation energy and entropy values increase in the full-length construct with respective to the single domains. This increase is about 10 ... 15%, and somewhat smaller in the case of the (N,N*C) pair. There is an important and striking difference between the two curves: in the N*C curve the dynamical transition is split into two parts, and notably, the activation parameters of the first step can be evaluated in terms of the presented two-step model. In the second step, an already somewhat activated dynamics is becoming even more activated, therefore the the ΔE and ΔS values in Table 9 for N*C 2 are in parenthesis, and are over-estimated, since the model assumes an inactive starting state, as shown in Figure 12. Therefore in this second case a better parameter is T_{MP}. If we compare the T_{MP} values, then it can be seen that in the N*C 1 partial activation the systems dynamics is close to the dynamics of the activated single N-domain, while after the N*C 2 transition it is somewhere between the C and C*N constructs. It has to be emphasized, that in PGK the two domains are thought to be largely

independent[150], and they supposed to interact mainly through the well-known hinge-bending motion. This partial autonomy of the domains is reflected also in the activation parameters. It is important to note, that according to Figure 12 during the entire activation the outer boundary of the system is still bound to the solid solvent matrix, thus the well-known, characteristic hinge-bending motion is blocked. *An important conclusion thus follows from the data: even if the hinge-bending motion is blocked, there is still some communication between the domains in the open configuration of the molecule, and this communication is manifested in the coupling of the slow, collective dynamics of the domains.* It can be seen best in the case of N*C, the activation "stops" at a partially activated state as it were somehow "waiting" for the C-domain to also become active, and then the collective dynamics finally reaches a fully activated state. This is best seen in the T_{MP} data, and this coupling is also supported by the increase in the ΔE value, as a larger, but finite sized collective system is expected to have an increased activation energy. Thus, it could be shown, that the hinge-bending motion is not the only result of inter-domain communication.

7

DUTP-ASE

This is very much work in progress, I have included it though, to show another example of the application of the method. Therefore, and also due to the space-limit, this chapter is very short, but the preliminary results obtained so far are interesting, and present a new possible application in the testing of interfaces of molecules.

7.1 SHORT INTRODUCTION TO DUTP-ASE

dUTPase (or dUTP-nucleotidohydrolase, DUT) is a homotrimeric molecule, which catalyzes the dUTP $\rightarrow$ dUMP + PP_i reaction[122]. It is an essential enzyme responsible for keeping a low cellular dUTP/dTTP ratio and thus maintaining DNA integrity [44, 140] by keeping their concentration low, and thus lowering their incorporation into DNA. Although uracil is tolerated in low incorporation-ratios, if it's level increases, it leads to increased probability of double-strand breaks of the DNA, which eventually causes cell death. This mechanism explains the importance of the up-regulation of DUT in tumor cells [22]. The role of DUT in the regulation of tumor cells, and bacteria makes it a target of drug-research, and the detailed understanding of it's structure and reaction mechanism is therefore important [139, 148, 132]. Most DUT enzymes are homotrimers, with a unique active-site architecture: each of the three active sites in a trimer is composed of five conserved motifs, four of these motifs are provided by two adjacent monomers, while the fifth is contributed by the C-terminal part of the third monomer. This C-terminal motif behaves much like an "arm", and is supposed to close-up on the active site during the chemical reaction [133, 84, 147]. The structure is shown in Figure 41. We have used a mutant from of the human DUT, in which a Trp residue is inserted (F158W) into the C-terminus [147]. It was confirmed based on fluorescence changes of the reporting Trp-158 that upon the binding of substrates the "arm" of the C-terminus is subject to a rearrangement, although large conformational changes are unlikely based on the relatively small changes in the acrylamide - quenching efficiency in various states (apo - enzyme and bound to various substrates or substrate - analogs). It was shown, that one of the analogs, 2´-deoxyuridine-5´-(α,β-

Figure 41: Schematic representation of DUT, the three subunits are colored differently. The key residues of the active sites are shown in a ball-and-stick model, note the long chain of the "arm" originating from the third subunits, and reaching the active site. Figure is reprinted from [147].

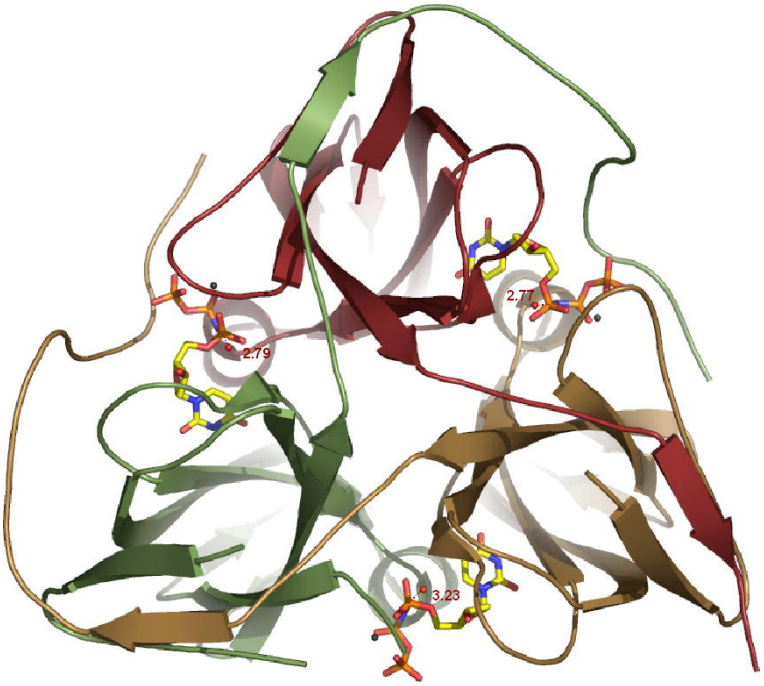

Figure 42: Decay curves of Trp phosphorescence in apo- human DUT at various temperatures: 10 K (blue) 210 K (red) and 235 K (green)

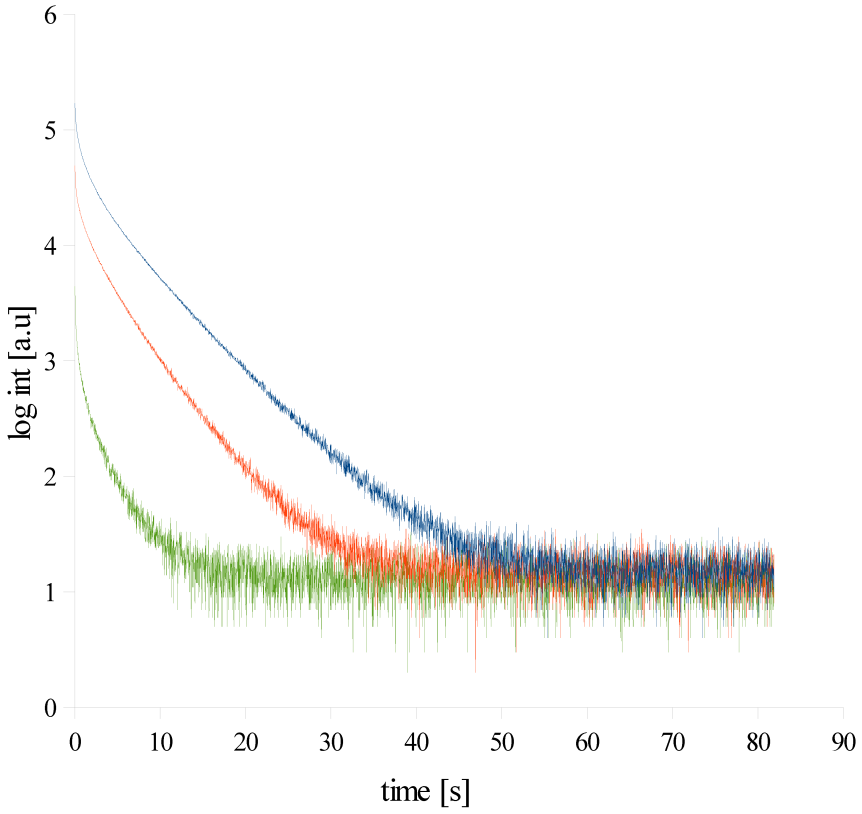

imido)triphosphate (dUPNPP) causes a relatively large change in the fluorescence parameters. Therefore this was selected as a staring point. We have up to now compared the apoenzyme and the dUPNPP-complex, in order to see if the already observed changes also manifest in the dynamical activation of the system.

7.2 TRANSITION IN DUTP-ASE

The phosphorescence decay curves at various temperatures are shown in Figure 42. The fitting was done in the same way as described in the case of Zn-HbA [118] and PGK. The temperature - dependence of the average lifetime values obtained by the fitting is shown in Figure 43. For comparison, the lifetime of Pd-CP and stripped Zn-HbA are also shown [1]. It can be seen, that in the apo-form the lifetime dependence of human DUT resembles more the case of a free chromophore in a buffer solution than the behavior of HbA. Although, this behavior is still different from

This is a first analysis of the data, evidently more states should be investigated to allow for firm conclusions. These are until then rather speculations.

1 They are scaled-up to 500ms to fit into the graph.

Figure 43: Temperature dependence of the average lifetime of human DUT in the apo form (blue squares) and bound to dUPNPP (green triangles). For comparison, the fitted curves of Pd-CP (dark green line) and stripped Zn-HbA (red line) scaled up to fit the graph are also shown.

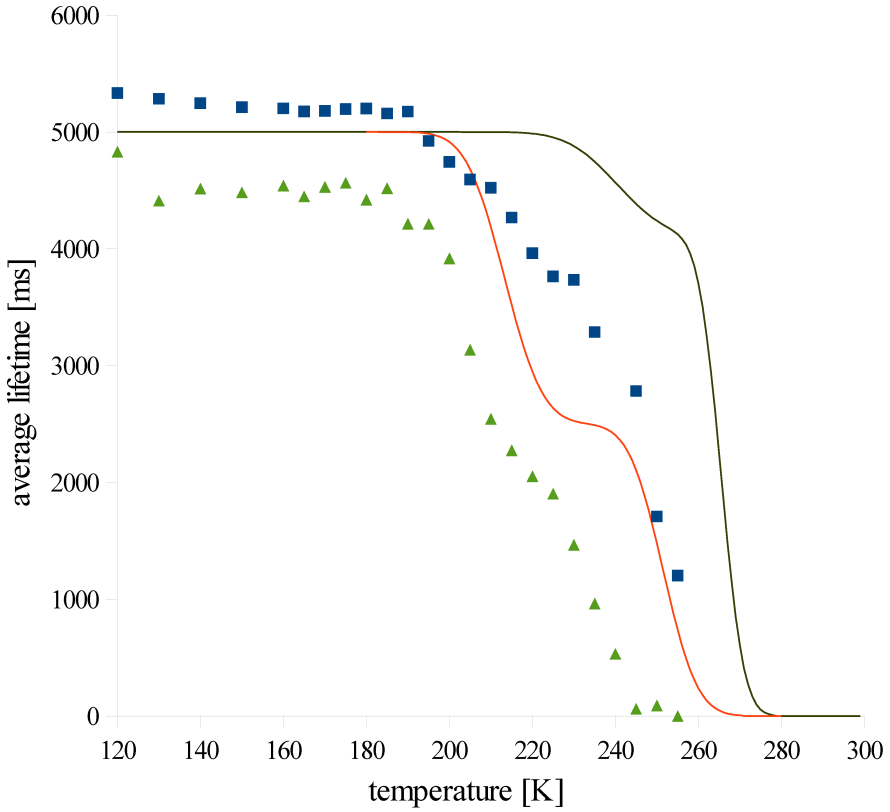

the Pd-CP, notably the transition temperature range is significantly lower. This indicates - in accord with previous findings - that the "arm" region is not completely exposed to the solvent. Moreover, it can be said, based on the difference in the activation between the apo-enzyme and Pd-CP that the "arm" is dynamically coupled to the rest of the protein even in the open, apo-form. It can also be seen, that the dynamic activation in the apo-form is a rather broad transition, whereas in the dUPNPP-bound form it closely resembles the behavior of HbA. This difference may arise from two factors: First, it can be, that the "arm" is not coupled strongly enough to the system in the open, apo-form to form a sufficiently "together-moving" unit with the rest of the protein, thus the activation of the "arm" may be somewhat separated from the rest of the protein. This, together with the coupling to the solvent may account for the observed differences of a higher activation temperature, and significant broadening of the transition. In short, it can be simply the case, that the "arm" is somehow in an intermediate state between being fully extended into the solvent and being tightly bound to the rest of the molecule, and as a consequence, the activation pattern is a simple "linear combination" of the closed configuration (dUPNPP-bound) and the Pd-CP curves.

A second possibility is, that in the apo-form there is a considerable structural heterogeneity in the system, and many different conformers co-exist, and this is the cause of the broadened transition. If a substrate is bound, and the "arm" closes, it may trigger a rearrangement in the conformational space of the molecule such, that the distribution becomes significantly narrower, and more resembles a cooperative tetramer such as HbA. The lower activation temperature, which is in the direction to the activation of Mb from the HbA-curve, may reflect the fact, that the size of human DUT is somewhat smaller than tetrameric HbA, but larger than Mb.

However, since this is not yet a finished study, these conclusions need to be verified and possibly extended with new experimental data.

8

CLOSING REMARKS

In this section I will briefly summarize the most important conclusions and add some further thoughts, speculations. It is important to note, that the speculations are what they are supposed to be: only ideas, which need further data and experiments to be confirmed, or rejected.

In the first part, which demonstrated the technique in the case of a zinc-hybrid human hemoglobin (and partly using non-hybrid HbA as well), the following conclusions were drawn:

- In the temperature dependence of the average phosphorescence lifetime in the 10 K ... 300 K temperature range two separate transitions can be observed. These transitions do not conform to the previous observations of a glass-transition as evident from an Arrhenius-type representation. Furthermore, the comparison of the above transition with the profile of a free chromophore leads to the conclusion, that this transition is primarily not an effect arising from the solvent matrix, but is rather a specific effect of the protein itself.

- The transition can be reliably detected only in the absence of glass-forming anti-freeze agents.

- The transition can be interpreted in terms of a dynamical activation of the protein matrix. This dynamics is supposed to be of a slow (ms ... s timescale) and collective nature. The latter is supported by the fact that the transition is independent from the position and type of the chromophore, until the conditions remain the same.

- A qualitative model was built, in which the observed quenching of the chromophore phosphorescence is caused by an increased diffusion of the small molecule quencher (mainly oxygen) inside the protein matrix. This increase in the diffusion coefficient is made possible by an onset of global motions in the structure, which allow a "hopping-like" movement of the quencher inside the protein. Any changes in the activation or type of these global motions are reflected in the quenching efficiency and its temperature-dependence.

Only the most important conclusions are summarized here, since each chapter and part has its own summary

- With a simple first-approximation type of thermodynamic model[1], the energy and entropy changes corresponding to the dynamical activation can be calculated from the data. These parameters depend on the conditions of the sample.
- The change in the activation parameters correlate with alterations in the structure caused by the addition of allosterically active molecules, and the change follows the trend observable by the biological effect of these molecules.
- With the help of another simple first-approximation type of model it was shown that these active molecules influence the strength of the inter - dimeric interface in both oxygen bound- and deoxy-states of HbA using pressure perturbation at room temperature and calculating the dissociation constant of the tetrameric HbA under different conditions.
- It was also shown by the cryogenic FLN technique, that the compressibility of the protein around the heme-group changes only by a small fraction, which is just above, or around the experimental error. However, the order of the change also resembles the order of the biological effect in this case.

The following ideas can be formulated:

1. It seems probable, that the change in the oxygen-binding function of

1 It has to be noted that in some cases (even in Hb), we have seen an up to 10 ... 20 % decrease in the average lifetime at a range of approximately 5 - 10 K lower temperature than the main transition itself, as can be seen, e.g., in the "N*" data of Figure 40. We have not taken this into account - see the fitted curve in Figure 40 - and it was also not always reproducible. It is not considered in this first approximation of the phenomenon, therefore we have discarded them from the analysis. It may, however, arise from a small-scale, partial onset of the dynamics, which causes a redistribution of the quenchers around the chromophore. It may also indicate that the phase transition could be much more complex than be described by this simple model, and it may have an onset at 5 - 10 K lower temperature. However, these considerations are beyond the scope of this thesis, and may more data, possibly under different quencher (oxygen) concentrations and freezing-speeds would need to be acquired to have enough data to enhance the model. Importantly, these possible further enhancements would only refine the model, but would not invalidate the present conclusions. It is also important that the dynamics, which is being activated in this type of experiment is only some kind of "partial" dynamics, since the boundary of the protein is being coordinated to a solid, still frozen matrix of the solvent. A possible separate phase-transition in this boundary may further complicate the situation. These considerations however only add to the complexity of the problem, but do not significantly alter the conclusions drawn from the very simple, first-approximation type of description presented in this thesis.

HbA is influenced in a dynamical way by allosteric effectors. This means that the presence of allosteric effectors may modify the slow, global dynamics of HbA, and this modified dynamics is what is being reflected in different ways in the experimental data.

2. Since the FLN technique is cryogenic, thus the vibrations are not [2] excited. This causes the technique to be largely insensitive to the slow, global dynamics, which is becoming activated only at higher temperatures, generally above 180 - 200 K. The changes in the dynamics may also have consequences in the low-energy vibrations, and may also modify the phonon-wing observable by FLN, thus a small effect is expected which is also seen in the data. Additionally to this change in the phonon-wings, the distribution of the molecules in the conformational space after fast freezing may be also changed, if the slow dynamics is changed, since every molecule will be trapped in its actual conformation at the time of freezing, and this conformation will not change significantly during the experiment any more.

3. The importance of dynamics may also explain - or at least is consistent with - the data obtained by the room-temperature pressure perturbation study. If there are significant changes in the slow global dynamics of the tetramer, the inter-dimeric interfaces being part of the system would also have a fluctuating interaction pattern [3]. A changed global dynamics would certainly cause a re-distribution of the interaction patterns in a hypothetical dynamical-conformational space, which would then lead to changes in the average interaction-strength between the two dimers. This is reflected in the change of the dissociation constant and dissociation volume.

4. All the above effects are possible *without* a change in the time or ensemble average structure, therefore it may be a purely dynamic effect [4]. This may also help to resolve an apparent controversy, that the allosteric effectors bind to the central cavity of the tetramer and affect the oxygen binding in every monomer at the distant heme-site, but no significant, statically observable structural changes happen there. This has

2 or in a very little proportion, as apparent from the high Debye-Waller factor below 10 K

3 It can be imagined, that the binding network is not constant in time, but it fluctuates between several different patterns, and the average is measurable by ensemble techniques, such as Raman spectroscopy or NMR.

4 There is of course a solid experimental evidence coming from a variety of techniques, that the addition of allosteric effectors do change some structural elements, mostly in the inter-dimeric interface region of HbA. However, it is interesting, that at least partly, the observed changes may result from a dynamical change, and not exclusively from static changes of the quaternary or tertiary structure.

been incorporated into the models describing the function of HbA by a changed network of equilibria, and the refined models quantitatively describe the oxygen-binding curves. However, the structural details are still not completely understood. The findings presented in this thesis support the "global-allostery" model published a few years ago. In this model it is supposed, that tertiary structural changes occur as a consequence of the binding of allosteric effectors in both oxy- and deoxy- states of HbA. This can now be extended with the idea, that not only tertiary structural changes occur, but importantly the pattern of global dynamics is changed, and this may play a significant, or possibly even major role in the regulation HbA.

In the second part of the thesis, two applications were introduced. The first is the case of phosphoglycerate kinase (PGK).

- It was shown, that the dynamical activation in both domains will pairwise a shift to a higher transition temperature, and both activation parameters increase if the other domain is also present.
- The change of the shift and of the parameters are asymmetric in the N and C domains.

The change showed up more strikingly in the N domain than in the C domain, even causing a splitting of the dynamical activation step. In the C domain the activation corresponds to a broad transition, while in the N domain a sharp transition is seen. This may reflect the known fact that the N domain has a very different folding kinetics than the C domain which is supposed to be a mixture of differently folding subconformations. This is in accord also with the observation, that the distribution of lifetimes in the C domain at 10 K (data not shown) is much broader than in the N domain. It has to be noted however, that the different lifetime distribution can also reflect a different local environment, and is not necessarily a consequence of a global structural heterogeneity of the C domain.

- Apparently, the hinge-bending motion is not essential for the interdomain communication: there is a collective dynamics of the two domains even when hinge bending is blocked. This finding further supports the speculation drawn from the HbA data, that the *slow, global* dynamics plays an important role in the regulation, and most

probably in the function of enzymes [5].

Second, the importance of dynamics is also apparent in the case of dUTPase (DUT). Albeit there are only limited experimental data available up to now, it can be seen that the apo-enzyme behaves significantly differently than the substrate-bound form. Both the width and the position of the dynamical transition are altered if the enzyme is bound to a substrate. The transition is shifted to a lower temperature and the width of the transition on the temperature scale is significantly reduced. It can be hypothesized, that the C terminal "arms" fold up to the main structure and this leads to the modified dynamics. While this folding up is already known, it is interesting to observe that the dynamical transition of the apo-enzyme somewhat resembles the transition of a free chromophore in buffer, whereas the substrate-bound form closely resembles the transition of a tightly coupled system, namely HbA. This may indicate that in dUTPase, there is a dynamic coupling between the "arm" and the main structure, even though the "arm" is also coupled somewhat to the solvent. The ratio of these two couplings change significantly if a substrate is added to the system. The case of dUTPase also shows that the new technique presented in this thesis is also capable of monitoring changes in the boundary region of a large molecule.

For further spculations it is inspiring that in all three - from a structural and functional point of view - very different cases the importance of slow, global dynamics is shown and that changes in this specific dynamics correlate with functionally, biologically important events (substrate binding, inter-domain communication, allosteric control). It may be the case that these ms - s timescale motions may somehow encode information, which is transmitted through the structure by a change in this global dynamics. Different parts of the molecule, albeit being in a relatively large distance, may "read out" this information simply by being part of those global fluctuations. Taking into account that most avergage enzyme cycles are in the time-range around the ms timescale, such a flow of information may be important in the regulation of these systems. The importance of

5 Of course the importance of dynamics is not new. What is new, is that a specific timescale (namely the ms - s range), and the global nature of these motions may be especially important. This is being discovered by NMR as well[86, 143], as recent developements make larger and larger systems accessible. An advantage of the phosphorescence-based method is that it can be applied to a protein, or even multi-protein complexes of almost any size.

these global fluctuations or dynamics may also be reflected in the fact that most allosteric systems - or systems which have a lot of fine-tuning possibilities - are fairly large. The larger size may be needed to have "enough space" to have an internal, independent dynamics, which can then somehow "store" and "encode" the information needed for the controlling and fine-tuning of the function.

As a closing remark let us remind ourselves again on the message from the *Bible*:

"... for *we see now through a mirror obscurely,*
and then face to face."

SDG.

BIBLIOGRAPHY

[1] G. Ackers and J. Holt. Asymmetric cooperativity in a symmetric tetramer: human hemoglobin. *Journal of Biological Chemistry*, 281(17):11441–11443, 2006. (Cited on pages 11 and 43.)

[2] R. G. Alden, J. D. Satterlee, J. Mintorovitch, I. Constantinidis, M. R. Ondrias, and B. I. Swanson. The effects of high pressure upon ligated and deoxyhemoglobins and myoglobin. an optical spectroscopic study. *Journal of Biological Chemistry*, 264 (4):1933–40, 1989. (Cited on page 57.)

[3] A. Ansari, C. Jones, E. Henry, J. Hofrichter, and W. Eaton. The role of solvent viscosity in the dynamics of protein conformational changes. *Science*, 256(5065): 1796–1798, 1992. (Cited on page 31.)

[4] E. Antonini and M. Brunori. *Hemoglobin and Myoglobin in their reactions with ligands*. North-Holland Biomedical Press, 1971. (Cited on page 76.)

[5] A. Arnone. X-ray diffraction study of binding of 2,3-diphosphoglycerate to human deoxyhaemoglobin. *Nature*, 237(5351):146–149, May 1972. (Cited on page 45.)

[6] D. H. Atha and A. Riggs. Tetramer-dimer dissociation in homoglobin and the bohr effect. *Journal of Biological Chemistry*, 251(18):5537–5543, 1976. (Cited on page 76.)

[7] E. Azenha, A. Serra, M. Pineiro, M. Pereira, J. Seixas de Melo, L. Arnaut, S. Formosinho, and A. Rocha Gonsalves. Heavy-atom effects on metalloporphyrins and polyhalogenated porphyrins. *Chemical physics*, 280(1-2):177–190, 2002. (Cited on page 27.)

[8] J. Baldwin and C. Chothia. Haemoglobin: the structural changes related to ligand binding and its allosteric mechanism. *J Mol Biol*, 129(2):175–220, Apr 1979. (Cited on page 45.)

[9] C. Balny, P. Masson, and K. Heremans. High pressure effects on biological macromolecules: from structural changes to alteration of cellular processes. *Biochim Biophys Acta*, 1595(1-2):3–10, Mar 2002. (Cited on page 57.)

[10] R. Banks, C. Blake, P. Evans, R. Haser, D. Rice, G. Hardy, M. Merrett, and A. Phillips. Sequence, structure and activity of phosphoglycerate kinase: a possible hinge-bending enzyme. 1979. (Cited on page 101.)

[11] O. Barabás, V. Pongrácz, J. Kövári, M. Wilmanns, and B. G. Vértessy. Structural insights into the catalytic mechanism of phosphate ester hydrolysis by dutpase. *Journal of Biological Chemistry*, 279(41):42907–42915, 2004. (Cited on page 5.)

[12] M. Berjis and V. S. Sharma. Double mixing stopped-flow method for the study of equilibria and kinetics of dimer-tetramer association of hemoglobins: studies on hb-carp, hb-a, and hb-rothschild. *Anal Biochem*, 196(2):223–228, Aug 1991. (Cited on page 76.)

[13] Y. Berlin, A. Burin, J. Friedrich, and J. Köhler. Spectroscopy of proteins at low temperature. part i: Experiments with molecular ensembles. *Physics of life reviews*, 3(4):262–292, 2006. (Cited on page 82.)

[14] M. Berman, R. Benesch, and R. E. Benesch. The removal of organic phosphates from hemoglobin. *Arch Biochem Biophys*, 145(1):236–239, Jul 1971. (Cited on page 12.)

[15] D. Bourgeois and A. Royant. Advances in kinetic protein crystallography. *Current opinion in structural biology*, 15(5):538–547, 2005. (Cited on pages 11 and 94.)

[16] D. Bourgeois, B. Vallone, F. Schotte, A. Arcovito, A. Miele, G. Sciara, M. Wulff, P. Anfinrud, and M. Brunori. Complex landscape of protein structural dynamics unveiled by nanosecond laue crystallography. *Proceedings of the National Academy of Sciences*, 100(15):8704, 2003. (Cited on pages 11 and 94.)

[17] K. Brady and D. Setzer. Is there a dynamic dna-protein interface in the transcription factor iiia-5 s-rrna gene complex? *Journal of Biological Chemistry*, 280(16):16115–16124, 2005. (Cited on page 11.)

[18] S. Bruno, S. Bettati, M. Manfredini, A. Mozzarelli, M. Bolognesi, D. Deriu, C. Rosano, A. Tsuneshige, T. Yonetani, and E. Henry. Oxygen binding by [alpha](fe2+) 2 [beta](ni2+) 2 hemoglobin crystals. *Protein Science*, 9(04):683–692, 2000. (Cited on page 58.)

[19] M. Brunori, D. Bourgeois, and B. Vallone. The structural dynamics of myoglobin. *J Struct Biol*, 147(3):223–234, Sep 2004. (Cited on pages 11 and 94.)

[20] R. Bryan. Maximum entropy analysis of oversampled data problems. *European Biophysics Journal*, 18:165–174, 1990. (Cited on page 16.)

[21] J. Carrero, D. Jameson, and E. Gratton. Oxygen penetration and diffusion into myoglobin revealed by quenching of zincprotoporphyrin-ix fluorescence. *Biophysical chemistry*, 54(2):143–154, 1995. (Cited on page 42.)

[22] T. Chano, K. Mori, K. Scotlandi, S. Benini, C. Lapucci, M. Manara, M. Serra, P. Picci, H. Okabe, and N. Baldini. Differentially expressed genes in multidrug resistant variants of u-2 os human osteosarcoma cells. *Oncology reports*, 11(6):1257–1263, 2004. (Cited on page 109.)

[23] A. H. Chu and G. K. Ackers. Mutual effects of protons, nacl, and oxygen on the dimer-tetramer assembly of human hemoglobin. the dimer bohr effect. *Journal of Biological Chemistry*, 256(3):1199–1205, 1981. (Cited on page 76.)

[24] P. Cioni and G. Strambini. Pressure effects on protein flexibility monomeric proteins. *Journal of molecular biology*, 242(3):291–301, 1994. (Cited on page 101.)

[25] J. Cohen, A. Arkhipov, R. Braun, and K. Schulten. Imaging the migration pathways for o2, co, no, and xe inside myoglobin. *Biophysical journal*, 91(5):1844–1857, 2006. (Cited on pages 22, 42, and 94.)

[26] G. Damaschun, H. Damaschun, K. Gast, and D. Zirwer. Denatured states of yeast phosphoglycerate kinase. *Biochemistry (Moscow)*, 63:259–275, 1998. (Cited on page 101.)

[27] A. Di Pace, A. Cupane, M. Leone, E. Vitrano, and L. Cordone. Protein dynamics. vibrational coupling, spectral broadening mechanisms, and anharmonicity effects in carbonmonoxy heme proteins studied by the temperature dependence of the soret band lineshape. *Biophysical journal*, 63(2):475–484, 1992. (Cited on pages 11 and 35.)

[28] W. Doster. The dynamical transition of proteins, concepts and misconceptions. *European Biophysics Journal*, 37(5):591–602, 2008. (Cited on page 35.)

[29] W. Doster, S. Cusack, and W. Petry. Dynamical transition of myoglobin revealed by inelastic neutron scattering. *Nature*, 337(6209):754–756, Feb 1989. (Cited on page 11.)

[30] D. L. Drabkin. Spectrophotometric studies. *Journal of Biological Chemistry*, 164(2): 703–723, 1946. (Cited on page 12.)

[31] M. R. Eftink. *Topics in Fluorescence Spectroscopy*, volume 2: Principles. Plenum Press, New York, 1991. (Cited on page 25.)

[32] J. Englander, C. Del Mar, W. Li, S. Englander, J. Kim, D. Stranz, Y. Hamuro, and V. Woods. Protein structure change studied by hydrogen-deuterium exchange, functional labeling, and mass spectrometry. *Proceedings of the National Academy of Sciences of the United States of America*, 100(12):7057, 2003. (Cited on page 95.)

[33] V. Feher and J. Cavanagh. Millisecond-timescale motions contribute to the function of the bacterial response regulator protein spoof. *Nature*, 400(6741):289–293, 1999. (Cited on page 11.)

[34] P. Fenimore, H. Frauenfelder, B. McMahon, and F. Parak. Slaving: solvent fluctuations dominate protein dynamics and functions. *Proceedings of the National Academy of Sciences*, 99(25):16047, 2002. (Cited on pages 32 and 35.)

[35] P. Fenimore, H. Frauenfelder, B. McMahon, and R. Young. Bulk-solvent and hydration-shell fluctuations, similar to α-and β-fluctuations in glasses, control protein motions and functions. *Proceedings of the National Academy of Sciences of the United States of America*, 101(40):14408, 2004. (Cited on pages viii, 31, 35, and 36.)

[36] J. Fidy, E. Balog, and M. Köhler. Proteins in electric fields and pressure fields: experimental results. *Biochim Biophys Acta*, 1386(2):289–303, Aug 1998. (Cited on pages 57 and 79.)

[37] J. Fidy, M. Laberge, A. Kaposi, and J. Vanderkooi. Fluorescence line narrowing applied to the study of proteins. *Biochimica et Biophysica Acta (BBA)-Protein Structure and Molecular Enzymology*, 1386(2):331–351, 1998. (Cited on pages 79 and 81.)

[38] R. Forman, G. Piermarini, J. Barnett, and S. Block. Pressure measurement made by the utilization of ruby sharp-line luminescence. *Science*, 176(4032):284–285, 1972. (Cited on page 84.)

[39] H. Frauenfelder, S. Sligar, and P. Wolynes. The energy landscapes and motions of proteins. *Science*, 254(5038):1598–1603, 1991. (Cited on pages 11, 31, and 35.)

[40] H. Frauenfelder, B. McMahon, and P. Fenimore. Myoglobin: the hydrogen atom of biology and a paradigm of complexity. *Proceedings of the National Academy of Sciences*, 100(15):8615, 2003. (Cited on pages 11 and 35.)

[41] H. Frauenfelder, P. Fenimore, G. Chen, and B. McMahon. Protein folding is slaved to solvent motions. *Proceedings of the National Academy of Sciences*, 103(42):15469–15472, 2006. (Cited on pages 11 and 35.)

[42] H. Frauenfelder, G. Chen, J. Berendzen, P. Fenimore, H. Jansson, B. McMahon, I. Stroe, J. Swenson, and R. Young. A unified model of protein dynamics. *Proceedings of the National Academy of Sciences*, 106(13):5129, 2009. (Cited on pages 11 and 35.)

[43] J. Friedrich and D. Haarer. Photochemical hole burning: a spectroscopic study of relaxation processes in polymers and glasses. *Angewandte Chemie International Edition in English*, 23(2):113–140, 1984. (Cited on pages 81 and 83.)

[44] M. Gadsden, E. McIntosh, J. Game, P. Wilson, and R. Haynes. dutp pyrophosphatase is an essential enzyme in saccharomyces cerevisiae. *The EMBO journal*, 12 (11):4425, 1993. (Cited on page 109.)

[45] M. Gonnelli and G. Strambini. Phosphorescence lifetime of tryptophan in proteins. *Biochemistry*, 34(42):13847–13857, 1995. (Cited on page 25.)

[46] P. J. Goodford, J. St-Louis, and R. Wootton. The interaction of human haemoglobin with allosteric effectors as a model for drug-receptor interactions. *Br J Pharmacol*, 68(4):741–748, Apr 1980. (Cited on page 45.)

[47] D. Gottfried, E. Peterson, A. Sheikh, J. Wang, M. Yang, and J. Friedman. Evidence for damped hemoglobin dynamics in a room temperature trehalose glass. *The Journal of Physical Chemistry*, 100(29):12034–12042, 1996. (Cited on page 11.)

[48] R. D. Gray and Q. H. Gibson. The effect of inositol hexaphosphate on the kinetics of co and o 2 binding by human hemoglobin. *J Biol Chem*, 246(23):7168–7174, Dec 1971. (Cited on page 47.)

[49] Z. Gryczynski, T. Tenenholz, and E. Bucci. Rates of energy transfer between tryptophans and hemes in hemoglobin, assuming that the heme is a planar oscillator. *Biophys J*, 63(3):648–653, Sep 1992. (Cited on pages 64 and 72.)

[50] Z. Gryczynski, S. Beretta, J. Lubkowski, A. Razynska, I. Gryczynski, and E. Bucci. Time-resolved fluorescence of hemoglobin species. *Biophys Chem*, 64(1-3):81–91, Feb 1997. (Cited on page 72.)

[51] S. Hagen, J. Hofrichter, and W. Eaton. Protein reaction kinetics in a room-temperature glass. *Science*, 269(5226):959–962, 1995. (Cited on page 11.)

[52] R. N. Haire and B. E. Hedlund. Thermodynamic aspects of the linkage between binding of chloride and oxygen to human hemoglobin. *Proceedings of the National Academy of Sciences*, 74(10):4135–4138, 1977. (Cited on page 47.)

[53] D. Hamdane, L. Kiger, G. H. B. Hoa, S. Dewilde, J. Uzan, T. Burmester, T. Hankeln, L. Moens, and M. C. Marden. High pressure enhances hexacoordination in neuroglobin and other globins. *Journal of Biological Chemistry*, 280(44):36809–36814, 2005. (Cited on page 65.)

[54] A. Harriman. Luminescence of porphyrins and metalloporphyrins. part 3: Heavy-atom effects. *J. Chem. Soc., Faraday Trans. 2*, 77(7):1281–1291, 1981. (Cited on page 27.)

[55] Y. He, P. Ku, J. Knab, J. Chen, and A. Markelz. Protein dynamical transition does not require protein structure. *Physical review letters*, 101(17):178103, 2008. (Cited on page 11.)

[56] K. Henzler-Wildman and D. Kern. Dynamic personalities of proteins. *Nature*, 450 (7172):964–972, 2007. (Cited on page 11.)

[57] K. Henzler-Wildman, M. Lei, V. Thai, S. Kerns, M. Karplus, and D. Kern. A hierarchy of timescales in protein dynamics is linked to enzyme catalysis. *Nature*, 450 (7171):913–916, 2007. (Cited on page 11.)

[58] K. Heremans and L. Smeller. Protein structure and dynamics at high pressure. *Biochim Biophys Acta*, 1386(2):353–370, Aug 1998. (Cited on pages 57 and 65.)

[59] T. Herskovits and V. Ibanez. Light-scattering investigations of the subunit dissociation of human hemoglobin a. effects of the aliphatic acid salts. *Biochemistry*, 15(26): 5715–5721, 1976. (Cited on page 76.)

[60] R. E. Hirsch and R. L. Nagel. Conformational studies of hemoglobins using intrinsic fluorescence measurements. *Journal of Biological Chemistry*, 256(3):1080–1083, 1981. (Cited on page 71.)

[61] R. E. Hirsch, R. S. Zukin, and R. L. Nagel. Intrinsic fluorescence emission of intact oxy hemoglobins. *Biochem Biophys Res Commun*, 93(2):432–439, Mar 1980. (Cited on page 71.)

[62] R. E. Hirsch, G. J. Vidugiris, J. M. Friedman, and J. P. Harrington. Alteration of tryptophan fluorescence properties upon dissociation of lumbricus terrestris hemoglobin. *Biochim Biophys Acta*, 1205(2):248–251, Apr 1994. (Cited on pages 71 and 72.)

[63] L. Hosszu, C. Craven, J. Spencer, M. Parker, A. Clarke, M. Kelly, and J. Waltho. Is the structure of the n-domain of phosphoglycerate kinase affected by isolation from the intact molecule? *Biochemistry*, 36(2):333–340, 1997. (Cited on page 101.)

[64] Y. Huang, M. L. Doyle, and G. K. Ackers. The oxygen-binding intermediates of human hemoglobin: evaluation of their contributions to cooperativity using zinc-containing hybrids. *Biophys J*, 71(4):2094–2105, Oct 1996. (Cited on pages 57 and 58.)

[65] K. Imai. *Allosteric Effects in Hemoglobin*. Cambridge University Press, 1982. (Cited on page 45.)

[66] R. Joseph and R. Lakowicz. *Principles of Fluorescence Spectroscopy*. Kluwer Academic/Plenum Publishers, New York, 1999. (Cited on page 81.)

[67] C. Jung, G. Hui Bon Hoa, D. Davydov, E. Gill, and K. Heremans. Compressibility of the heme pocket of substrate analogue complexes of cytochrome p-450cam-co. the effect of hydrostatic pressure on the soret band. *Eur J Biochem*, 233(2):600–606, Oct 1995. (Cited on pages 64 and 68.)

[68] A. Kaposi. *High resolution fluorescence spectroscopy in the study of the structure of chromoproteids.* PhD thesis, Hungarian Academy of Sciences, Biophysics Research Laboratory, 1993. (Cited on pages ix, 80, and 95.)

[69] M. Karplus, T. Ichiye, and B. Pettitt. Configurational entropy of native proteins. *Biophysical journal*, 52(6):1083–1085, 1987. (Cited on pages 41 and 94.)

[70] J. K. Kauppinen, D. J. Moffatt, H. H. Mantsch, and D. G. Cameron. Fourier self-deconvolution: A method for resolving intrinsically overlapped bands. *Applied Spectroscopy*, 35(3):271 – 276, 1981. (Cited on page 61.)

[71] M. Köhler, J. Friedrich, and J. Fidy. Proteins in electric fields and pressure fields: basic aspects. *Biochim Biophys Acta*, 1386(2):255–288, Aug 1998. (Cited on page 57.)

[72] I. Kövesi, G. Schay, T. Yonetani, M. Laberge, and J. Fidy. High pressure reveals that the stability of interdimeric contacts in the r- and t-state of hba is influenced by allosteric effectors: Insights from computational simulations. *Biochim Biophys Acta*, 1764(3):516–521, Mar 2006. (Cited on pages 48, 55, and 71.)

[73] M. Laberge, I. Kövesi, T. Yonetani, and J. Fidy. R-state hemoglobin bound to heterotropic effectors: models of the dpg, ihp and rsr13 binding sites. *FEBS Lett*, 579 (3):627–632, Jan 2005. (Cited on page 47.)

[74] B. B. Laird and J. L. Skinner. Microscopic theory of reversible pressure broadening in hole-burning spectra of impurities in glasses. *The Journal of Chemical Physics*, 90 (6):3274–3281, 1989. (Cited on pages 68 and 83.)

[75] I. Lalezari, P. Lalezari, C. Poyart, M. Marden, J. Kister, B. Bohn, G. Fermi, and M. F. Perutz. New effectors of human hemoglobin: structure and function. *Biochemistry*, 29(6):1515–1523, Feb 1990. (Cited on page 45.)

[76] L. Landau and E. Lifshitz. Theoretical physics. *V*, 6:288–289, 1988. (Cited on page 82.)

[77] M. Lucas and V. Guallar. An atomistic view on human hemoglobin carbon monoxide migration processes. *Biophysical Journal*, 102(4):887 – 896, 2012. ISSN 0006-3495. (Cited on page 3.)

[78] S. Lusceac, M. Vogel, and C. Herbers. 2h and 13c nmr studies on the temperature-dependent water and protein dynamics in hydrated elastin, myoglobin and collagen. *Biochimica et Biophysica Acta (BBA)-Proteins & Proteomics*, 1804(1):41–48, 2010. (Cited on page 35.)

[79] B. Ma, T. Elkayam, H. Wolfson, and R. Nussinov. Protein–protein interactions: structurally conserved residues distinguish between binding sites and exposed protein surfaces. *Proceedings of the National Academy of Sciences*, 100(10):5772, 2003. (Cited on page 11.)

[80] A. Massari, I. Finkelstein, B. McClain, A. Goj, X. Wen, K. Bren, R. Loring, and M. Fayer. The influence of aqueous versus glassy solvents on protein dynamics: Vibrational echo experiments and molecular dynamics simulations. *Journal of the American Chemical Society*, 127(41):14279–14289, 2005. (Cited on pages 11 and 33.)

[81] K. Mayo, D. Kucheida, F. Parak, and J. Chien. Structural dynamics of human deoxyhemoglobin and hemochrome investigated by nuclear gamma resonance absorption (mössbauer) spectroscopy. *Proceedings of the National Academy of Sciences*, 80(17):5294, 1983. (Cited on page 36.)

[82] J. G. McLean and I. M. Lewis. Oxygen affinity responses to 2,3-diphosphoglycerate, and methaemoglobin formation in horse and human haemoglobins. *Res Vet Sci*, 19 (3):259–262, Nov 1975. (Cited on page 45.)

[83] F. Meersman, L. Smeller, and K. Heremans. Extending the pressure-temperature state diagram of myoglobin. *Helvetica Chimica Acta*, 88(3):546–556, 2005. ISSN 1522-2675. (Cited on page 65.)

[84] B. Mészáros, J. Tóth, B. Vértessy, Z. Dosztányi, and I. Simon. Proteins with complex architecture as potential targets for drug design: A case study of mycobacterium tuberculosis. *PLoS computational biology*, 7(7):e1002118, 2011. (Cited on page 109.)

[85] D. Missiakas, J. Betton, P. Minard, and J. Yon. Unfolding-refolding of the domains in yeast phosphoglycerate kinase: comparison with the isolated engineered domains. *Biochemistry*, 29(37):8683–8689, 1990. (Cited on page 101.)

[86] A. Mittermaier and L. Kay. New tools provide new insights in nmr studies of protein dynamics. *Science's STKE*, 312(5771):224, 2006. (Cited on page 119.)

[87] G. Miyazaki, H. Morimoto, K. Yun, S. Park, A. Nakagawa, H. Minagawa, and N. Shibayama. Magnesium (ii) and zinc (ii)-protoporphyrin ix's stabilize the lowest oxygen affinity state of human hemoglobin even more strongly than deoxyheme1. *Journal of molecular biology*, 292(5):1121–1136, 1999. (Cited on pages 58 and 73.)

[88] K. Modig, E. Liepinsh, G. Otting, and B. Halle. Dynamics of protein and peptide hydration. *J Am Chem Soc*, 126(1):102–114, Jan 2004. (Cited on page 11.)

[89] J. Monod, J. Wyman, and J. P. Changeux. On the nature of allosteric transitions: A plausible model. *J Mol Biol*, 12:88–118, May 1965. (Cited on page 45.)

[90] G. B. Ogunmola, A. Zipp, F. Chen, and W. Kauzmann. Effects of pressure on visible spectra of complexes of myoglobin, hemoglobin, cytochrome c, and horse radish peroxidase. *Proceedings of the National Academy of Sciences*, 74(1):1–4, 1977. (Cited on page 57.)

[91] M. Orrit, J. Bernard, and R. Personov. High-resolution spectroscopy of organic molecules in solids: from fluorescence line narrowing and hole burning to single molecule spectroscopy. *The Journal of Physical Chemistry*, 97(40):10256–10268, 1993. (Cited on page 79.)

[92] S. Osváth and M. Gruebele. Proline can have opposite effects on fast and slow protein folding phases. *Biophysical journal*, 85(2):1215–1222, 2003. (Cited on page 101.)

[93] S. Osváth, J. Sabelko, and M. Gruebele. Tuning the heterogeneous early folding dynamics of phosphoglycerate kinase. *Journal of molecular biology*, 333(1):187–199, 2003. (Cited on page 101.)

[94] S. Osváth, G. Köhler, P. Závodszky, and J. Fidy. Asymmetric effect of domain interactions on the kinetics of folding in yeast phosphoglycerate kinase. *Protein science*, 14(6):1609–1616, 2005. (Cited on pages x, 102, and 106.)

[95] S. Osváth, G. Köhler, P. Závodszky, and J. Fidy. Assymetric effect of domain interactions on the kinetics of folding in yeast phosphoglycerate kinase. *Protein Science*, 14:1609 – 1616, 2005. (Cited on page 24.)

[96] A. Paciaroni, S. Cinelli, and G. Onori. Effect of the environment on the protein dynamical transition: A neutron scattering study. *Biophysical Journal*, 83(2):1157 – 1164, 2002. ISSN 0006-3495. (Cited on page 52.)

[97] F. Parak, E. W. Knapp, and D. Kucheida. Protein dynamics: Moessbauer spectroscopy on deoxymyoglobin crystals. *Journal of Molelcular Biology*, 161:177–194, 1982. (Cited on pages 11, 35, and 36.)

[98] S. Y. Park, A. Nakagawa, and H. Morimoto. High-resolution crystal structure of magnesium (mgii)-iron (feii) hybrid hemoglobin with liganded beta subunits. *J Mol Biol*, 255(5):726–734, Feb 1996. (Cited on page 58.)

[99] F. Pecorari, C. Guilbert, P. Minard, M. Desmadril, and J. Yon. Folding and functional complementation of engineered fragments from yeast phosphoglycerate kinase. *Biochemistry*, 35(11):3465–3476, 1996. (Cited on page 101.)

[100] R. Personov. Site selection spectroscopy of complex molecules in solutions and its applications. *Spectroscopy and excitation dynamics of condensed molecular systems*, 4: 555–580, 1983. (Cited on page 79.)

[101] M. F. Perutz. Stereochemistry of cooperative effects in haemoglobin. *Nature*, 228 (5273):726–739, Nov 1970. (Cited on page 45.)

[102] M. F. Perutz, G. Fermi, B. Luisi, B. Shaanan, and R. C. Liddington. Stereochemistry of cooperative mechanisms in hemoglobin. *Accounts of Chemical Research*, 20(9): 309–321, 1987. (Cited on pages 45 and 47.)

[103] M. F. Perutz, A. J. Wilkinson, M. Paoli, and G. G. Dodson. The stereochemical mechanism of the cooperative effects in hemoglobin revisited. *Annu Rev Biophys Biomol Struct*, 27:1–34, 1998. (Cited on page 47.)

[104] M. F. Perutz, M. F., W. Bolton, R. Diamond, H. Muirhead, and H. C. Watson. Structure of haemoglobin.an x-ray examination of reduced horse haemoglobin. *Nature*, 203:687–690, Aug 1964. (Cited on page 45.)

[105] S. Pin, C. Royer, E. Gratton, B. Alpert, and G. Weber. Subunit interactions in hemoglobin probed by fluorescence and high-pressure techniques. *Biochemistry*, 29(39):9194 – 9202, 1990. (Cited on pages 43, 57, 68, and 73.)

[106] C. Poyart, M. C. Marden, and J. Kister. Bezafibrate derivatives as potent effectors of hemoglobin. *Methods Enzymol*, 232:496–513, 1994. (Cited on page 45.)

[107] Y. Reshetnyak and E. Burshtein. Assignment of the components of the fluorescence spectrum of protein to tryptophan residues based on the properties of their microenvirons in a three-dimensional structure. *Biophysics*, 42(2):267–274, 1997. (Cited on page 71.)

[108] D. Ringe and G. Petsko. The glass transition'in protein dynamics: what it is, why it occurs, and how to exploit it. *Biophysical chemistry*, 105(2-3):667–680, 2003. (Cited on pages 11 and 35.)

[109] M. Ritco-Vonsovici, B. Mouratou, P. Minard, M. Desmadril, J. Yon, M. Andrieux, E. Leroy, and E. Guittet. Role of the c-terminal helix in the folding and stability of yeast phosphoglycerate kinase. *Biochemistry*, 34(3):833–841, 1995. (Cited on page 101.)

[110] K. Ruan, S. Tian, R. Lange, and C. Balny. Pressure effects on tryptophan and its derivatives. *Biochem Biophys Res Commun*, 269(3):681 – 686, Mar 2000. (Cited on page 69.)

[111] U. Samuni, L. Juszczak, D. Dantsker, I. Khan, A. J. Friedman, J. Pérez-González-de Apodaca, S. Bruno, H. L. Hui, J. E. Colby, E. Karasik, L. D. Kwiatkowski, A. Mozzarelli, R. Noble, and J. M. Friedman. Functional and spectroscopic characterization of half-liganded iron-zinc hybrid hemoglobin: evidence for conformational plasticity within the t state. *Biochemistry*, 42(27):8272–8288, Jul 2003. (Cited on pages 58 and 73.)

[112] U. Samuni, D. Dantsker, L. J. Juszczak, S. Bettati, L. Ronda, A. Mozzarelli, and J. M. Friedman. Spectroscopic and functional characterization of t state hemoglobin conformations encapsulated in silica gels. *Biochemistry*, 43(43):13674–13682, Nov 2004. (Cited on pages 57, 58, 71, and 73.)

[113] U. Samuni, C. J. Roche, D. Dantsker, L. J. Juszczak, and J. M. Friedman. Modulation of reactivity and conformation within the t-quaternary state of human hemoglobin: the combined use of mutagenesis and sol-gel encapsulation. *Biochemistry*, 45(9): 2820–2835, Mar 2006. (Cited on pages 58, 71, and 73.)

[114] A. Savitzky and M. Golay. Smoothing and differentiation of data by simplified least squares procedures. *Analytical chemistry*, 36(8):1627–1639, 1964. (Cited on page 60.)

[115] G. Schay, F. Tölgyesi, and J. Fidy. A polymer sensor to measure oxygen concentration in liquids and gases., 1998. (Cited on page 4.)

[116] G. Schay, F. Tölgyesi, J. Fidy, G. Csík, and F. Gábor. A method to determine the antibiotic susceptibility of oxygen consuming microorganisms., 1998. (Cited on page 4.)

[117] G. Schay, L. Smeller, A. Tsuneshige, T. Yonetani, and J. Fidy. Allosteric effectors influence the tetramer stability of both r-and t-states of hemoglobin a. *Journal of Biological Chemistry*, 281(36):25972–25983, 2006. (Cited on pages 3, 33, 48, 55, 71, 75, and 76.)

[118] G. Schay, L. Hereényi, M. Kellermayer, K. Moódos, T. Yonetani, and J. Fidy. Millisecond time-scale protein dynamics exists prior to the activation of the bulk solvent matrix. *The Journal of Physical Chemistry B*, 115 (19):5707 – 5715, 2011. (Cited on page 111.)

[119] F. A. Seixas, W. de Azevedo, Jr, and M. F. Colombo. Crystallization and x-ray diffraction data analysis of human deoxyhaemoglobin a(0) fully stripped of any anions. *Acta Crystallogr D Biol Crystallogr*, 55(Pt 11):1914–1916, Nov 1999. (Cited on page 47.)

[120] N. Shibayama, H. Morimoto, and T. Kitagawa. Properties of chemically modified ni(ii)-fe(ii) hybrid hemoglobins. ni(ii) protoporphyrin ix as a model for a permanent deoxy-heme. *J Mol Biol*, 192(2):331–336, Nov 1986. (Cited on page 58.)

[121] N. Shibayama, S. Miura, J. R. H. Tame, T. Yonetani, and S.-Y. Park. Crystal structure of horse carbonmonoxyhemoglobin-bezafibrate complex at 1.55-åresolution. *Journal of Biological Chemistry*, 277(41):38791–38796, 2002. (Cited on page 47.)

[122] J. Shlomai and A. Kornberg. Deoxyuridine triphosphatase of escherichia coli. purification, properties, and use as a reagent to reduce uracil incorporation into dna. *Journal of Biological Chemistry*, 253(9):3305–3312, 1978. (Cited on page 109.)

[123] J. Silva and G. Weber. Pressure stability of proteins. *Annual Review of Physical Chemistry*, 44(1):89–113, 1993. (Cited on pages 57 and 68.)

[124] J. L. Silva, D. Foguel, and C. A. Royer. Pressure provides new insights into protein folding, dynamics and structure. *Trends Biochem Sci*, 26(10):612 – 618, Oct 2001. (Cited on pages 57 and 68.)

[125] L. Smeller. Pressure-temperature phase diagrams of biomolecules. *Biochim Biophys Acta*, 1595(1-2):11–29, Mar 2002. (Cited on page 57.)

[126] L. Smeller and J. Fidy. The enzyme horseradish peroxidase is less compressible at higher pressures. *Biophysical Journal*, 82(1):426 – 436, 2002. ISSN 0006-3495. (Cited on pages 3 and 83.)

[127] L. Smeller, K. Goossens, and K. Heremans. How to minimize certain artifacts in fourier self-deconvolution. *Applied spectroscopy*, 49(10):1538–1542, 1995. (Cited on page 61.)

[128] L. Smeller, K. Goossens, and K. Heremans. *High Pressure Science and Technology*. World Scientific Co. Pte. Ltd., Singapore, 1996. (Cited on pages 65 and 68.)

[129] X. Song, V. Simplaceanu, N. Ho, and C. Ho. Effector-induced structural fluctuation regulates the ligand affinity of an allosteric protein: Binding of inositol hexaphosphate has distinct dynamic consequences for the t and r states of hemoglobin. *Biochemistry*, 47(17):4907–4915, 2008. (Cited on page 11.)

[130] V. Šrajer, Z. Ren, T. Teng, M. Schmidt, T. Ursby, D. Bourgeois, C. Pradervand, W. Schildkamp, M. Wulff, and K. Moffat. Protein conformational relaxation and ligand migration in myoglobin: a nanosecond to millisecond molecular movie from time-resolved laue x-ray diffraction. *Biochemistry*, 40(46):13802–13815, 2001. (Cited on pages 11 and 94.)

[131] A. Szabo and M. Karplus. A mathematical model for structure-function relations in hemoglobin. *J Mol Biol*, 72(1):163–197, Dec 1972. (Cited on page 45.)

[132] E. Takács, O. Barabás, M. Petoukhov, D. Svergun, and B. Vértessy. Molecular shape and prominent role of β-strand swapping in organization of dutpase oligomers. *FEBS letters*, 583(5):865–871, 2009. (Cited on page 109.)

[133] E. Takács, G. Nagy, I. Leveles, V. Harmat, A. Lopata, J. Tóth, and B. Vértessy. Direct contacts between conserved motifs of different subunits provide major contribution to active site organization in human and mycobacterial dutpases. *FEBS letters*, 584(14):3047–3054, 2010. (Cited on page 109.)

[134] P. Tamarat, A. Maali, B. Lounis, and M. Orrit. Ten years of single-molecule spectroscopy. *The Journal of Physical Chemistry A*, 104(1):1–16, 2000. (Cited on page 79.)

[135] N. Tanaka, C. Ikeda, K. Kanaori, K. Hiraga, T. Konno, and S. Kunugi. Pressure effect on the conformational fluctuation of apomyoglobin in the native state. *Biochemistry*, 39(39):12063–12068, Oct 2000. (Cited on page 73.)

[136] R. Tilton Jr, I. Kuntz Jr, and G. Petsko. Cavities in proteins: structure of a metmyoglobin xenon complex solved to 1.9. ang. *Biochemistry*, 23(13):2849–2857, 1984. (Cited on pages 22, 42, and 94.)

[137] K. Tompa, P. Bánki, M. Bokor, P. Kamasa, G. Lasanda, and P. Tompa. Interfacial water at protein surfaces: Wide-line nmr and dsc characterization of hydration in ubiquitin solutions. *Biophysical journal*, 96(7):2789–2798, 2009. (Cited on pages 29, 35, and 37.)

[138] P. Tompa, P. Bánki, M. Bokor, P. Kamasa, D. Kovács, G. Lasanda, and K. Tompa. Protein-water and protein-buffer interactions in the aqueous solution of an intrinsically unstructured plant dehydrin: Nmr intensity and dsc aspects. *Biophysical journal*, 91(6):2243–2249, 2006. (Cited on pages 27, 29, 35, and 37.)

[139] J. Tóth, B. Varga, M. Kovács, A. Málnási-Csizmadia, and B. Vértessy. Kinetic mechanism of human dutpase, an essential nucleotide pyrophosphatase enzyme. *Journal of Biological Chemistry*, 282(46):33572–33582, 2007. (Cited on page 109.)

[140] T. Traut. Physiological concentrations of purines and pyrimidines. *Molecular and cellular biochemistry*, 140(1):1–22, 1994. (Cited on page 109.)

[141] A. Tsuneshige and T. Yonetani. Preparation of mixed metal hybrids. *Methods in Enzymology*, 231:215–222, 1994. (Cited on pages 12 and 48.)

[142] A. Tsuneshige, S. Park, and T. Yonetani. Heterotropic effectors control the hemoglobin function by interacting with its t and r states–a new view on the principle of allostery. *Biophys Chem*, 98(1-2):49–63, Jul 2002. (Cited on pages 12, 47, and 48.)

[143] S. Tzeng and C. Kalodimos. Protein dynamics and allostery: an nmr view. *Current opinion in structural biology*, 21(1):62–67, 2011. (Cited on page 119.)

[144] G. G. Van Beek and S. H. De Bruin. The ph dependence of the binding of d-glycerate 2,3-bisphosphate to deoxyhemoglobin and oxyhemoglobin. determination of the number of binding sites in oxyhemoglobin. *Eur J Biochem*, 100(2):497–502, Oct 1979. (Cited on page 47.)

[145] J. Vanderkooi, G. Maniara, T. Green, and D. Wilson. An optical method for measurement of dioxygen concentration based upon quenching of phosphorescence. *Journal of Biological Chemistry*, 262(12):5476–5482, 1987. (Cited on page 25.)

[146] A. Varga, B. Flachner, É. Gráczer, S. Osváth, A. Szilágyi, and M. Vas. Correlation between conformational stability of the ternary enzyme–substrate complex and domain closure of 3-phosphoglycerate kinase. *FEBS Journal*, 272(8):1867–1885, 2005. (Cited on pages 101 and 106.)

[147] B. Varga, O. Barabás, J. Kovári, J. Tóth, É. Hunyadi-Gulyás, É. Klement, K. Medzihradszky, F. Tölgyesi, J. Fidy, and B. Vértessy. Active site closure facilitates juxtaposition of reactant atoms for initiation of catalysis by human dutpase. *FEBS letters*, 581(24):4783–4788, 2007. (Cited on pages x, 109, and 110.)

[148] B. Veértessy and J. Toóth. Keeping uracil out of dna: physiological role, structure and catalytic mechanism of dutpases. *Accounts of chemical research*, 42(1):97–106, 2008. (Cited on page 109.)

[149] J. T. Vivian and P. R. Callis. Mechanisms of tryptophan fluorescence shifts in proteins. *Biophys J*, 80(5):2093–2109, May 2001. (Cited on page 71.)

[150] H. Watson, N. Walker, P. Shaw, T. Bryant, P. Wendell, L. Fothergill, R. Perkins, S. Conroy, M. Dobson, M. Tuite, et al. Sequence and structure of yeast phosphoglycerate kinase. *The EMBO journal*, 1(12):1635, 1982. (Cited on pages 101 and 107.)

[151] B. Weinstein. Ruby thermometer for cryobaric diamond-anvil cell. *Review of Scientific Instruments*, 57(5):910–913, 1986. (Cited on page 84.)

[152] S. L. White. Titration of the carboxyhemoglobin tetramer-dimer equilibrium by inositol hexaphosphate. *Journal of Biological Chemistry*, 251(15):4763–4769, 1976. (Cited on page 76.)

[153] P. Wong and D. Moffat. A new internal pressure calibrant for high-pressure infrared spectroscopy of aqueous systems. *Applied Spectroscopy*, 43(7):1279–1281, 1989. (Cited on page 61.)

[154] T. Yonetani and M. Laberge. Protein dynamics explain the allosteric behaviors of hemoglobin. *Biochimica et Biophysica Acta (BBA)-Proteins & Proteomics*, 1784(9): 1146–1158, 2008. (Cited on page 43.)

[155] T. Yonetani, S. Park, A. Tsuneshige, K. Imai, and K. Kanaori. Global allostery model of hemoglobin. *Journal of Biological Chemistry*, 277(37):34508–34520, 2002. (Cited on pages 3, 47, 48, and 77.)

[156] L. Zhang, L. Wang, Y. Kao, W. Qiu, Y. Yang, O. Okobiah, and D. Zhong. Mapping hydration dynamics around a protein surface. *Proceedings of the National Academy of Sciences*, 104(47):18461, 2007. (Cited on page 11.)

[157] J. Zollfrank, J. Friedrich, J. Fidy, and J. M. Vanderkooi. Photochemical holes under pressure: Compressibility and volume fluctuations of a protein. *The Journal of Chemical Physics*, 94(12):8600–8603, 1991. (Cited on pages 31, 68, and 83.)

[158] J. Zollfrank, J. Friedrich, J. M. Vanderkooi, and J. Fidy. Conformational relaxation of a low-temperature protein as probed by photochemical hole burning. horseradish peroxidase. *Biophys J*, 59(2):305–312, Feb 1991. (Cited on pages 11, 68, and 83.)

ÖSSZEFOGLALÓ

A dolgozatban egy új, foszforeszcencián alapuló módszer kerül bemutatásra, mellyel fehérjék lassú (ma ... s időskálájú), kollektív mozgásainak aktivációja vizsgálható. Bemutatom, hogy ez az aktiváció specifikusan a fehérjére jellemző. Az aktivációs jelenség kvalitatív és kvantitatív értelmezésére is sor kerül egy nagyon egyszerű modell segítségével, amely azonban a jelenség lényegét leírja, és segítségével meghatározható (becsülhető) az aktivációs energia és entrópia. A módszert az első fejezetben humán hemoglobin esetében mutatom be, más spektroszkópiai módszerekkel kapható adatokkal együtt. A foszforeszcencián alapuló módszerrel kapható adatokat összevetem egy nyomás-perturbációs kísérletből kapható disszociációs állandókkal, illetve a fluoreszcencia vonal-keskenyedés módszerével kapható izotermikus kompresszibilitás változások adataival. Megállapítható, hogy hemoglobin esetében mindhárom módszer adatai korrelálnak az alloszterikus effektorok ismert hatáserősség-sorrendjével. Mindhárom módszer adatait figyelembe véve feltételezhető, hogy az alloszterikus effektorok hatásmechanizmusában a lassú, kollektív dinamika befolyásolásának fontos szerepe lehet. A második fejezetben bemutatom az új foszforeszcencián alapuló módszer alkalmazását két másik fehérje, a foszfoglicerát kináz (PGK) és a dUTP pirofoszfatáz (dUTPáz) esetében. Foszfoglicerát kináz esetében kimutatható, hogy a fehérje két (N és C) doménje között aszimmetrikus kommunikáció valósul meg abban az esetben is, amikor a szerkezet ismert csuklómozgása gátolt. Az adatok alapján feltételezhető egy más, nem az ismert csuklómozgáson alapuló dinamikai kölcsönhatás megléte is. dUTPáz esetében eltérés tapasztalható a homotrimer molekula C-terminális kar-szerű végének dinamikai viselkedése között az apo-enzim és a szubsztrát-analógot kötött forma esetében. Mivel ez a kar fontos szerepet tölt be az aktív centrum kialakításában, így felvetődik a kollektív mozgások esetleges szerepe a funkció szabályozásában, azonban ennek pontosabb tisztázására ebben az esetben további kísérletekre van szükség. Összefoglalva megállapítható, hogy az új foszforeszcencián alapuló módszer több fehérje esetében is a funkcióval összefüggésbe hozható eredményeket szolgáltat, ami felveti annak lehetőségét, hogy a lassú kollektiv dinamika fontos szerepet játszhat a több-doménes fehérjék működésének szabályozásában.

ABSTRACT

A new phosphorescence-based method is presented, by which the activation of slow (ms - s time-scale) global dynamics of proteins can be monitored. It is shown, that the activation of this slow, global dynamics is specific for the protein. A simple model is also presented by which the activation energy and entropy can be calculated (estimated) from the experimental data. The new method is presented in the case of human hemoglobin. The experiments were performed also in the presence of allosteric effector molecules, which modify the oxygen-binding of hemoglobin. As a consequence of the presence of these effectors we have observed changes in the activation of the collective dynamics of hemoglobin, changes in the dissociation constant of the tetramer obtained by pressure perturbation, and also changes in the isothermal compressibility obtained by fluorescence line narrowing spectroscopy. All these changes are in accordance with the efficiency of the effectors in modifying the oxygen binding of hemoglobin. This shows that changes in the global, slow dynamics of hemoglobin, caused by allosteric effectors may play a significant role in the regulation of hemoglobin function. The phosphorescence-based method is also applied to two other proteins, namely phosphoglycerate kinase, and dUTP-pyrophosphatase. In the case of phosphoglycerate kinase it was shown that the activation of the dynamics is asymmetric, and depends on the presence of both domains. Apparently, the hinge-bending motion is not essential for the inter-domain communication: there is a collective dynamics of the two domains even when hinge bending is blocked. In the case of dUTP-pyrophosphatase it was shown that the C-terminal arm-like structures of the trimeric molecule have a distinct dynamics in the apo-enzyme and in the substrate-bound form. It may thus be hypothesized that the special type of dynamics being monitored in these experiments may be important in the regulation of multi-domain proteins.

Part III

APPENDIX

GENERAL REMARKS

It would not be possible to acquire the data presented in this thesis without the use of custom-designed and custom-built instrumentation. During the years of my PhD work, a significant amount if time had to be devoted to engineering work. Since this thesis is not an engineering thesis, and there are also space considerations, I will show only some aspects of the instrumental developments, and will try to give an overview of that side of my work. Would it be an electrical engineering diploma-thesis, then I could explain all the electronics schematics, and all the software codes, but this is not my intention here. This appendix is not strictly needed to understand the thesis itself, but I think it is important to see, that experimental science sometimes also involves a lot of engineering. I had my joy also in designing and building instruments, and the motivation to have this appendix is partly to show these results as well.

A

PHOSPHORESCENCE SETUP

A.1 SYSTEM DESIGN

The development of a new technique inevitably involves the need of instrumentation developments. This case in not different from the others, I first had to change our old fluorimeter setup, and then gradually build a completely new system re-using as many building blocks of the modular Edinburg Analytical Instruments (EAI) FL/CD-900 spectrofluorimeter. The need for a new system arose, when it became clear, that the absence of anti-freeze agents is key to the successful measurement of the thermodynamic activation. This absence of glass-forming substances from the protein solution caused the samples to freeze into an opaque structure, also having a considerable light-scattering. This resulted in a dramatic decrease of the light intensity at the detector side, since both the excitation efficiency, and the detectable fluorescence intensity decreased by more than a magnitude. Even with a cooled, high quantum-yield photomultiplier (PMT) (Hamamatsu R928, cooled to -65 °C) the photon count / minute on average was 50 ... 100 only. To have a reliable fit taking into account the Poisson distribution of the photons (thus the variance is equal to the expectation value) the estimated data acquisition time is in the range of 9 ... 15 hours on average. If the quenching efficiency at the dynamical transition is large, then the signal level will decrease significantly, and the needed data acquisition time will increase accordingly. Generally this means, that a single temperature-scan required around two - three weeks of continuous operation and data acquisition. At each temperature one has to wait for equilibrium to be reached, at least in a sense, that no further significant changes should occur during the data-acquisition time [1]. Then, after waiting for equilibrium, the data-acquisition can be started. After that, the new temperature has to be set, and the cycle can restart. While this can also be done manually, it is practically impossible to have two temperature-scans which are exactly the same in terms of all parameters, and this may introduce an excess of uncertainty into the data. It is also useful if the data acquisition is adjusted always to the actual signal level, and not set "by the eye". A third problem arising from the unusually long time of the experiment, is that short power or cooling-water outages can occur. This may not be a problem, if the closed-cycle helium cryostat is promptly shut down in the event of a drop in the water-pressure, and it can be re-started as soon the water-flow reaches the minimally required level. To have this done, however a constant, non-stop su-

1 Of course very slowly happening changes can not be totally excluded. If there is a kinetic barrier, thus the system is not perfectly in equilibrium, then the repeatability will even more depend on the waiting and acquisition times to be uniform.

Figure 44: Picture of the integrated phosphorescence lifetime spectrometer. The main blocks are marked in the picture.

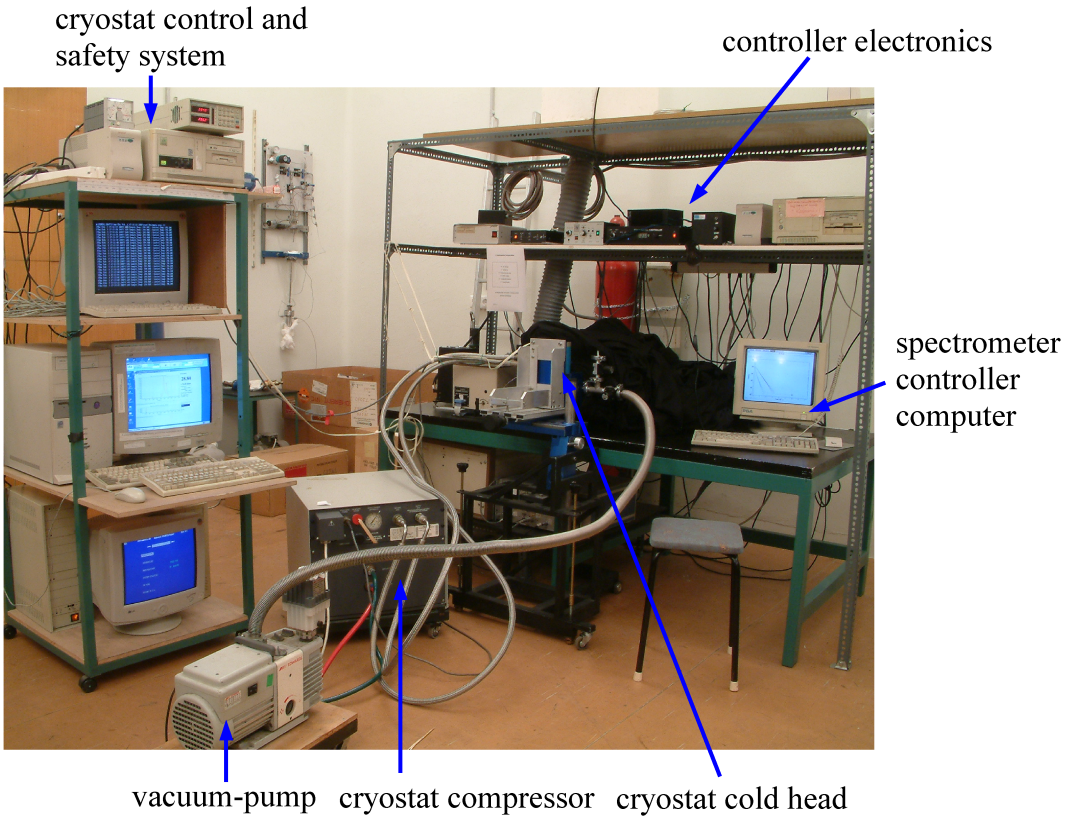

pervision, and more importantly rapid intervention to avoid cryostat damage is required.

All these considerations lead to the design, and build of a computer-controlled, integrated measurement system. The image of the system (in the days when the Zn-HbA data were taken) is shown in Figure 44. As can be seen in the first days the integration involved multiple computers, they were working in a network, each had it's own task, and I always had issues with one computer falling out. The next step was to re-design and re-build the whole system to achieve reliable operation. The block-diagram of the new system is shown in Figure 45. It is built around the optical building blocks of the old EAI instrument, since it is a modular system, and the building-blocks could be re-used in the new system. In the new design three main controllers are used: The central controller is a Linux-based Pentium-I PC (data acquisition and programming unit). This runs the main data-acquisition software, which controls the rest of the system, and outputs its data to a web-server (User interface) for display and download. This design alleviates the risk of data-loss due to possible over-loading of the processing capacity of the machine by graphics-intensive tasks. A newer, more powerful PC can not be used, since the these PC-s do not have an ISA-standard card slot. This is however needed for the proprietary controller-cards. The next unit, the Optics controller (OC) is inherited from the original system: it

Figure 45: Block diagram of the new system design.

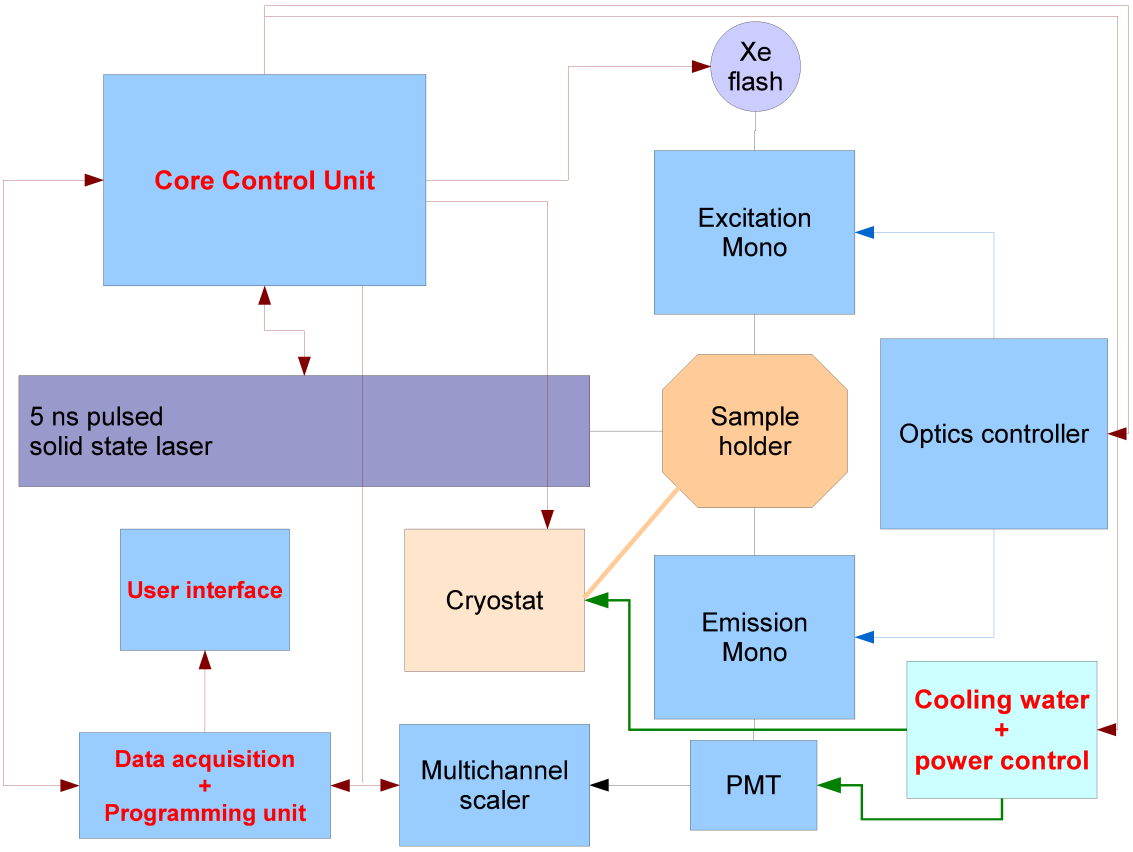

is responsible for the monochromators (setting the wavelength to a given value) and the shutters protecting the PMT. For this task the original controller could be used, it communicates with a proprietary protocol on an IEEE-488 General Purpose Interface Bus (GPIB-bus). This protocol had to be reverse-engineered to integrate the original controller into the new design. It turned out to be a text-based communication protocol with added byte-code parts to program the stepping-motor driver cards at system start-up. The third unit (Core Control Unit, CCU) is a 8-core parallel microprocessor (Parallax Propeller[2]) responsible for the hardware-integration of the solid-state tunable flash-laser, for driving the power-electronics of the safety-subsystem, for controlling the cryostat, and for the timing-synchronization of the light sources (Xenon flash-lamp and the laser) to the data-acquisition unit. The original multichannel card was replaced by a new photon-counting unit made by Károly Módos based on the photon-counting unit he built for the dynamic light scattering instrument of the department.

A.2 CONTROLLER PROGRAM

The system is integrated via a hierarchical master-slave mechanism: the PC running the main program is the master, and the other two controllers (CCU and OC) are slaved to it. The CCU is however the master of the controller of the solid-state laser, the Xenon flash-lamp driver, and the power electronics. There is an "emergency-network" built into the system, in this system the CCU is the absolute master. One core of the 8-core microprocessor is dedicated to this network, it reads the power and water-flow sensors built into the PMT-cooling line and into the cryostat cooling line. In the event of an emergency the CCU will promptly (within a few milliseconds) shut down the cryostat and disable the high-voltage on the PMT. It will additionally signal the main program of the emergency situation, so that it can adapt it's behavior. This prevents damage of the system in an event of power or cooling water outage. The main program will then restore operations if conditions return to normal, an depending on the temperature of the sample will either terminate the experiment, or return to a temperature slightly below the last setting, insert an extra temperature point (as an internal control of the experiment) and resume the temperature scan. The main program is also responsible for data-logging. It not only saved the decay curves, but also periodically logs the temperature, the wavelength, and other parameters of the system. It created separate files for each decay, but it also produces a single log-file, in which all the data are compressed. This is for convenience, and also to have a safety-backup of the experimental data. The Linux operating system is configured to remotely synchronize the output-directory of

2 http://www.parallax.com/propeller

the controller program every night to a backup-server. The individual data files are also synchronized periodically (for eg. in every minute) to the web-server[3].

As an example I will show two representative parts of the main controller program. The code is several thousand lines long, so the whole can not be included here.

The GPIB initialization, using a custom-modified version of the Linux GPIB communication library is shown in 1. The code is well-commented, and does not need much additional description.

Listing 1: The GPIB initialization code

```
// ********************************************************************
// EAI comm routine (c) 2008 G.Schay
// uses a hacked linux gpib c API
int eaicomm ( char * buffer , int * commlen ) {
    /* write it to EAI */
        int cl=0 ;
        int cn=0 ;
        int status;
        cl = *commlen;
        if(DEBUG){
          printf("# Sending EAI command: ");
          for(cn=0;cn<=cl;cn++) printf("%c",buffer[cn]);
          printf(" ; ");
          }
        status = ibwrt(dev,buffer,cl);
        if( status & ERR )
        {
                printf("! ibwrtf() failed, massage comes:\n" );
                printf("! %s\n# ", gpib_error_string( ThreadIberr() ) );
                return -1;
        }
    if(buffer[0]=='P') return 0 ; /* implement "P" bug of EAI */
     /* read back response */
        status = ibrd(dev,buffer,1023);
        if( status & ERR )
        {
                printf("! ibwrtf() failed, massage comes:\n" );
                printf("! %s\n# ", gpib_error_string( ThreadIberr() ) );
                return -1;
        }
        if(DEBUG) printf("Read from EAI: %s  ; bytes transfered:%d\n",buffer,ibcnt);
        *commlen=ibcnt;
        return iberr;
}
int eaiinit (char systpye){
        int board_index = 0;
        int pad = 1;
        int sad = 0;
        int send_eoi = 1;
        int eos_mode = 0;
/* PAD=1, board=0, send EOI with last byte of write */
        int status;
        int commlen;
        char buffer [1024];
 /* EAI monochromator and polariser program sequence */
        char monoinitfs[14]={0x00,0x00,0x00,0x3e,0x07,0xd0,0x46,0x50,0x00,0x01,0x4e,0x20,0x46,0x50
              };
        char polainitfs[14]={0x00,0x02,0x00,0x32,0x00,0x01,0x00,0x05,0xff,0xff,0x00,0x00,0x00,0x00
              };
        char monoinitfl[14]={0x00,0x00,0x00,0x3e,0x00,0x64,0x03,0x84,0x00,0x14,0x4e,0x20,0x46,0x50
              };
        char polainitfl[14]={0x00,0x02,0x00,0x3e,0x00,0x01,0x00,0x05,0xff,0xff,0x00,0x00,0x00,0x00
              };
        char * monoinit = monoinitfl;
        char * polainit = polainitfl;
/* init board */
        dev = ibdev( board_index, pad, sad, TNONE, send_eoi, eos_mode );
```

3 nightowl.sote.hu

```
        if( dev < 0 )
        {
                printf("! ibdev() failed, massage comes:\n" );
                printf("! %s\n", gpib_error_string( ThreadIberr() ) );
                return -1;
        }
        if(DEBUG) printf( "# EAI online: board index=%i, pad=%i, sad=%i\n",board_index, pad, sad);
// System setup sequence.
        if(systype==FL) {
            monoinit=monoinitfl;
            polainit=polainitfl;
            if(DEBUG) printf("# Mode = FL-style\n");
            }
        if(systype==FS) {
            monoinit=monoinitfs;
            polainit=polainitfs;
            if(DEBUG) printf("# Mode = FS-style\n");
            }
        if(DEBUG) printf("# Runing init sequence\n");
/* init EAI */
        strcpy(buffer,"R,0"); commlen=strlen(buffer);
        eaicomm(buffer,&commlen);
        strcpy(buffer,"R,0,0"); commlen=strlen(buffer);
        eaicomm(buffer,&commlen);
        strcpy(buffer,"M,26,0"); commlen=strlen(buffer);
        eaicomm(buffer,&commlen);
    if(systype==FS){
        strcpy(buffer,"I,1,58063"); commlen=strlen(buffer);
        eaicomm(buffer,&commlen);
        if(buffer[4]=='-' && buffer[5]=='2'){
        /* mono init error, most probably "Stepper config does not match" Run mono setup */
            strcpy(buffer,"P,1"); commlen=strlen(buffer);
            eaicomm(buffer,&commlen);
            bcopy(monoinit,buffer,14); commlen=14;
            eaicomm(buffer,&commlen);
            strcpy(buffer,"I,1,58063"); commlen=strlen(buffer);
            eaicomm(buffer,&commlen);
            }
    }
    if(systype==FL){
        strcpy(buffer,"I,1,39082"); commlen=strlen(buffer);
        eaicomm(buffer,&commlen);
        if(buffer[4]=='-' && buffer[5]=='2'){
        /* mono init error, most probably "Stepper config does not match" Run mono setup */
            strcpy(buffer,"P,1"); commlen=strlen(buffer);
            eaicomm(buffer,&commlen);
            bcopy(monoinit,buffer,14); commlen=14;
            eaicomm(buffer,&commlen);
            strcpy(buffer,"I,1,39082"); commlen=strlen(buffer);
            eaicomm(buffer,&commlen);
            }
    }
        strcpy(buffer,"M,5,0"); commlen=strlen(buffer); // defaulting to us lamp
        eaicomm(buffer,&commlen);
    if(systype==FS){
        strcpy(buffer,"I,2,58063"); commlen=strlen(buffer);
        eaicomm(buffer,&commlen);
        if(buffer[4]=='-' && buffer[5]=='2'){
        /* mono init error, most probably "Stepper config does not match" Run mono setup */
            strcpy(buffer,"P,2"); commlen=strlen(buffer);
            eaicomm(buffer,&commlen);
            bcopy(monoinit,buffer,14); commlen=14;
            eaicomm(buffer,&commlen);
            strcpy(buffer,"I,2,58063"); commlen=strlen(buffer);
            eaicomm(buffer,&commlen);
            }
    }
    if(systype==FL){
        strcpy(buffer,"I,2,39082"); commlen=strlen(buffer);
        eaicomm(buffer,&commlen);
        if(buffer[4]=='-' && buffer[5]=='2'){
        /* mono init error, most probably "Stepper config does not match" Run mono setup */
            strcpy(buffer,"P,2"); commlen=strlen(buffer);
            eaicomm(buffer,&commlen);
            bcopy(monoinit,buffer,14); commlen=14;
            eaicomm(buffer,&commlen);
            strcpy(buffer,"I,2,39082"); commlen=strlen(buffer);
```

```
131             eaicomm(buffer,&commlen);
                }
    }
        strcpy(buffer,"M,6,1"); commlen=strlen(buffer);
        eaicomm(buffer,&commlen);
136 if(systype==FS){
        strcpy(buffer,"I,9,57"); commlen=strlen(buffer);
        eaicomm(buffer,&commlen);
        if(buffer[4]=='-' && buffer[5]=='2'){
        /* polariser init error, most probably "Stepper config does not match" Run mono setup */
141         strcpy(buffer,"P,9"); commlen=strlen(buffer);
            eaicomm(buffer,&commlen);
            bcopy(polainit,buffer,14); commlen=14;
            eaicomm(buffer,&commlen);
            strcpy(buffer,"I,9,57"); commlen=strlen(buffer);
146         eaicomm(buffer,&commlen);
            }
        }
    if(systype==FL){
        strcpy(buffer,"I,9,69"); commlen=strlen(buffer);
151     eaicomm(buffer,&commlen);
        if(buffer[4]=='-' && buffer[5]=='2'){
        /* polariser init error, most probably "Stepper config does not match" Run mono setup */
            strcpy(buffer,"P,9"); commlen=strlen(buffer);
            eaicomm(buffer,&commlen);
156         bcopy(polainit,buffer,14); commlen=14;
            eaicomm(buffer,&commlen);
            strcpy(buffer,"I,9,69"); commlen=strlen(buffer);
            eaicomm(buffer,&commlen);
            }
161     }
    if(systype==FS){
        strcpy(buffer,"I,10,57"); commlen=strlen(buffer);
        eaicomm(buffer,&commlen);
        if(buffer[5]=='-' && buffer[6]=='2'){
166     /* polariser init error, most probably "Stepper config does not match" Run mono setup */
            strcpy(buffer,"P,10"); commlen=strlen(buffer);
            eaicomm(buffer,&commlen);
            bcopy(polainit,buffer,14); commlen=14;
            eaicomm(buffer,&commlen);
171         strcpy(buffer,"I,10,57"); commlen=strlen(buffer);
            eaicomm(buffer,&commlen);
            }
    }
    if(systype==FL){
176     strcpy(buffer,"I,10,69"); commlen=strlen(buffer);
        eaicomm(buffer,&commlen);
        if(buffer[5]=='-' && buffer[6]=='2'){
        /* polariser init error, most probably "Stepper config does not match" Run mono setup */
            strcpy(buffer,"P,10"); commlen=strlen(buffer);
181         eaicomm(buffer,&commlen);
            bcopy(polainit,buffer,14); commlen=14;
            eaicomm(buffer,&commlen);
            strcpy(buffer,"I,10,69"); commlen=strlen(buffer);
            eaicomm(buffer,&commlen);
186         }
    }
        if(DEBUG) printf("# EAI init sequence finished.\n# System type is now set to %s \n",(
            systype==FS)? ("FS"):("FL"));
/* init ready */
return o;
191 }
```

As can be seen, the communication routine is from line 17 to line 47. The controller needs to send byte-code along the text-formed communication to the OC unit at start-up, this is declared in lines 60 ... 65. From line 49 the main initialization routine follows. This is full of optional debugging messages, the DEBUG variable is set by the main routine.

The photon counting unit also needs special communication, the routine is listed as the code snippet shown in 2.

Listing 2: Communication code of the photon counting unit

```
int acqcomm (char * acqbuffer , long commwait){
long counter=0;
long cntr=0;
int code=0;
int tempcode=0;
char stay=1;
char tmp=0;
int slwt=0;
if (DEBUG>1) printf("# AcqBoard: command is: %s\n",acqbuffer);
if(acqbuffer[0]=='q') stay=0;
cntr=0;
fflush(acqport);
if(stay){
 if(acqbuffer[0]=='.') {
    bzero(acqbuffer,BLEN);
    // read resp.
    // DataAck resp format: M.....<CR> for every line
    counter=0;
    code=0;tempcode=0;
    if(fgetc(acqport)!='M') printf("! DataAqBorad: No response.\n"); // first 'M' indicates
         response, read it and check..
    while(code!=EOF&&counter<BLEN)
     {
     code=fgetc(acqport);
     if(code=='M'&&tempcode==0x0d)
      { // new line comes, this is the leading 'M', skip it, make a space instead.
      code=' ';
      }
     tempcode=code;
     if(code==0x0d) code='\n'; // replace <CR> with \n
     if(code!=EOF) acqbuffer[counter]=code;
     counter++;
     }
    counter-=3;
    acqbuffer[counter]=0;
    if(DEBUG) printf("# AcqBoard: Read response: %s \n",acqbuffer);
    }
 else {
  for(cntr=0;acqbuffer[cntr]>0;cntr++);
  // cntr--;
  if(DEBUG) printf("# AcqBoard: Command length: %d bytes\n",cntr);
  counter=0;
  while (counter<cntr){
   tmp=acqbuffer[counter];
   code=fprintf(acqport,"%c",tmp);
   // printf("\ncounter=%d , wrote: '%c', code:%d\n",counter,tmp,code);
   fflush(acqport);
   fflush(stdout);
   // printf("next.\n");
   counter++;
   }
   // tmp=0x0a; // linefeed
   tmp=0x0d; // Carriage Return
  code=fprintf(acqport,"%c",tmp);
   // printf("\ncounter=%d , wrote: '%c', code:%d\n",counter,tmp,code);
   fflush(acqport);
   fflush(stdout);
  bzero(acqbuffer,BLEN);
   counter=0;
    code=0;tempcode=0;
    if(commwait) {
         // possible wait needed before resp can be read do it.
        if(commwait<=1000000) usleep (commwait);
        else {
            slwt=(int)ceil(commwait/1000000);
            // printf("sleeping for %d sec",slwt);
            sleep(slwt);
            }
        }
    if(fgetc(acqport)!='M') printf("! DataAqBorad: No response.\n"); // first 'M' indicates
         response, read it and check..
    while(code!=EOF&&counter<BLEN)
     {
     code=fgetc(acqport);
```

```
      if(code=='M'&&tempcode==oxod)
74     { // new line comes, this is the leading 'M', skip it, make a space instead.
       code=' ';
       }
      tempcode=code;
      if(code==oxod) code='\n'; // replace <CR> with \n
79    if(code!=EOF) acqbuffer[counter]=code;
      counter++;
      }
     counter-=3;
     acqbuffer[counter]=0;
84   if(DEBUG) printf("# AcqBoard: Read response: %s \n",acqbuffer);
    }
  }
return(counter); // read resp length
}
```

It can be seen, that the code checks for specific return values, and if a possible error is found, then it prints a warning.

A.3 MICRO-CONTROLLER HUB

The CCU consits of a Parallax Propeller chip, and several external electronics to couple it's digital low-voltage (3V) logic to the power-electronics of the system. The Propeller is a versatile platform, the chip has eight parallel running processors, that share a common memory, and I/O lines. The picture of the CCU board is shown in Figure 46.

The Propeller runs a special interpreted proprietary language called "spin", but each processor can also be programmed in assembly.

The spin code is again very long, as an example I only show part a simple debugging version in 3 used for beta-testing, which is small, and for an example of the assembly code, the programming of a synchronization timer is also shown in 4. Both codes are fairly well commented, so I will not add additional comments to them.

Listing 3: Beta-testing laser-synchronization code of the CCU

```
CON
2    _clkmode        = xtal1 + pll16x
     _xinfreq        = 5_000_000
     Rx = 31
     Tx = 30
     SerialMode = %0000
7    SerialBaud = 9600
     Bl_Pin = 26
OBJ
      Serial   : "Mod_Extended_FDSerial"
      Timer    : "timer8"
12  VAR
     long  blinkDeadline
     long  blinkDelay
     long  PerT
     long  QSWON
17   long  MCSON
     long  ATT
     byte  Freq
     byte  Error
     byte  serial_on
22   byte  cmd[20]
     byte  DEBUG
     long  PreHT
...
```

Figure 46: Image of the CCU main board (top, © G.Schay) and block diagram of the propeller chip (bottom, image used with permission from the Parallex website)

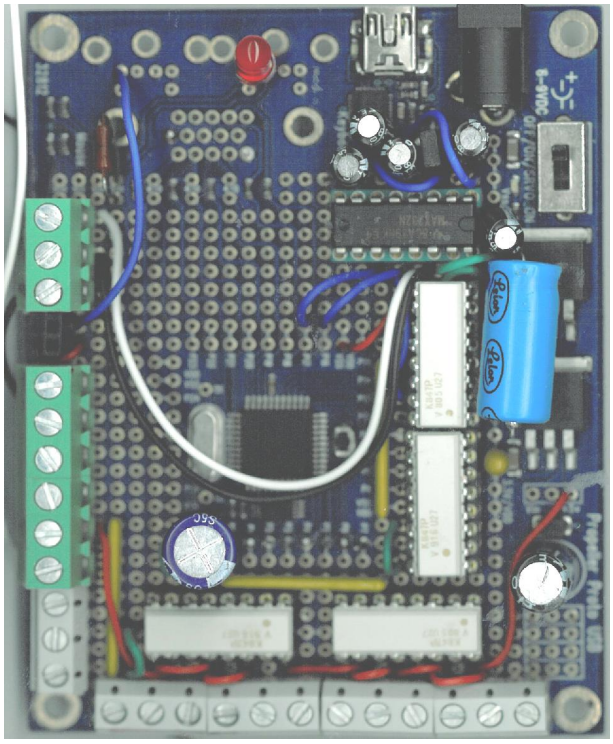

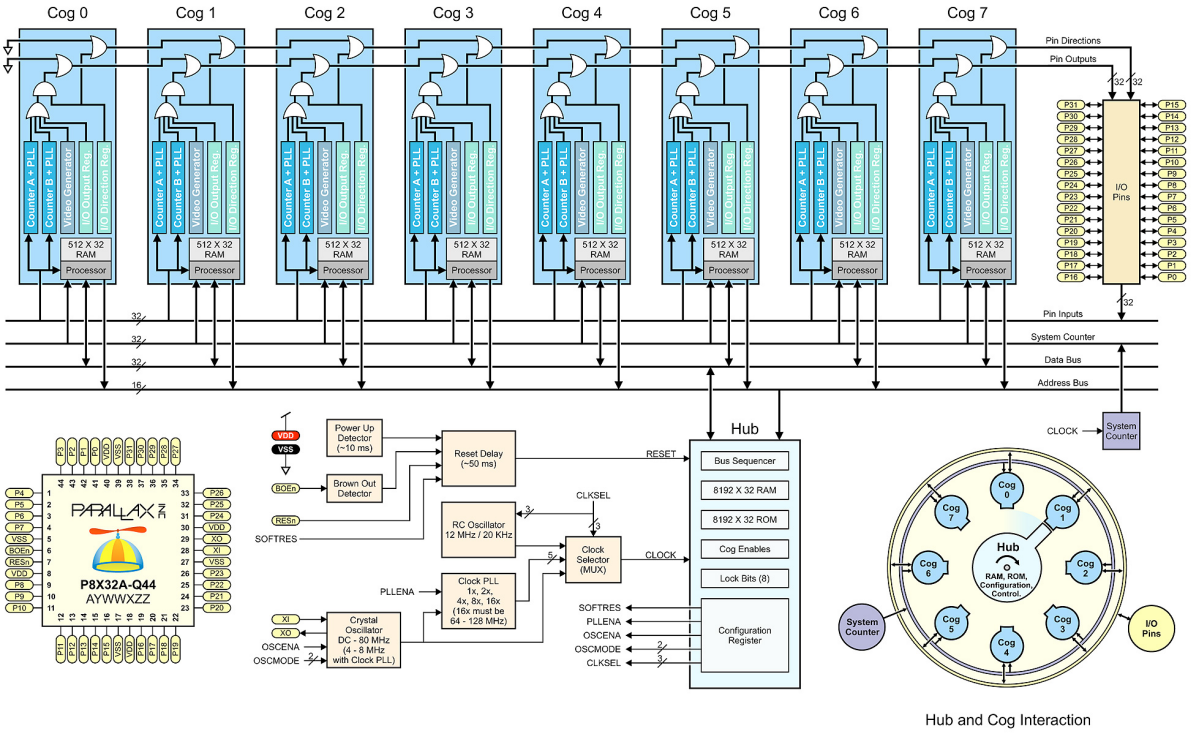

Hub and Cog Interaction

```
PUB Main  | command , ser_cog
' INIT
    Freq  :=10
    Error :=0
    PerT  :=0
    QSWON :=0
    MCSON :=0
    ATT   :=150
    DEBUG :=1
    PreHT :=50
    ' make the PIN an output
    dira[Bl_Pin]:=1
    command := -1
    serial_on := 0
    dira [Rx] :=0
    dira [Tx] :=0
    ' MAIN LOOP
     repeat
       ' wait for target time to be exceeded
       if cnt > blinkDeadline
           ' toggle the pin state...
           !outa[Bl_Pin]
           blinkDeadline := cnt + blinkDelay
       ' check if to start serial_driver
       if (serial_on==0 AND (ina [Rx]==1 AND ina [Tx]==1))
         ser_cog := Serial.Start(Rx,Tx,SerialMode,SerialBaud)
         serial_on := 1
         waitcnt(cnt+clkfreq)
       if (serial_on == 1 AND Error<>0 AND DEBUG<>0)  'there is an error msg to send
         Serial.str(@_erro)
         Serial.dec(Error)
         Serial.str(@_nl)
         Serial.str(@_error)
         Serial.rxflush
         Error:=0
       if serial_on == 1
         command := Serial.rxcheck
       if command <> -1
         if command == "." ' all commands start with "."
           Serial.RxStr(@cmd)
           ' we have new data, update delay and clear buffer
           if StrComp(@cmd,String("period")) ' set period time
             PerT := Serial.RxDec
             Serial.str(String("New period time: "))
             Serial.dec(PerT)
             Serial.str(String(" x 0.1s"))
             Serial.str(@_nl)
             if(timer.setup(PerT,ATT,QSWON,MCSON,PreHT))
               Error:=2
           if StrComp(@cmd,String("qsw")) ' set qswitched mode
             QSWON := Serial.RxDec
             if(QSWON)
              QSWON:=1
             Serial.str(String("Q-switched mode: "))
             if(QSWON)
              Serial.str(String(" ON"))
             if(QSWON==0)
              Serial.str(String(" OFF"))
             Serial.str(@_nl)
             if (timer.setup(PerT,ATT,QSWON,MCSON,PreHT))
               Error:=2
           if StrComp(@cmd,String("mcs")) ' set qswitched mode
             MCSON := Serial.RxDec
             if(MCSON)
              MCSON:=1
             Serial.str(String("MCS triggering: "))
             if(MCSON)
              Serial.str(String(" ON"))
             if(MCSON==0)
              Serial.str(String(" OFF"))
             Serial.str(@_nl)
             if(timer.setup(PerT,ATT,QSWON,MCSON,PreHT))
               Error:=2
           if StrComp(@cmd,String("start")) ' start timer
             timer.setup(PerT,ATT,QSWON,MCSON,PreHT)
             if( timer.start == 0 )
               Freq:=2 'on error set low blink rate
```

```
                Error:=1 'set error msg codeATT := Serial.RxDec
              Serial.str(String("Laser driver started "))
              Serial.str(@_nl)
            if StrComp(@cmd,String("stop")) ' stop timer
107           timer.stop
              Serial.str(String("Laser driver stopped "))
              Serial.str(@_nl)
            Serial.rxflush
```

Listing 4: Assembly timer code of the CCU

```
{{ ---------------------------------------------------
| Timer for the Laser Controller                     |
| (c) 2010 G.Schay                                   |
| VER. 1.1 Beta                                      |
5 ---------------------------------------------------  }}
'CON
'     _clkmode        = xtal1 + pll16x
'     _xinfreq        = 5_000_000
VAR
10   long  timerCog                        ' This is in hub ram
     long  Dataready
     long  PeriodTime
     long  Npulses
     long  QswON
15   long  MCSON
     long  QswDelay
     long  PMTDelay
     long  MCSDelay
     long  Preheat
20 'PUB main
PUB start : success
     dira[7]:=1
     dira[6]:=1
     dira[5]:=1
25   dira[4]:=1
     outa[7]:=0
     outa[6]:=0
     outa[5]:=0
     outa[4]:=0
30 'setup to do nothing with safe params
     PeriodTime :=0
     Npulses    :=1
     QswON      :=0
     MCSON      :=0
35   QswDelay   :=15200
     MCSDelay   :=80
     PMTDelay   :=14800
     Dataready  :=1
     Preheat    :=50
40 ' Now to start the cog,
pinLXe :=   |<7
pinQsw :=   |<6
pinPMT :=   |<5
pinMCS :=   |<4
45 success := (timerCog := cognew(@asm_code,@Dataready) + 1)
waitcnt(clkfreq/100+cnt)
PUB stop
  if timerCog
    cogstop(timerCog~ -  1)
50 ' clear the bits of output, and set them to input
     outa[7]:=0
     outa[6]:=0
     outa[5]:=0
     outa[4]:=0
55   dira[7]:=0
     dira[6]:=0
     dira[5]:=0
     dira[4]:=0
PUB setup(PT,ATT,QSW,MCS,PreHT) : ready
60 ' This sets up the timer
' PT is the period Time in 0.1s increments
' ATT is the attenuation factor 0=max power, 100 = +100us delay
PeriodTime:=PT
Preheat:=PreHT
```

```
QswON:=QSW
MCSON:=MCS
if QSWON
 QswDelay:=15200+(ATT*80)-960
if(MCSON)
  MCSDelay := 800
ifnot(MCSON)
  MCSDelay :=0
PMTDelay := 420                 'MUST be >400
if (PT)
  Npulses:=1                    'if no QSW, let it flash slow
if(QswON AND PT>2)                    'but if QSW is ON, short period, 1 preflash
  Npulses:=PT
  if (PT>Preheat)
   Npulses:=Preheat
Dataready:=1
waitcnt(clkfreq/100+cnt)
ready:=Dataready                'if cog reads the data it clears the flag
DAT
                        org
asm_code                or      DIRA,pinLXe
                        or      DIRA,pinQsw
                        or      DIRA,pinMCS
                        or      DIRA,pinPMT
                        ' pins set
                        mov     _tst,#0
                        or      _tst,pinLXe
                        or      _tst,pinQsw
                        or      _tst,pinMCS
                        or      _tst,pinPMT
                        andn    OUTA,_tst
                        mov     head,PAR
:read                   mov     ptr,PAR
                        add     ptr,#4
                        rdlong  _pt,ptr         ' get period time
                        add     ptr,#4
                        rdlong  _np,ptr         ' get Npulses
                        add     ptr,#4
                        rdlong  _Qon,ptr        'get QSW=ON?
                        add     ptr,#4
                        rdlong  _MCS,ptr        'get MCS=ON?
                        add     ptr,#4
                        rdlong  _qsw,ptr        'get Qsw delay
                        add     ptr,#4
                        rdlong  _pmt,ptr        'get PMT delat
                        add     ptr,#4
                        rdlong  _mcsd,ptr       'get MCS delay
                        wrlong  _zero,head
:inf_loop               mov     ptime,CNT       'get start of period
                        rdlong  _tst,head
                        tjnz    _tst,#:read     'if new data,read it
                        tjz     _pt,#:inf_loop    ' if period time =0 do nothing, read
                        mov     _tst,_np        'copy npulses
:pulse                  mov     time,CNT
                        add     time,_ptbase    'add 0.1 sec delay
                        waitcnt time,#10            'wait
                        ' blind PMT for security
                        or      OUTA,pinPMT
                       ' mov     time,CNT
                       ' add     time,_trigtime
                       ' waitcnt time,#10
                       ' andn    OUTA,pinPMT
                        ' pmt e.shutter triggered
                        ' now flash laser
                        or      OUTA,pinLXe     'set LXe ON
                        mov     time,CNT
                        add     time,_trigtime
                        waitcnt time,#10            'wait 12 us
                        andn    OUTA,pinLXe     'clear LXe, trigger end
                        andn    OUTA,pinPMT     're-enable PMT after pulse
                        sub     _tst,#1
                        tjnz    _tst,#:pulse    'if more pulses repeat
                        tjz     _Qon,#:waitperiod       'QSW will not flash, wait
                        mov     time,CNT
                        add     time,_qsw
                        sub     time,_pmt
                        waitcnt time,#10
```

```
                        mov     p,CNT
                        or      OUTA,pinPMT     'blind PMT again
                        mov     time,p
                        add     time,_pmt
                        waitcnt time,#10
                        or      OUTA,pinQsw     'trigger QSW
                        add     time,_trigtime
                        waitcnt time,#10
                        andn    OUTA,pinQsw
                        andn    OUTA,pinPMT     're-enable PMT after pulse
                        tjz     _MCS,#:waitperiod       'no MCS start
                        mov     time,CNT
                        add     time,_mcsd
                        waitcnt time,#10
                        or      OUTA,pinMCS
                        mov     time,_us
                        shl     time,#2
                        add     time,CNT
                        waitcnt time,#10
                        andn    OUTA,pinMCS

:waitperiod             mov     _tst,_np
                        mov     _ticks,_pt
                        ' count for Npulses
:cntpt                  add     ptime,_ptbase
                        sub     _tst,#1
                        sub     _ticks,#1
                        tjnz    _tst,#:cntpt
                        ' npulses time added
                        ' if _ticks=_npulses -> end of period
                        tjz     _ticks,#:inf_loop
                        ' no, need to wait more, do it in ticks
                        mov     time,CNT
:waitticks              add     time,_ptbase
                        waitcnt time,#10
                        sub     _ticks,#1
                        mov     time,CNT
                        tjnz    _ticks,#:waitticks
                        jmp     #:inf_loop
' Initialized data
_us                     long    80
_trigtime               long    960
_ptbase                 long    8_000_000
pinLXe                  long    0
pinQsw                  long    0
pinPMT                  long    0
pinMCS                  long    0
_zero                   long    0
' Uninitialized data
p                       res     1
ptime                   res     1
_tst                    res     1
head                    res     1
ptr                     res     1
time                    res     1
_pt                     res     1
_np                     res     1
_pmt                    res     1
_qsw                    res     1
_Qon                    res     1
_MCS                    res     1
_mcsd                   res     1
nextperiod              res     1
_ticks                  res     1
                        FIT
```

A.4 WEB-SERVER ARCHITECTURE

The web-interface is very minimalistic. It is optimized for viewing also on low-resolution devices, such as smart-phones. The reason behind this is, that in

an event of emergency the main program also sends an email, and one can promptly check the status of the system by opening the web-page it generates. The main controller program outputs data files in two formats, one as a text-file to download, which is simply copied to the server, and a link is inserted into the HTML-code accordingly. The second file is for processing with the "Gnuplot" program[4] which makes a small image of the data accordingly to the data type: excitation or emission spectrum, or phosphorescence decay. In the latter case the decay is shown in a half-logarithmic representation. The content of the web-site is generated by some very simple commands driving Gnuplot, and the line-oriented file-processor "awk"[5]. This is possible since the main controller program outputs the files in formats suitable for these programs, and it also generates a text-file from which for eg. the status-message on the web-page can easily be generated. As an example an image of the website's page in an emergency situation is shown in Figure 47. Note the status message at the beginning, the power status is "OFF".

4 http://www.gnuplot.info
5 http://www.gnu.org/software/gawk

Figure 47: The first page of the web-site of the data-acquisition program as displayed on a remote computer.

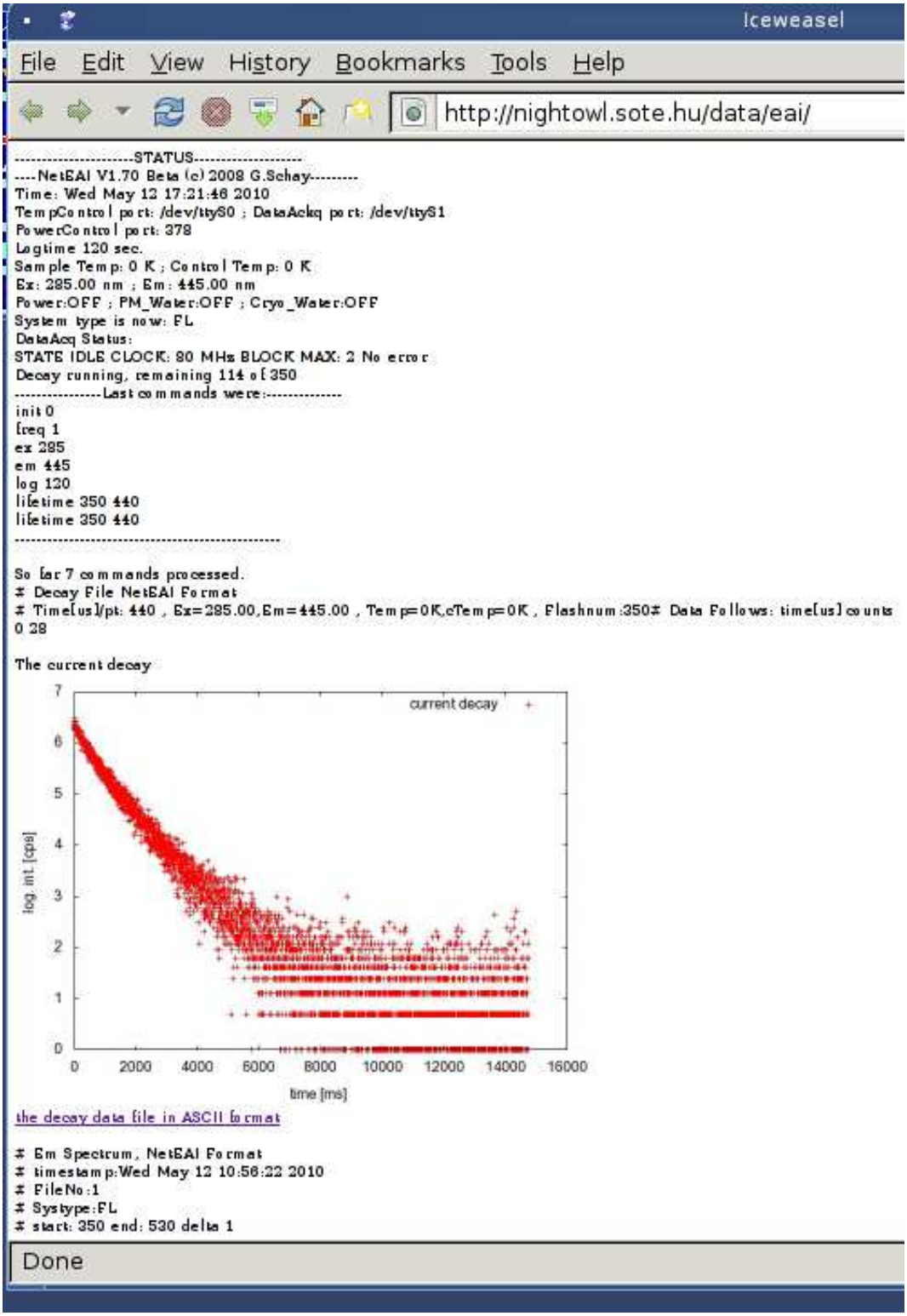

B

FLN SETUP

In the FLN setup, there were two separate tasks to be solved. The first was the development of a program to help tune the ring dye-laser once it was operating in a power-stabilization loop-back. The second task was to develop a program package to help analyze the data.

B.1 LASER SCANNING

The computer control of the scanning was important, since at the edge of the scanning range the laser-dye bleaches more quickly, and to be able to measure the IDF, the scanning has to be made as quick as possible. With a manual scanning this would not be possible. Therefore I have written a very simple Delphi language program to run under Windows to control the stepper motor driving the scanning mechanics. The choice of Delphi comes from the fact that the CCD camera's software also runs under Windows, so this way the whole setup could be controlled with a single computer. The image of the controller program is shown in Figure 48. The program is very simple: it first calibrates itself to the speed of the computer it is running on, and then uses this calibration to output pulses to drive the stepper motor. Since there is no feed-back of the actual position, the laser's wavenumber-position has to be read manually at the beginning of the experiment, and input into the program. Then by pressing the buttons on the screen the laser can be moved with a given wavenumber-increase or decrease to the new position. For convenience two different steps are also implemented,

Figure 48: Image of the laser-scanning program, together with a list of files of the source code.

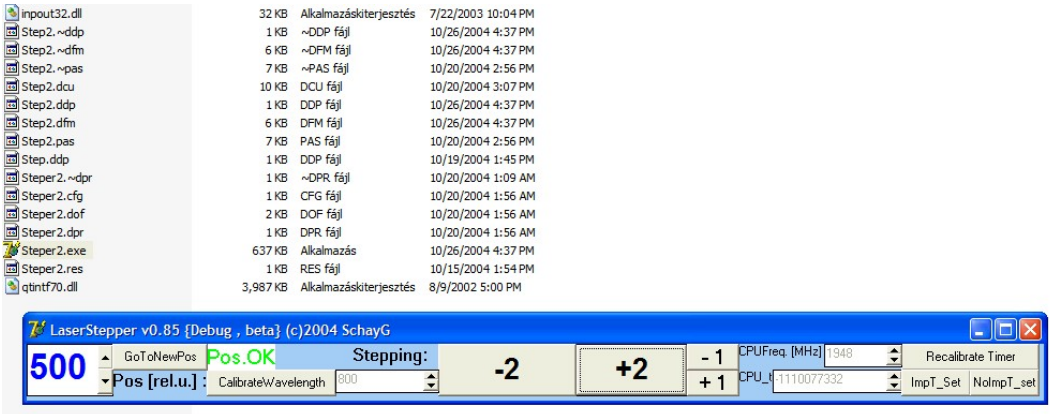

along with a numeric input possibility.

B.2 DATA EVALUATION

The data evaluation on the FLN experiment involves the processing of hundreds of spectra. As shown in Figure 35 several peaks in each spectrum can be evaluated, and ideally all of the observable peaks have to be followed, and the position and the amplitude of the peaks have to be recorded. Another problem is the subtraction of the non-resolved baseline, since that would introduce artifacts into the peak-height data. Therefore the spectra had to be subjected to a baseline-subtraction first.
I have developed a software package written in "octave"[1], a free alternative to the well-known Matlab® program. The package consist of several small programs, each performing a different task. The tasks are the following:

- Calibrating the CCD camera data (turning the pixel-number into wavenumber scale). The CCD camera's image is turned into a quasi-spectrum by the data-acquisition software, which integrates the image along the vertical axis. This is useful, since the camera is mounted onto the exit slit of the monochromator, and thus a given spectral line is a vertical line in the image of the camera. The calibration is done by processing this vertically integrated image taken of a glimm-lamp through the monochromator, and recorded with the camera. The known emission lines of the neon gas can be used to find them in the image of the camera, and make a pixel to wavenumber conversion. I have used a simple linear fit to the pixel-number vs. glimm-lamp emission line wavelength data pairs to obtain the calibration.
- Converting the spectral images to real spectra by using the established calibration.
- Baseline-correcting the spectra by removing non-resolved background from the spectra.
- Finding and tracking the peaks in a series of spectra, together with the corresponding excitation wavenumbers.
- Fitting the IDF to the multiple peak-series by a global-fitting algorithm.

The programs were designed in a way to build upon each other, each is processing the files from the program before it in the processing chain, and outputs a format required by the program performing the next step. This makes it possible, that the processing can be halted at any stage, and it opens the way for manual intervention if possible, by simply editing the intermediate files before running the next program on them. For convenience, a wrapper program is also

1 http://www.gnu.org/software/octave

Figure 49: Output of the "Peakfinder" program of the FLN data evaluation package. The sample is Zn-HbA + 100 mM NaCl at 1.4 kbar pressure.

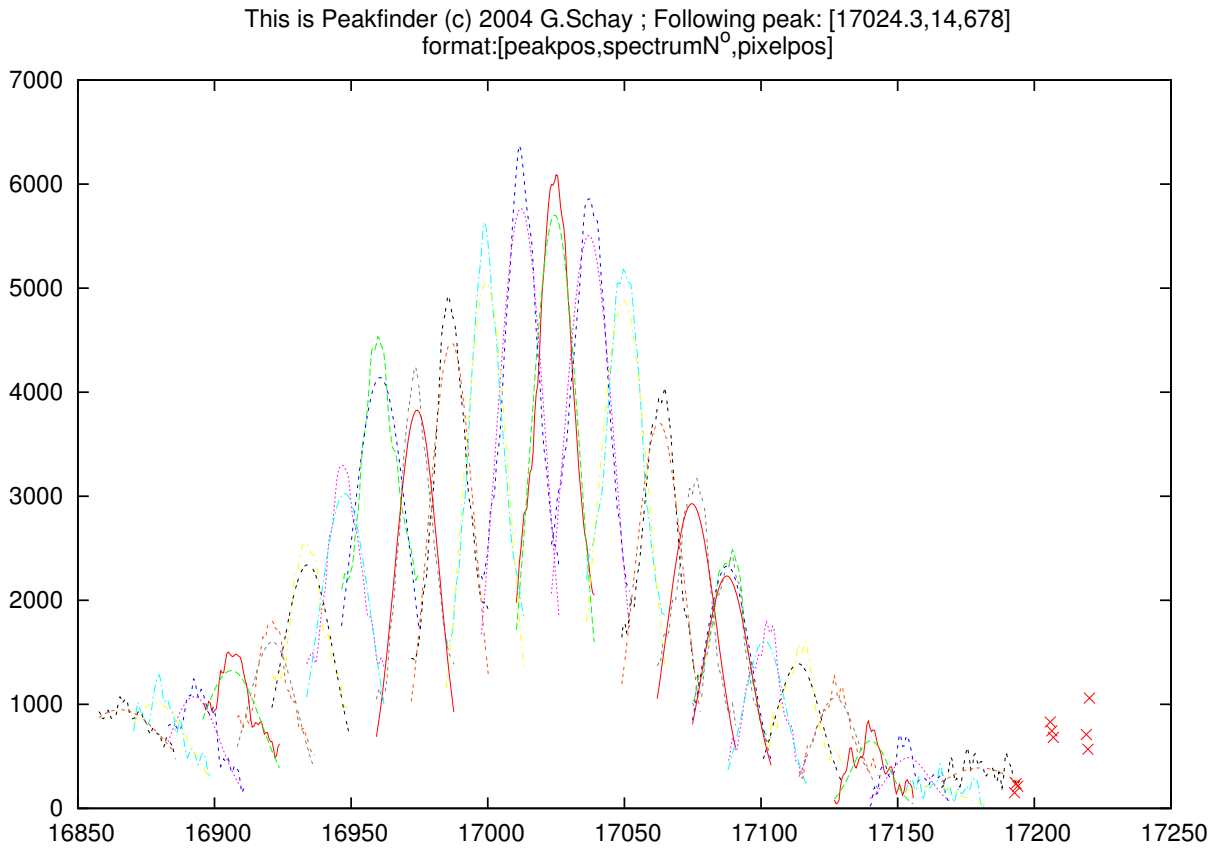

included in the package, which finds all experimental files in a directory structure, and runs the evaluation on each spectral series. It also prints a report is postscript format about every stage. As an example of the outputs generated by the package such a report from the peak-tracking stage ("Peakfinder" program) is shown in Figure 49.